MEASUREMENT AND APPLICATION OF RESIDENCE TIME OF PLASTIC LITTER ON BEACHES

January, 2014

DOCTOR OF ENGINEERING

Tomoya Kataoka

TOYOHASHI UNIVERSITY OF TECHNOLOGY

ABSTRACT

Understanding the residence time of plastic litter on beaches is crucial to take countermeasures against plastic pollution, and yet few studies have examined this issue. This research attempted to measure the residence time of litter on a beach, and to understand the physical mechanisms determining the residence time. In addition, the application of residence time to beach cleanups is discussed.

Firstly, mark-recapture (MR) experiments for certain fishery floats were conducted on Wadahama Beach, Niijima Island, Japan for two years at one- to three-month intervals. In the MR experiments, we used a permanent marker to number individual floats found along the whole beach which is 900 m long, and measured the position of each float to investigate the physical mechanisms determining the residence time. In addition, beach topography was measured using a real-time kinematic GPS system.

The remnants of the floats decreased during the two years according to an exponential function. If a decrease in floats is seen over a long period, it means that the remnants can be assumed to have decreased at a constant rate which determines the average residence time. The average residence time was calculated from the exponential decay of remnants, which was 224 days. We investigated the movement of the remnant floats in the alongshore direction (northward−southward). The floats moved both northward and southward, and consequently became concentrated in the northern and southern areas of the beach. These areas of concentration were located in the lee of low crested structures (LCSs) offshore of Wadahama Beach. The alongshore distribution of the concentration of remnant floats was similar to that for floats had been backwashed offshore (i.e., emigration). The alongshore movement of floats was significantly correlated with the rate of decrease and the frequency of wind-waves running up as far as the backshore. In addition, the area with the highest concentration of floats matched the area where sediment transported alongshore was deposited. Therefore, we assume that the floats were concentrated by being transported due to longshore currents, and were backwashed offshore in the transportation process.

To understand the physical mechanisms determining the residence time of the floats on Wadahama Beach, we discussed the physical mechanism of the backwashing of floats by identifying where the floats were most likely to be backwashed offshore through numerical experiments. Firstly, we divided the total length of the beach (i.e., 900 m long) into nine 100-m wide transects in the alongshore direction, and calculated the residence time in each 100-m wide transect based on the positions of the floats measured in the MR experiments. The residence time in the 100-m wide transect that

corresponded to the area of highest concentration was the closest to the residence time in the whole beach (224 days). The backwash transects were identified by comparing the alongshore concentration for emigration and the residence time in the 100-m wide transects revealed by the MR experiments with those calculated by the numerical experiments using a one-dimensional advection-diffusion equation. Consequently, we found that the physical mechanism of backwashing is as follows: the floats are transported in the alongshore direction due to longshore currents, and are backwashed offshore due to the return flow generated in the lee of the LCSs corresponding to the area of high concentration of remnant floats.

The exponential decay of the remnant floats corresponded to a unit impulse response in a time-invariant linear system, which enables us to understand the system characteristics. Thus, we investigated the dependence of the effects of beach cleanups on the residence time based on a linear system analysis. We focused on three beach cleanup effects (BCEs): improvement of the landscape of a beach, decrease of the total mass of toxic metals, and prevention of the generation of plastic fragments. The BCEs depended strongly on a dimensionless residence time obtained by dividing the residence time by the period of litter input flux (litter input period), and the BCEs increased as the dimensionless residence time became longer. Furthermore, the BCEs depended on the time when the beach cleanups were conducted: beach cleanups were more effective when the remnants of floats reached the peak (cleaning time). Therefore it is crucial to understand the three factors for effective cleanups: the residence time, the predominant litter input period and the effective cleaning time.

To understand the predominant litter input period and the effective cleaning time (i.e. when the remnants become peaks), we attempted to develop a new technique on Sodenohama Beach in Tobishima Island, Japan for sequential monitoring of remnants of plastic litter on sites where plastic litter with various colors has been stranded. The new technique involves three steps: (1) Color references (ellipsoid bodies in CIELUV color space) to detect plastic pixels from images are generated by converting RGB values obtained from the original photographs into CIELUV values. (2) The plastic pixels are detected using the color reference and a composite image method. (3) The area covered by plastic litter (covered area) is calculated by applying a projective transformation to webcam images. We successfully monitored the temporal variability of the covered areas on Sodenohama Beach for 14 months. The advantage of this technique is that it can detect plastic pixels with various colors except black and transparent pixels. The new technique enables us to sequentially monitor the temporal variability of remnants of plastic litter on various beaches.

CONTENTS

CHAPTER 1

Introduction

1.1 Plastic pollution

Plastics have been widely used in everyday life for the last half-century because they are lightweight, strong, durable, inexpensive, and have suitable characteristics for the manufacture of a wide range of products (Derraik, 2002). However, if these handy plastic products end up in the ocean due to improper disposal on land or illegal dumping from ships, they become marine litter (or debris). Most marine debris enters the ocean from land-based sources such as runoff from rivers, wastewater systems, wind-blown litter and recreational litter left on beaches (Ryan et al., 2009). The International Convention for the Prevention of Pollution from Ships (MARPOL) was adopted by the International Marine Organization in November 1973 in an attempt to reduce pollution from oil, chemicals, harmful substances in packaged form, sewage, and garbage. MARPOL Annex V, which was enforced on December 31, 1988, prohibits dumping of litter from ships. However, marine debris continues to be found on beaches and oceans (e.g., Ryan et al., 2009; Barnes et al., 2009; Law et al., 2010).

Plastic litter has numerous adverse impacts on marine and/or coastal environments. The primary impacts are entanglement and ingestion of plastic litter (Derraik, 2002). For instance, plastics have been found in the stomachs of marine animals around the world (e.g., Moser and Lee, 1992; Shaw and Day, 1994; Gregory, 2009; Boerger et al., 2010; van Franeker et al., 2011). The ingestion of plastics can cause weight loss in marine animals (Derraik, 2002). For instance, Ryan (1988) found that seabirds with large plastic loads consume less food, which limits their ability to lay down fat deposits, and Spear et al. (1995) found a negative relationship between the number of plastic particles ingested and the body weight of seabirds from the tropical Pacific. Entanglement in plastic litter, especially in discarded fishing gear, also poses a risk to marine animals. Sea turtles, mammals, seabirds and fish are frequently drawn to or accidentally entangled in netting, rope and monofilament lines that have been discarded or lost during commercial fishing activities (Gregory, 2009).

In the last decade, plastic litter has become widely recognized as a contaminant in the marine environment (e.g., Mato et al., 2001; Derraik, 2002; Thompson et al., 2004; Ogata et al., 2009; Teuten et al., 2009; Nakashima et al., 2012). It is well-known that hydrophobic persistent organic pollutants (POPs) such as polychlorinated biphenyls

(PCBs) are distributed globally via atmospheric and ocean currents (Mato et al., 2001). Plastic particles absorb these pollutants in ambient seawater due to the hydrophobic nature of the plastic surfaces (Mato et al., 2001). Takada (2006) started global monitoring of POPs by collecting polyethylene pellets from beaches around the world, and has identified areas with high concentrations of these pollutants (Ogata et al., 2009). During the production of plastics several metals are used as additives to function as catalysts, pigments, and plastic stabilizers. Nakashima et al. (2012) showed that lead stearate ($Pb(C_{18}H_{35}O_2)_2$), which is a toxic metal, could leach into a beach environment. Thus, plastic litter plays a role as a transport vector for marine pollutants (Mato et al., 2001; Nakashima et al., 2012).

Plastics released into the ocean are carried long distances and for long periods by the ocean currents, and during the transportation process, they slowly break down through a combination of photodegradation, oxidation and mechanical abrasion (Gregory and Andrady, 2003). Consequently, plastics are gradually changed into meso- (2−20 mm), micro- (0.06−2 mm), and nanoplastics (< 0.06 mm). Note that these size ranges of plastics have been differently defined by various researchers (Andrady, 2011). In this study, they are defined based on Gregory and Andrady (2003) and Ryan et al. (2009). Plastic fragments such as micro- and nanoplastics have already been found around the world (Barnes et al., 2009), and this fragmentation makes the plastics difficult to remove from the marine environment, and enables their easy entry into ecosystems.

Many researchers have been investigating the behavior of plastic litter in oceans (e.g., Kubota, 1994; Kako et al., 2011a; Maximenko et al., 2012). Kubota (1994), for instance, demonstrated that floating marine debris has been accumulating to the north of the Hawaiian Islands in the North Pacific via surface currents including the Stokes drift, Ekman drift, and geostrophic currents. The accumulation of floating materials in this area has also been confirmed by the trajectories of satellite-tracked Lagrangian drifters (Maximenko et al., 2012), and many plastic fragments have accumulated on several beaches in the Hawaiian Islands (Cooper and Corcoran, 2010). These studies demonstrate that plastics are broken down into smaller pieces during transportation by ocean currents.

1.2 Residence time of plastics on beaches

Plastics litter does not remain on a beach after washing ashore. Bowman et al. (1998) investigated the budget of marine litter (including natural debris) on six Israeli beaches facing the Mediterranean Sea. Their results indicate that marine litter is backwashed offshore by wind waves because the amount of backwash is significantly high

during the stormiest season. Therefore, the litter is returned offshore by the hydrodynamics in a nearshore area. Garrity and Levings (1993) identified the temporal decay of fifty representative items in a 1 × 50 m transect at four sites along the Caribbean Coast of Panama. They speculated that an average residence time on beaches is less than 1 year based on the transect survey. However, at present, the residence time of plastic litter on beaches is not investigated.

Understanding the residence time would be crucial to investigate the transportation process of plastic litter in open oceans, mitigate the generation of microplastic and collect greater amounts of plastic litter from beaches with less effort. Plastic litter is repeatedly washed ashore and backwashed offshore in the transportation process in the ocean. However, most research that has investigated the transportation or the accumulation of marine litter in oceans rarely considers the physical process in nearshore regions (e.g., Potemra, 2012, Maximenko et al., 2012). Also, during its residence time on the beach surface, plastic litter is rapidly degraded by solar UV radiation and/or the surface temperature on the beach (Andrady, 2011). Therefore, the transportation of plastic litter in the ocean and the generation of plastic fragments are greatly affected by the residence time of plastic litter on the beaches.

On the other hand, plastic litter in the marine environment has mainly been collected from the beaches. The Ministry of Land, Infrastructure and Transport (MLIT) has been collecting marine litter (including natural debris) using cleanup vessels on the sea surface of enclosed inner bays in Japan (Kataoka et al., 2013). Although this way of collecting marine litter takes less effort than beach cleanup, it is costly, and also difficult to do in open oceans. As a result, the removal of plastic litter from the marine environment relies on beach cleanup. The amount of beach litter may fluctuate on a monthly or shorter time scale as shown by Kako et al. (2010). To collect more plastic litter from beaches, it is important to understand the temporal variability of the amount of litter on the beach because the remnants of beach litter are determined by the balance between the amounts of plastic litter washed ashore and backwashed offshore. Therefore, it is essential to understand the residence time in order to effectively conduct beach cleanup.

1.3 Purpose of this study

The purpose of this study is to understand the residence time of plastic litter on beaches, and to suggest ways of applying the residence time to beach cleanups. The flow of this study is shown in Fig. 1-1. Basically, the residence time would be not a constant, and be determined by various factors (e.g., beach morphology, wind, wind waves and litter type). Thus, for the first purpose, we not only measure the residence

time, but also investigate the physical mechanism determining the residence time (i.e., backwash process). For the second purpose, we suggest quantification of cleanup effects on the beach environment using the residence time, and an effective beach cleanup strategy. The aim of each chapter is described below.

In Chapter 2, the residence time of plastic litter on the beach is measured by determining the remnant function based on fundamental concepts for seawater exchange in a coastal sea as proposed by Takeoka (1984). The amount of plastic litter that washes ashore at once decreases due to backwashing. The remnant function is represented by the decrease in the remnants of plastic litter. In addition, to understand the physical mechanism of the backwash process, we investigate the movement of plastic litter until it is backwashed offshore.

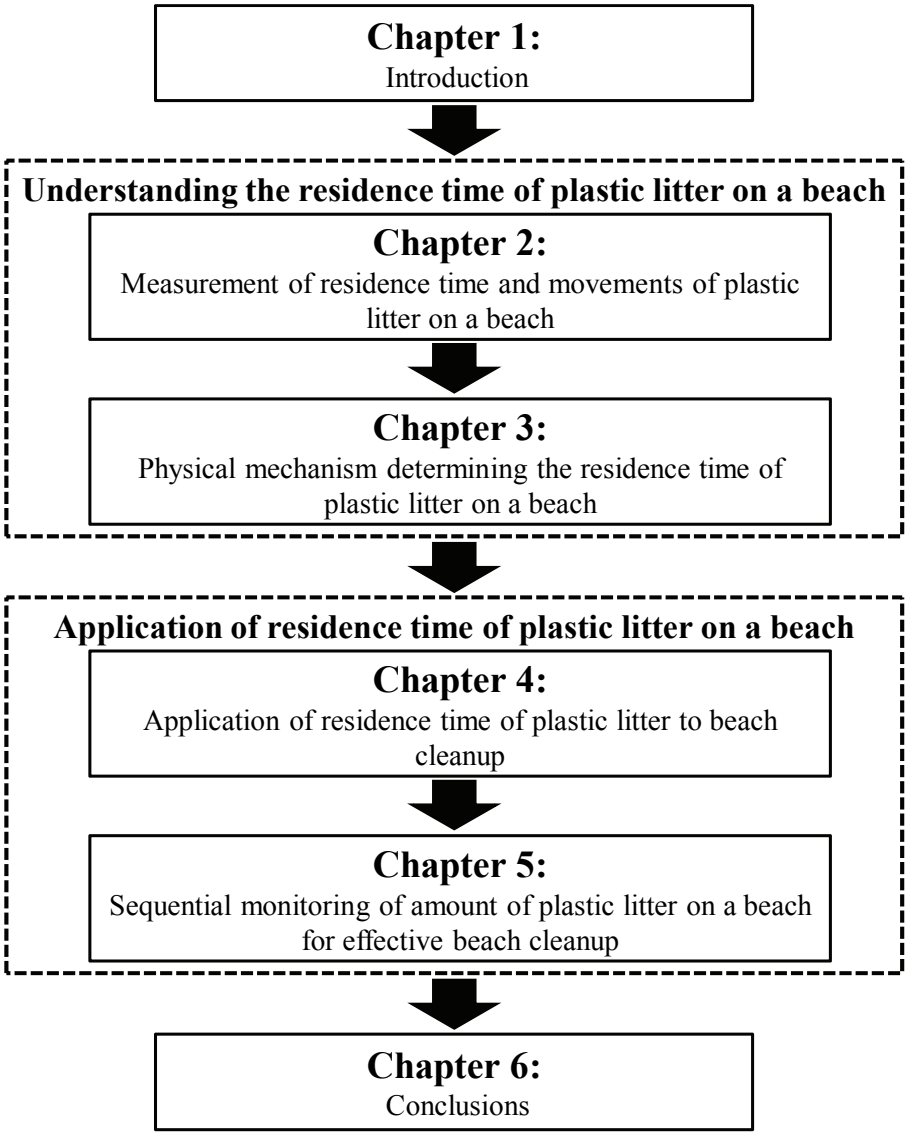

Figure 1-1. Flow of this study.

In Chapter 3, we investigate the physical mechanism determining the residence time based on the movement of plastic litter. In general, to determine the remnant function, it is necessary to measure the decrease in remnants based on regular surveys in situ. However, this is difficult for multiple beaches due to the high cost and/or extensive labor. By understanding the physical mechanism of the backwash process in a nearshore area in the future, the residence time could be estimated, for example, by using wave statistics.

In Chapter 4, we focus on three effects of beach cleanups: to improve the landscape of the beach, to reduce the chance of plastic fragmentation, and to prevent beach pollution from toxic chemicals contained in the plastics (e.g. Nakashima et al., 2012). Based on the remnant function determined in Chapter 2, we attempt to quantify these cleanup effects, and suggest effective cleanup strategies.

In Chapter 5, a new technique for sequential monitoring of the amount of plastic litter on a beach is developed to facilitate effective cleanup. Usually, the temporal variability of the amount of plastic litter is monitored by monthly or yearly surveys in situ (e.g., Ribic, 1998; Ryan et al., 2009; Ribic et al., 2010). However, the long-term interval of the surveys makes it difficult to apply the observed temporal variability to beach cleanups, and to simultaneously monitor multiple beaches. Thus, we attempt to establish remote monitoring of the amount of plastic litter.

Finally, Chapter 6 presents the general conclusions of this study.

CHAPTER 2

Measurement of residence time and movement of plastic litter on Wadahama Beach

2.1 Introduction

Understanding the residence time is crucial for assessing the adverse impact of plastic litter on beaches. For example, Andrady (2011) indicates that beaches are the most likely source of plastic fragments because plastics lying on a beach rapidly undergo photo-oxidative degradation through exposure to solar ultraviolet radiation and the surface temperature of the beach. Thus, to prevent the generation of plastic fragments, it is important to measure the residence time and to clarify the factors determining the residence time.

Nevertheless, few studies have focused on the residence time of plastics on beaches (e.g., Garrity and Levings, 1993). A number of surveys on the abundance and categorization of beach litter and its spatial-temporal variability have been conducted at beaches around the world (e.g., Walker et al., 1997; Williams and Tudor, 2001; Kusui and Noda, 2003; Ivar do Sul and Costa, 2007; Ryan et al., 2009; Ribic et al., 2012). These surveys have generally clarified the present environmental conditions of the beaches and, in some cases, their variability trends.

To understand the residence time on a beach, it is necessary to measure the temporal variation of the remnants of plastic litter. Thus, in this study, mark-recapture (MR) experiments are used to obtain such measurements. MR experiments are utilized for estimating population and related parameters such as the survival, recruitment, and population growth rate of animals and fish (e.g., Peterson and Cederholm, 1984; Smith et al., 1999). The MR method has also been applied to beach litter studies (e.g., Garrity and Levings, 1993; Bowman et al., 1998; William and Tudor, 2001). In these experiments, all of the target items were sprayed with the same color in accordance with the experimental date or location of the strandline where the items were found. This method makes it possible to understand the population decay and movement of each cohort, but not the movement of individual items.

Garrity and Levings (1993) found that debris tended to move upshore of strandlines and then enter into upland areas, and that the movement of debris was seasonal with a greater rate of disappearance from transects in the dry season than in the wet season.

They speculated that the average residence time on beaches is less than one year. From comparative analyses of the MR experiment results from six Israeli Mediterranean beaches, Bowman et al. (1998) concluded that beach geomorphology—beach width, ridge-and-runnel morphology, and beach porosity—made the backshore of beaches an efficient trap for litter. William and Tudor (2001) revealed that the residence time of litter on the beach surface depended on its size: items smaller than the substrate size had a shorter residence time mainly because they became buried in the sand.

Our major aims in this chapter are to measure the residence time and to understand the movement of plastic litter on a beach. By understanding the movement, we expect to clarify the physical process whereby plastic litter is backwashed offshore. Clearly, the residence time differs according to the type of plastic litter. For example, the behavior of plastic PET bottles on the beach would differ from that of PET bottle lids because the bottles are strongly affected by the wind. As a first step in measuring the residence time, three types of plastic fishing floats, which are comparatively small and hardly moved by the wind pressure on the beach, are selected as the target litter items of this study.

2.2 Materials and Methods

2.2.1 Study site

Wadahama Beach is located on the west coast of Niijima Island, about 150 km south of Tokyo (Fig. 2-1a). When the Kuroshio Current takes the nearshore nonlarge meander path or the large meander path (e.g., Hinata et al., 2005), it strikes the west coast of the island. Wadahama Beach is 900 m long and 30–50 m wide (Fig. 2-1b), with coarse sand having a mean sediment diameter of d_{50} = 1.43 mm. The beach is not a public bathing site and thus there are generally few visitors even in the summer. There are two isolated mountains in the northern and southern parts of the island (Fig. 2-1a). The mountain behind the beach creates the local characteristics of the wind field on and around the beach by blocking the easterly winds. Typhoons passing by the island during the summer and autumn seasons episodically produce larger and longer sea surface waves. The beach slope ranges from 0.09 to 0.18 (i.e., an angle of about 5° to 10°). An escarpment with an average angle of about 35° connects the beach to the coastal hinterland (Fig. 2-1b). This steep escarpment blocks the migration of beach litter to the hinterland except lower-density litter such as plastic PET bottles, plastic sheets and plastic bags. Four low-crested structures (LCSs) of 250 m, 250 m, 100 m and 150 m in length are located approximately 100 m from the shoreline and 6 m deep (Fig. 2-1b). The crest of the LCSs is 35 m wide and at a depth of 1.5 m below the mean water level (MWL).

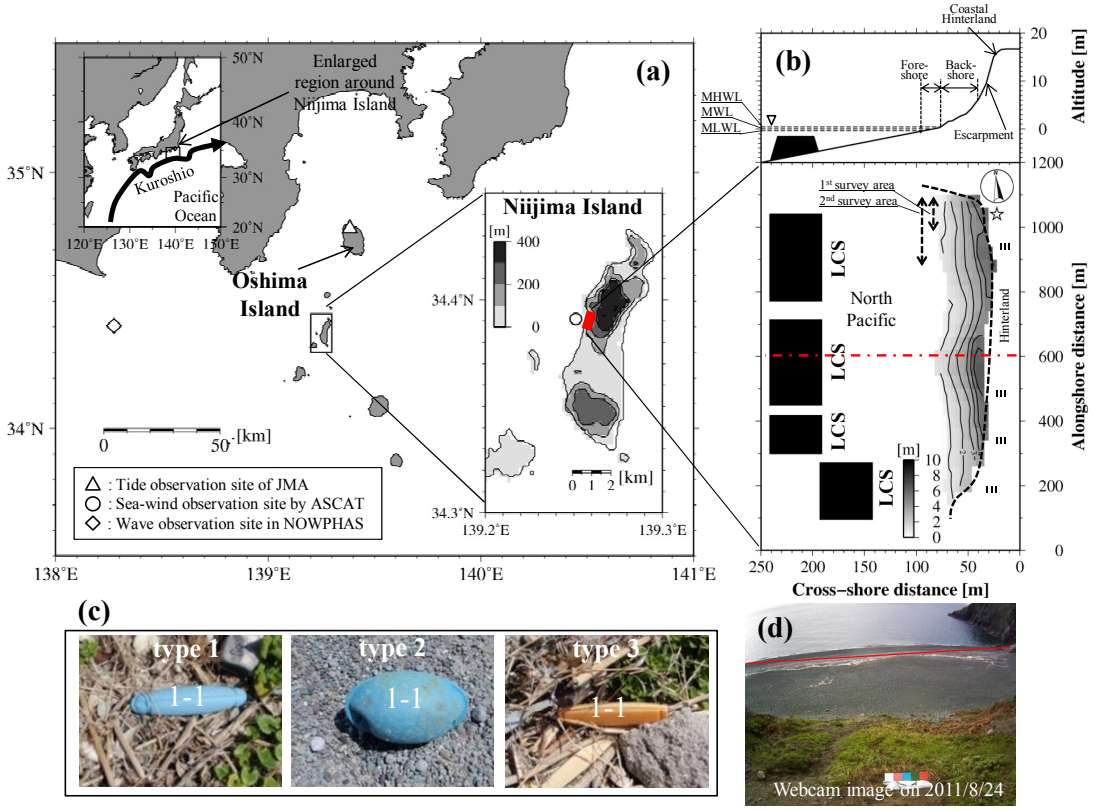

Figure 2-1. (a) Location of Niijima Island, tide observation (triangle), sea-wind observation (circle) and wave observation (diamond). In the enlarged map of Niijima Island in panel (a), contour lines and gray-white gradation denote the altitudes of Niijima Island. (b) Enlarged map of Wadahama Beach showing the altitudes (contour lines and gray-white gradation) and position of the webcam (white star). Note that the scale in the latitudinal direction is 3.2 times as large as that in the longitudinal direction. The upper panel of (b) shows the cross-sectional beach topography along the red dash-dotted line in the lower panel. Black boxes in panel (b) denote low-crested structures (LCSs). (c) Pictures of target items. (d) Sample of webcam images taken on August 24, 2011. Red line denotes the boundary between the foreshore and backshore of the beach.

2.2.2 Target items

The target litter items are three types of plastic fishing floats (Fig. 2-1c). The dimensions and weight of these floats measured in situ are as follows: Type 1: 13.0 cm × ϕ_{max} 2.4 cm, on average 38.8±5.4 g; Type 2: 13.1 cm × ϕ_{max} 7.8 cm, on average 134.0±15.6 g; Type 3: 11.0 cm × ϕ_{max} 1.9 cm, on average 12.8±0.7 g. The floats on the beach showed little movement even during the strong westerly winter monsoon. We found all three types of floats stranded on eight beaches distributed from the northernmost to the southernmost ends of the Japanese Archipelago, where a webcam beach litter monitoring system has been installed. The specification of the webcam system is shown in 5.2.2. Thus, in the future, the movement of floats on Wadahama Beach revealed in this study will be compared with that of other beaches based on the MR experiments, which will improve our understanding of the dynamics of plastic litter on beaches. In addition, Nakashima et al. (2012) found that the Type 1 plastic floats con-

tain a high concentration (13.5±8.4 g/kg) of lead (Pb), which could leach into the beaches via the water surrounding the floats (e.g., rainwater). It is not known if Types 2 and 3 contain a high concentration of Pb. Thus, it is important to establish a method for calculating the residence time of floats on actual beaches in order to estimate the total mass of Pb leaching into the natural environment.

2.2.3 Mark-recapture experiments

To measure the residence time and to understand the movement of plastic litter on the beach, mark-recapture (MR) experiments have been conducted since September 2011 at one- to three-month intervals. The first and second experiments were carried out in the northernmost 100- and 200-m-long areas, respectively (Fig. 2-1b), while the other experiments covered the entire beach. All of the target items on the beach were collected, numbered with a permanent marker and replaced where they were found. The number consists of the experiment number and a sequential number allocated to each type of float (Fig. 2-1c). A thorough search for floats was conducted until no unnumbered target items could be found by repeated observations. The position of each item was recorded by a handheld GPS receiver (GARMIN GPSMAP 60CSx) with a measurement error of about ±3 m. The MR experiments make it possible for us to understand the temporal variation of the number of floats, spatial concentration and movement of each float.

Based on the MR experiments, we calculated the temporal variation of the number of floats that had been newly washed ashore (immigration), had been backwashed offshore (emigration), had been buried (reemergence) and had remained on the beach surface (remnant) during the previous and present MR experiments (hereafter "experiment period"). In addition, to calculate the residence time of the floats, the temporal decay of the number of floats newly washed ashore during each experiment (hereafter "cohort population") was continuously calculated.

The alongshore and cross-shore concentration of floats was determined according to the horizontal position of the floats recorded by the handheld GPS. We divided the beach into 100-m wide (5-m wide) transects in the alongshore (cross-shore) direction. The concentration in each transect was calculated by dividing the number of floats in each transect by that on the entire beach. The vertical distribution of concentration was determined using beach elevation data measured by a real-time kinematic GPS system (see 2.2.4) corresponding to the horizontal position recorded by the handheld GPS. The vertical concentration was calculated by dividing the number of floats per vertical distance of 0.5 m by the number of floats remaining on the whole beach. The spatial concentration was determined according to the three states of the floats: immigration, emi-

gration and remnant. The spatial concentration for the emigration state was determined by the position of the floats in the previous experiment because the position where the floats were backwashed offshore cannot be identified by our MR experiments. The spatial movement of floats was evaluated based on the distance that remnants had moved during the experiment period.

2.2.4 Measurement of beach topography

Starting with the third experiment, the beach elevation was monitored based on point measurements using a real-time kinematic (RTK) GPS system (Trimble 5800 II, Trimble) with a horizontal and vertical measurement error of about ±5 mm. The alongshore and cross-shore distance between adjacent measurement points is about 10 m and about 5 m, respectively.

The raw measured data was interpolated to a grid with both alongshore and cross-shore spacing of 5 m using a nearest-neighbor algorithm and a spline function. First, the elevation at each grid was calculated by the following nearest-neighbor rule:

$$\bar{z} = \sum_{i=1}^{n} z_i w_i \Big/ \sum_{i=1}^{n} w_i , \quad w_i = \left(1 + 9 r_i^2 / R^2\right)^{-1} \tag{2.1}$$

where $\bar{z}$ and z_i denote the interpolated elevation at a grid point and the measured elevation near the grid point, respectively. w_i is a weighting function for distance r_i between the grid and the measurement points in the search radius R. n is the number of measurement points in the search radius. In this study, the search radius R is 7 m. Next, the elevation at all grid points on the beach was interpolated using a cubic spline function (McKinley and Levine, 1998). The cubic spline interpolation was applied to the grid data for both the alongshore and cross-shore direction.

2.2.5 Observation data on waves, winds and tides

Surface wind waves at about 90 km west of Niijima Island with a water depth of 120 m (white diamond in Fig. 2-1a) are monitored by the Nationwide Ocean Wave information network for Ports and Harbours (NOWPHAS) of the Ministry of Land, Infrastructure, Transport and Tourism (MLIT). Since the floats cannot be moved unless the swash waves reach where the floats were washed ashore because of little movement by wind pressure, the runup height was calculated using the hourly significant wave height and period as follows:

$$\frac{R}{H_0} = \xi , \tag{2.2}$$

where R is the runup height from MWL and H_0 is the deep-water significant wave

height (Hunt, 1959). ξ is called the Iribarren number, which is defined as (Battjes, 1974):

$$\xi = \frac{\tan\beta}{(H_0/L_0)^{1/2}}, \tag{2.3}$$

where $\tan\beta$ is the beach slope, L_0 is the deep-water wavelength given by $L_0 = (g/2\pi)T_0^2$ where g is the acceleration due to gravity and T_0 is the significant wave period. In this chapter, the beach slope was determined as $\tan\beta = 0.14$ based on measurements of beach topography. The Iribarren number can be interpreted as dynamic beach steepness, comparing beach slope to the square root of deepwater wave steepness.

In addition, sea wind data observed by the Advanced Scatterometer (ASCAT) and webcam images taken on the northern hinterland (star in Fig. 2-1b) since August 2011 were used to investigate factors determining the residence time. The sea wind data has been gridded using an optimal interpolation method (Kako et al., 2011b). We used the sea wind data at a grid point located in front of Wadahama Beach (white circle in Fig. 2-1a). The specifications of the webcam monitoring system are shown in 5.2.2. Swash events, in which the waves run up through the shoreward line on the foreshore (red line in Fig. 2-1d), were identified by analyzing the webcam images. To compare the movement of floats with the frequency of swash events, the probability of swash events (hereafter "event probability") was calculated by dividing the frequency of swash events in each experiment period by the experiment period. Also, the sea level records measured at Oshima Island (white triangle in Fig. 2-1a), which is situated about 50 km north of Niijima Island, were analyzed to understand the Kuroshio path variability. The mean high water level (MHWL), mean water level (MWL) and mean low water level (MLWL) were calculated from the sea level records obtained during September 2011 to May 2013 at the JMA tide station (triangle in Fig. 2-1a).

2.3 Results

2.3.1 Temporal variation of number of floats

The number of floats obtained in the MR experiments is described in Table 2-1. The total population denotes the summation of immigration and remnant. The time series of immigration, remnant, total population and emigration of all three types is shown in Fig. 2-2. Immigration has a local maximum in October 2011, June 2012 and May 2013, whereas emigration takes a local maximum in November 2012. The resultant total population has a local maximum in November 2011, June 2012 and June 2013.

Generally, the time series of the immigration, remnant and emigration of each float type (Table 2-1) has a local maximum in the corresponding months of the time series of

Table 2-1. Number of floats recovered by the MR experiments and cohort population and abundance of reemergence (within parentheses) in each MR experiment. The abundance of reemergence is added to the cohort population of the previous experiments. The summation in each column of cohort population is consistent with the total population of all types.

Experiment No.	1	2	3	4	5	6	7	8	9	10	11	12	13	14
Experiment date	2011/09/30	2011/10/27	2011/11/24	2011/11/26	2012/01/26	2012/03/23	2012/06/29	2012/08/21	2012/11/08	2012/12/27	2013/02/27	2013/05/08	2013/06/27	2013/08/31
Type 1														
Immigration	10	4	9	1	1	0	14	4	2	2	4	24	8	3
Remnant	0	8	11	20	21	19	14	27	14	16	12	10	34	34
Total population	10	12	20	21	22	19	28	31	16	18	16	34	42	37
Emigration	0	2	1	0	0	3	5	1	17	0	5	6	0	8
Reemergence	0	0	0	0	1	0	4	0	3	3	1	3	1	1
Type 2														
Immigration	18	30	31	3	8	4	29	7	16	3	8	65	19	11
Remnant	0	14	42	72	59	49	40	56	29	42	36	31	92	108
Total population	18	44	73	75	67	53	69	63	45	45	44	96	111	119
Emigration	0	4	2	1	16	18	13	13	34	3	8	13	4	3
Reemergence	0	0	0	1	2	5	9	0	4	4	1	13	1	5
Type 3														
Immigration	19	43	21	16	9	14	93	15	39	15	16	102	37	7
Remnant	0	14	52	71	59	44	31	105	54	83	89	82	168	163
Total population	19	57	73	87	68	58	124	120	93	98	105	184	205	170
Emigration	0	5	5	2	28	24	27	19	66	10	9	23	16	42
Reemergence	0	0	1	3	4	7	9	1	6	5	3	44	4	8
All types														
Immigration	47	77	61	20	18	18	136	26	57	20	28	191	64	21
Remnant	0	36	105	163	139	112	85	188	97	141	137	123	294	305
Total population	47	113	166	183	157	130	221	214	154	161	165	314	358	326
Emigration	0	11	8	3	44	45	45	33	117	13	22	42	20	53
Reemergence	0	0	1	4	7	12	22	1	13	12	5	60	6	14
Cohort Population														
No.1	47 (0)	36 (0)*	34 (1)	34 (2)	28 (2)	17 (0)	12 (3)	10 (0)	6 (3)	6 (0)	6 (1)	6 (3)	5 (0)	5 (0)
No.2	-	77 (0)	71 (0)	71 (2)	52 (5)	38 (2)	27 (8)	23 (1)	12 (4)	10 (2)	8 (0)	7 (2)	7 (0)	4 (1)
No.3	-	-	61 (0)	58 (0)	44 (0)	34 (6)	25 (7)	21 (0)	13 (2)	11 (2)	10 (0)	7 (4)	7 (0)	6 (2)
No.4	-	-	-	20 (0)	15 (0)	12 (4)	6 (1)	5 (0)	4 (1)	4 (3)	4 (0)	1 (0)	1 (1)	1 (0)
No.5	-	-	-	-	18 (0)	11 (0)	8 (3)	7 (0)	4 (0)	4 (2)	2 (0)	2 (1)	2 (0)	2 (0)
No.6	-	-	-	-	-	18 (0)	7 (0)	6 (0)	2 (0)	2 (1)	2 (0)	1 (0)	1 (1)	1 (0)
No.7	-	-	-	-	-	-	136 (0)	116 (0)	48 (3)	46 (2)	38 (1)	35 (22)	34 (1)	27 (2)
No.8	-	-	-	-	-	-	-	26 (0)	8 (0)	8 (0)	7 (0)	6 (3)	5 (1)	4 (0)
No.9	-	-	-	-	-	-	-	-	57 (0)	50 (0)	44 (3)	31 (18)	29 (2)	29 (0)
No.10	-	-	-	-	-	-	-	-	-	20 (0)	16 (0)	14 (7)	11 (0)	11 (1)
No.11	-	-	-	-	-	-	-	-	-	-	28 (0)	13 (0)	13 (0)	12 (1)
No.12	-	-	-	-	-	-	-	-	-	-	-	191 (0)	179 (0)	158 (7)
No.13	-	-	-	-	-	-	-	-	-	-	-	-	64 (0)	45 (0)
No.14	-	-	-	-	-	-	-	-	-	-	-	-	-	21 (0)

* Population of cohort No. 1 in the second experiment is not used in Figs. 2-3 and 2-4 because the second experiment was carried out in the northernmost 200 m-long area.

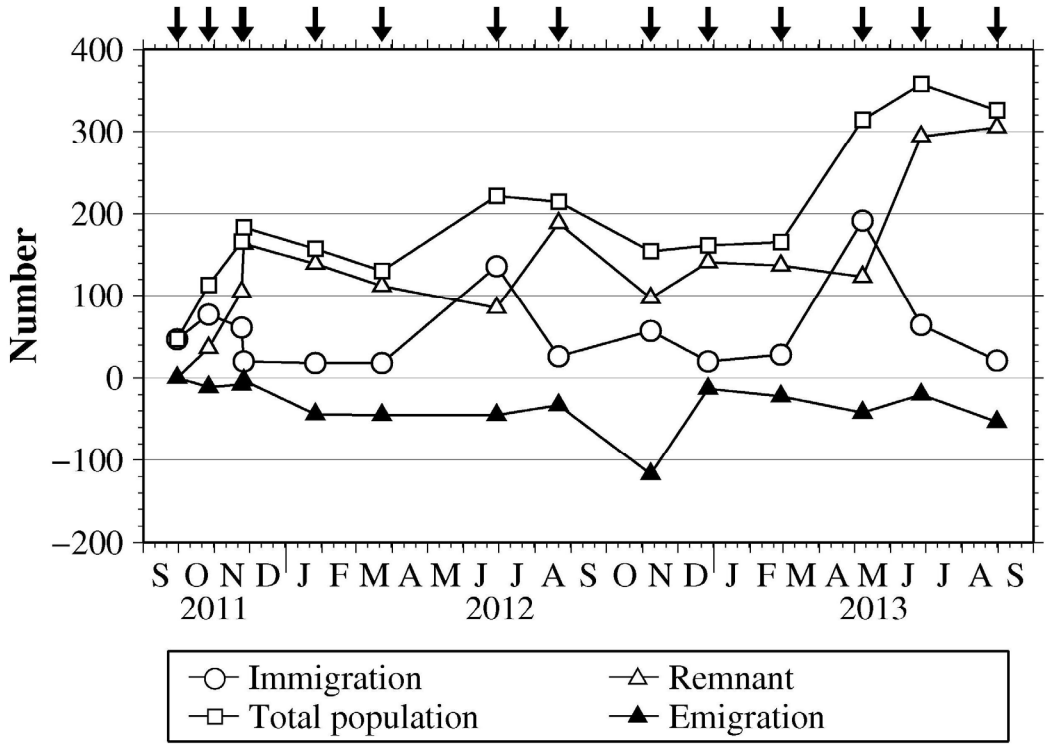

Figure 2-2. Time series of the total number of immigration, remnant, total population and emigration revealed by the MR experiments. The meanings of symbols are shown in the lower box. Black arrows show the date of each experiment.

the totals shown in Fig. 2-2. The similar temporal variation pattern of immigration suggests that all types have similar spatial distribution and drifting characteristics in the offshore region, while the similar emigration time series would be the result of similar movement of all three types on the beach. Thus, we investigated the temporal variation of population of each cohort regardless of the float type.

2.3.2 Residence time of floats on Wadahama Beach

The population decay of each cohort is tabulated in Table 2-1. The remnants include the number of reemerged floats that were not recovered in the previous experiments but were found in the present experiment. The ratio of reemerged floats to the remnants is very small (6% on average). Natural or anthropogenic large debris, such as logs and lumber, was not common on the beach: it did not form any strandline, but rather was stranded separately and sparsely. In the experiments, we searched for target items behind and beneath such debris. Presumably, reemerged floats had been buried in the sand. William and Tudor (2001) found that litter items larger than the surrounding substrate accumulated more readily on the beach surface, since these items would be uncovered by strong wind waves. Thus, we assume that the emigration of floats is driv-

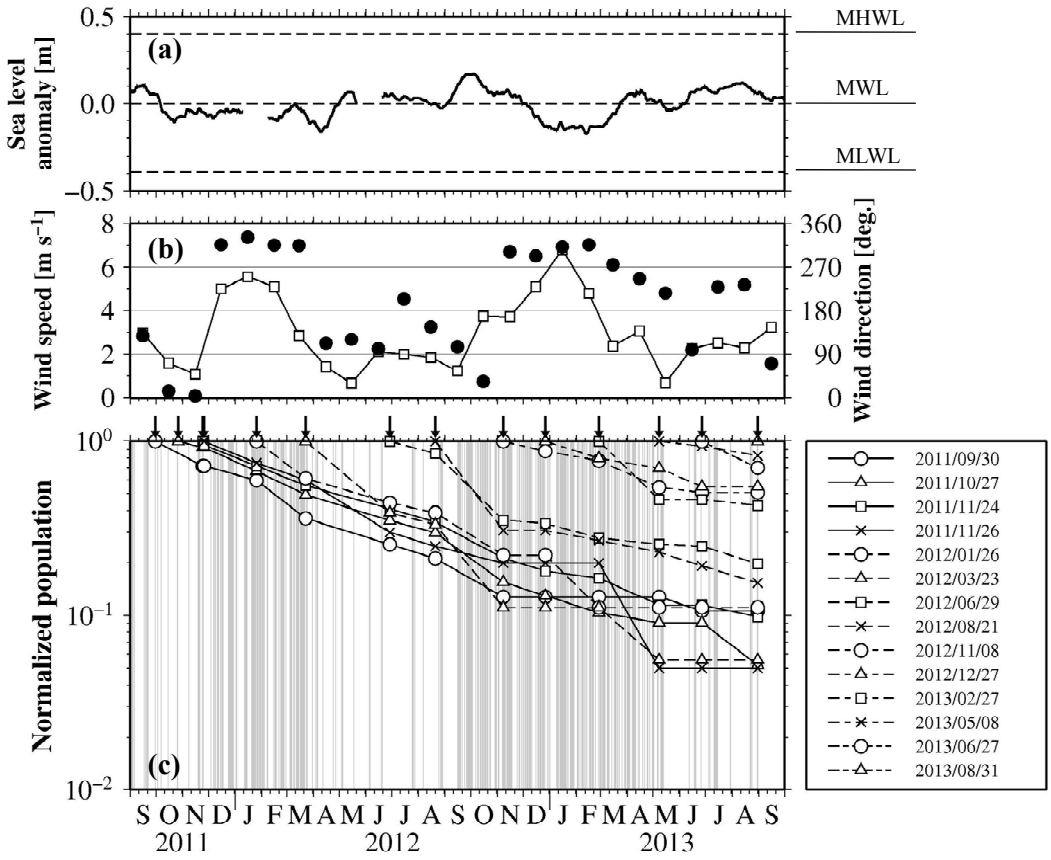

Figure 2-3. Time series of (a) 30-day moving average of adjusted sea level anomaly at the JMA tide station (see white triangle in Fig. 3-1(a)), (b) monthly average wind speed (solid line with white square) and direction in degrees clockwise from the north (black circle) observed by ASCAT (white circle in Fig. 3-1(a)) and (c) the population decay of each cohort. Black arrows in (c) show the date of each experiment. Light gray line denotes swash events.

en by backwashing to the sea.

Figure 2-3c shows the population decay of all cohorts normalized by the initial values. Interestingly, the populations decrease exponentially. The plot of the normalized population produced from all the experiment data setting the experiment dates equal to 0 (Fig. 2-4) provides a much clearer exponential decay. We approximated the plots as an exponential function $h(t)$ (=exp[$-kt$]) with a 95% confidence level (n = 104, R^2 = 0.852, $P = 6.47\times10^{-47} < 0.05$) as follows:

$$h(t) = \begin{cases} \exp\left(-4.471\times10^{-3}t\right), & (t \geq 0) \\ 0, & (t < 0) \end{cases} \tag{2.4}$$

where t is elapsed time in days. From the integral of this function from t = 0 to infinity, the residence time of the floats on the beach is estimated as $\tau_r = 1/k$ = 224 days, that is, about 7.5 months. The margin of error of the coefficient k was estimated as 0.340×10^{-3}

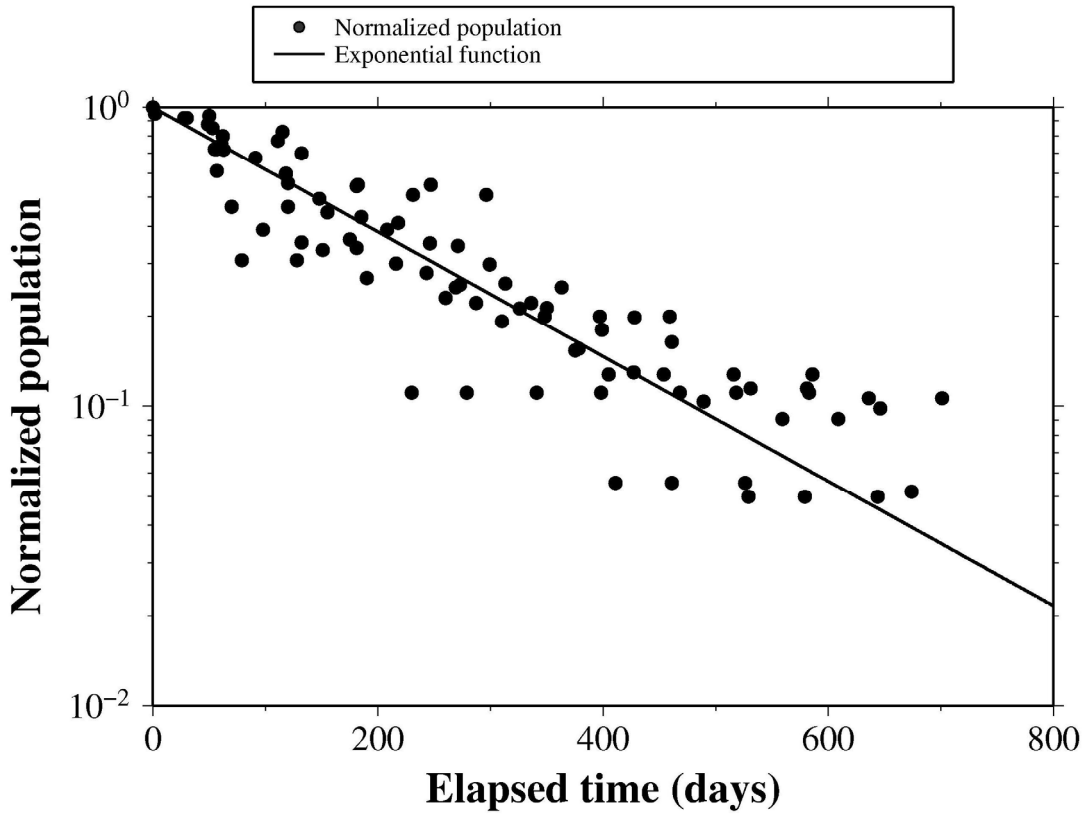

Figure 2-4. Exponential function revealed by all the MR experiments at Wadahama Beach.

by a *t*-distribution with a 95% confidence limit. Therefore, the residence time has a 95% confidence interval from 208 days (i.e., $1/(4.471\times10^{-3} + 0.340\times10^{-3})$) to 242 days (i.e., $1/(4.471\times10^{-3} - 0.340\times10^{-3})$). The exponential decay of cohort population means that the remnant floats can be considered to have decreased at a constant rate determined as $1-e^{-1/\tau_r}$ (i.e., 0.5% per day), if a decrease in floats is seen during a period longer than one year. This corresponds to a unit impulse response in a time-invariant linear system, and enables us to understand the linear response of the beach to the input of floats. The system characteristics are presented in Chapter 4.

2.3.3 Spatial concentration of floats

Figure 2-5 shows the alongshore (Figs. 2-5a–2-5c), cross-shore (Figs. 2-5d–2-5f) and vertical (Figs. 2-5g–2-5i) concentration of the floats at each experiment. The spatial concentration is described for the respective state (i.e., immigration, remnant and emigration). The concentration at September and October 2011 is disregarded because the MR experiment was conducted in the northernmost 100- and 200-m-long areas.

The alongshore concentration for remnant and emigration tends to be high in the northern area from 700 to 1100 m of the alongshore distance corresponding to the lee of

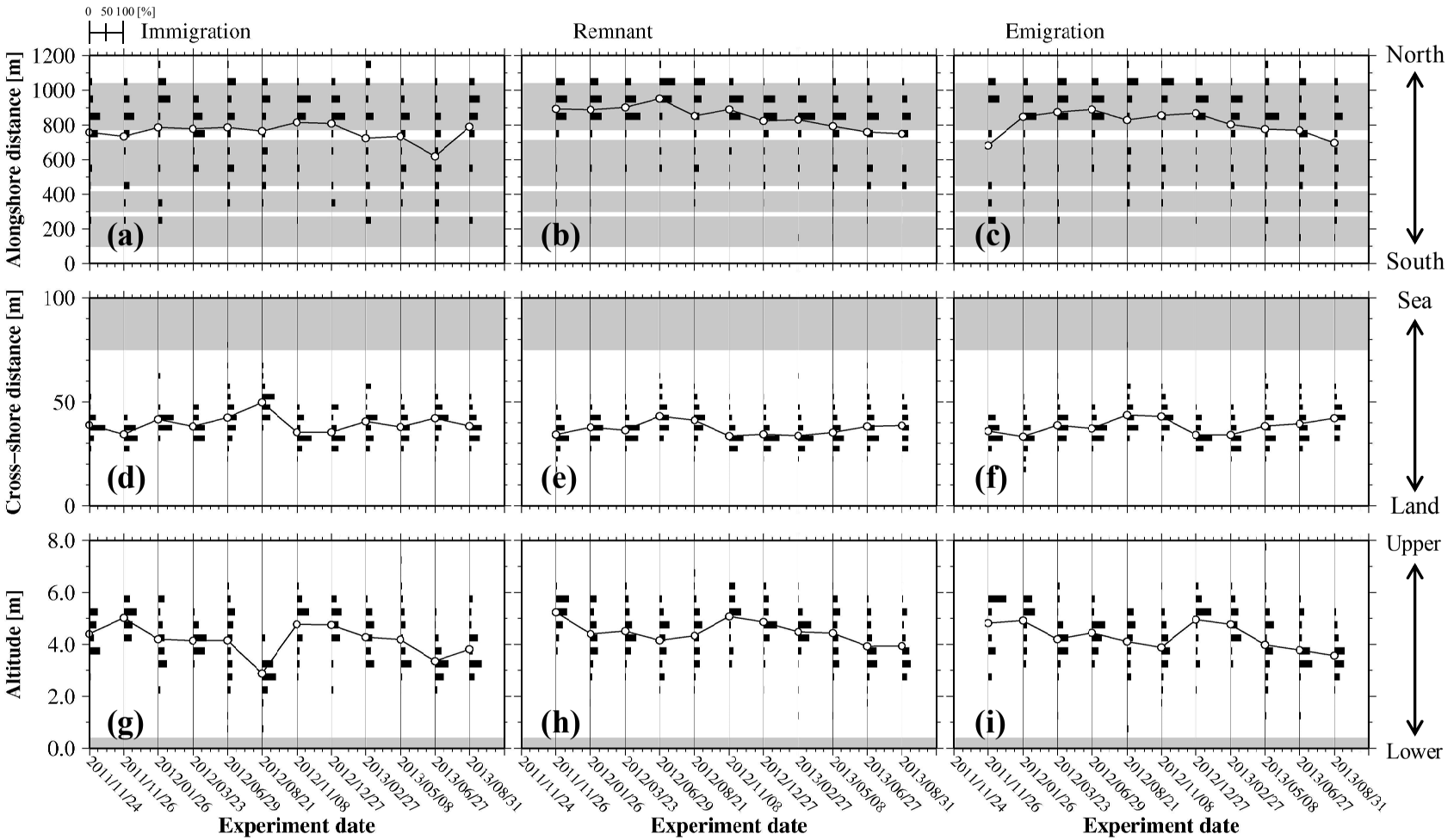

Figure 2-5. Alongshore concentration (immigration (a), remnant (b) and emigration (c)), cross-shore concentration (immigration (d), remnant (e) and emigration (f)) and vertical concentration (immigration (g), remnant (h) and emigration (i)). Length of black bar denotes the concentration at each distance (see upper left). Gray areas in panels (a)-(c) denote alongshore distance where the LCSs are located. Gray areas in panels (d)-(f) and (g)-(i) denote the cross-shore distance and altitude where the sea level has been lower than the MHWL, respectively. Circle in all panels denotes the average position of floats.

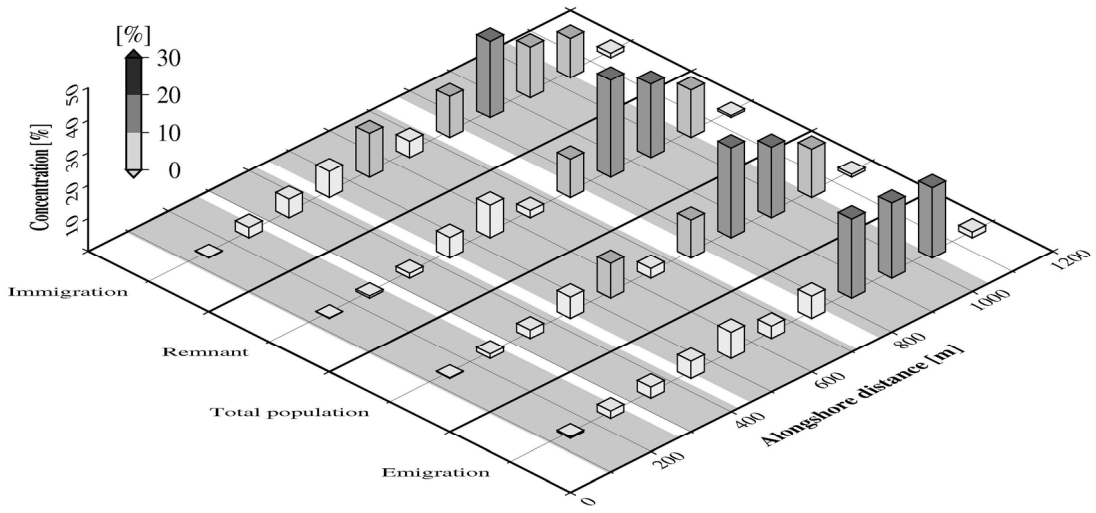

Figure 2-6. Average alongshore concentration for immigration, remnant, total population and emigration in each alongshore transect through all experiments. Light gray area means the alongshore position of the LCSs. The concentration color scale is shown in the upper left of the diagram.

the northernmost LCS (Figs. 2-5b and 2-5c). On the other hand, the alongshore concentration for immigration (Figs. 2-5a) is distributed more uniformly than that for remnant and emigration (Figs. 2-5b and 2-5c). Basically, the alongshore concentration for remnant and emigration would be more strongly affected by hydrodynamics in the nearshore region (e.g., swash waves) than that for immigration because of a longer stay at the beach. This implies that the floats are concentrated in the northern area by the hydrodynamics. The relationship between the alongshore concentration and movement is discussed in 2.4.4.

The cross-shore concentration for all states was high in the range from 20 to 50 m of the cross-shore distance (Figs. 2-5d–2-5f). Thus, the width for the cross-shore direction in which floats washed ashore was approximately 30 m. The cross-shore concentration for remnant in the summer was transferred seaward because many floats had washed up near the shoreline on June 29, 2012 and May 8, 2013 (Fig. 2-5d and circle in Fig. 2-2). Naturally, the variation pattern of the vertical concentration (Figs. 2-5g–2-5i) corresponds well with that of the cross-shore concentration (Figs. 2-5d–2-5f), and the vertical concentration for immigration also fluctuated according to the season (Fig. 2-5g): the beach elevation was high (low) from November 2011 to January 2012 and from November 2012 to February 2013 (from January 2012 to November 2013 and from February 2013 to August 2013).

Figure 2-6 shows the average alongshore concentration for immigration, remnant, total population (i.e., summation of immigration and remnant) and emigration in the MR experiments except the first and second experiments. The average alongshore con-

centration was calculated by dividing the total number of floats in 100-m-wide alongshore transects by the total number on the whole beach in all experiments. The average alongshore concentration for all states was relatively high from 400 to 600 m and from 700 to 1100 m of the alongshore distance. Overall, the floats tend to be highly concentrated on the lee of the LCSs (gray area in Fig. 2-6), and the concentration behind the gap of the LCSs is lower. The average alongshore concentration of the total population was significantly correlated with that of emigration (n = 11, R = 0.95, $P = 2.61\times10^{-7} <$ 0.05). This suggests that the floats were randomly backwashed offshore, being proportional to the concentration for the total population.

2.3.4 Spatial movement of floats

Figure 2-7 shows the movement distance of the floats remaining on the beach in the alongshore (a), cross-shore (b) and vertical (c) direction in each experiment period. The average movement distance denotes the direction in which the floats moved overall (white circle in Fig. 2-7). The standard deviation of the movement distance denotes the estimator for movement of floats in each experiment period (error bar in Fig. 2-7). The average and standard deviation are shown in Table 2-2. The spatial movement from September 30 and October 27, 2011 is also disregarded.

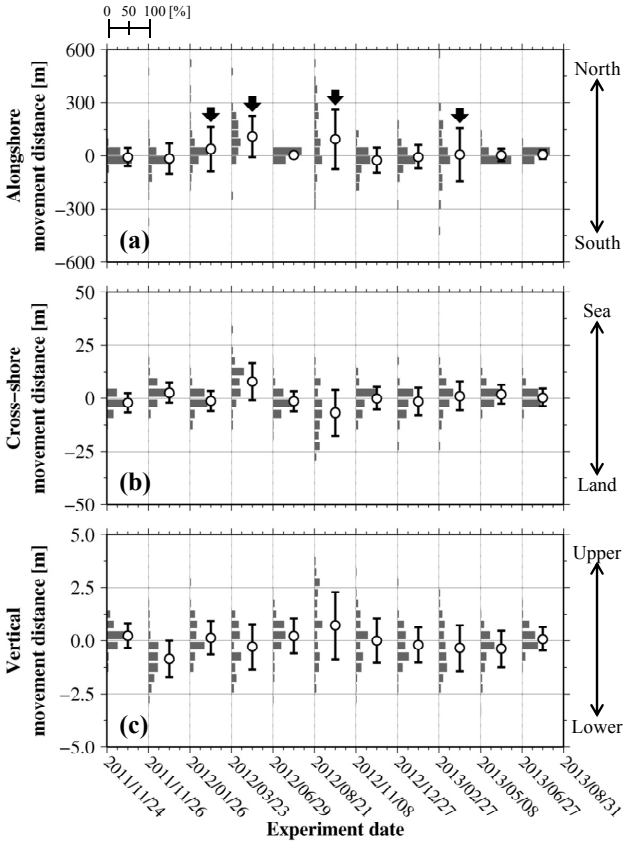

Figure 2-7. Distance that floats were moved in the alongshore (a), cross-shore (b) and vertical (c) direction in each experiment period. Gray bar, white circle and error bar denote frequency, and average and standard deviation of movement distance, respectively. Length of gray bar denotes frequency of movement distance in each experiment period (see upper left). For example, the frequency from November 26, 2011 to January 26, 2012 is shown between the grid lines at these dates. Black arrow denotes when the floats were moved in an alongshore distance longer than 100 m.

The alongshore movement distance indicates wide float movement in both the north and south direction (Fig. 2-7a). The standard deviation of the alongshore movement distance in four

Table 2-2. Spatial movement of floats, decreasing rate and event probability in each experiment period.

Experiment number	1	2	3	4	5	6	7	8	9	10	11	12	13	14
Experiment date	2011/9/30	2011/10/27	2011/11/24	2011/11/26	2012/1/26	2012/3/23	2012/6/29	2012/8/21	2012/11/8	2012/12/27	2013/2/27	2013/5/8	2013/6/27	2013/8/31
Experiment period [days]	27	28	2	61	57	98	53	79	49	62	70	50	65	
Spatial movement of the floats during experiment period														
Alongshore movement distance [m]														
Average	4.61	3.25	-8.91	-16.97	37.79	107.87	4.16	92.02	-25.98	-7.48	6.86	2.76	5.98	
Standard deviation	4.44	33.72	52.31	85.11	126.29	116.43	14.95	169.21	70.13	65.77	151.23	35.81	25.21	
Movement velocity [m day^{-1}]	0.16	1.20	26.16	1.40	2.22	1.19	0.28	2.14	1.43	1.06	2.16	0.72	0.39	
Cross-shore movement distance [m]														
Average	0.18	-0.64	2.23	-2.55	1.40	-7.65	1.53	6.96	0.19	1.62	-0.98	-1.72	-0.25	
Standard deviation	6.06	3.79	4.61	4.76	4.80	8.69	4.76	10.76	5.29	6.44	6.87	4.43	4.16	
Vertical movement distance [m]														
Average	-0.04	0.03	0.22	-0.86	0.13	-0.29	0.21	0.71	0.00	-0.21	-0.35	-0.39	0.07	
Standard deviation	0.77	0.51	0.58	0.85	0.79	1.05	0.82	1.58	1.04	0.82	1.06	0.85	0.55	
Decrease of remnants during experiment period														
Survival ratio	0.77	0.93	0.98	0.76	0.71	0.65	0.85	0.45	0.92	0.85	0.75	0.94	0.85	
Decreasing rate [%]	0.98	0.26	0.91	0.45	0.59	0.43	0.30	1.00	0.18	0.26	0.42	0.13	0.25	
Swash event during experiment period														
Frequency [days]	5	5	2	31	38	16	4	40	34	37	41	9	13	
Event probability [%]	19	18	100	51	67	16	8	51	69	60	59	18	20	

experiment periods (i.e., from January 26 to March 23, 2012; from March 23 to June 29, 2012; from August 21 to November 8, 2012 and from February 27 to May 8, 2012) was larger than that in the other experiment periods (black arrows in Fig. 2-7a), which was from 116 to 169 m (Table 2-2). In addition, the average alongshore movement distance (white circle in Fig. 2-7a) was around zero except during two experiment periods: March 23 to June 29, 2012 and August 21 to November 8, 2012.

The cross-shore movement distance indicates that the floats were not only pushed landward, but were also pulled seaward by swash waves (Fig. 2-7b). In particular, float movement was generally seaward from March 23 to June 29, 2012, and landward from August 21 to November 8, 2012, and the average cross-shore movement distance in these periods was ±6.5 m. On the other hand, the average cross-shore movement distance was around zero in the other experiment periods. The standard deviation of the cross-shore movement distance ranged from 4 to 10 m. The cross-shore movement distance was maximized from August 21 to November 8, 2012.

The vertical movement distance fluctuated in each experiment period according to the movement in the cross-shore direction (Fig. 2-7c). The standard deviation was significant in relation to that of the cross-shore distance at a 95% confidence level ($n = 12$, $R = 0.92$, $P = 1.88\times10^{-5} < 0.05$). In general, the average vertical movement distance was also around zero except in the two experiment periods from November 26, 2011 to January 26, 2012 and from August 21 to November 8, 2012. The floats were washed down from November 26, 2011 to January 26, 2012, whereas they were washed up from August 21 to November 8, 2012. The largest average vertical movement distance was from November 26, 2011 to January 26, 2012.

2.3.5 Temporal variation of beach topography

Figures 2-8 and 2-9 show the beach topography at each experiment date and the temporal variation of the beach topography. From November 2011 to August 2013, the shoreline of Wadahama Beach was consistently prominently seaward in the center area and the northernmost area of the beach ranging from 500 to 700 m and from 900 to 1100 m (Fig. 2-8 and Fig. 2-9a), respectively. However, the temporal variation of the beach topography in the center area differed from that in the northernmost area. Figure 2-9b shows the yearly linear trend of beach elevation calculated from the temporal variability of the altitude. The trend in the northernmost area indicates that sand has been deposited at a rate of 0.0–0.4 m yr^{-1}. In other areas, the beach elevation has been decreasing at a rate of 0.0–1.0 m yr^{-1} (Fig. 2-9b). This suggests that sand has been supplied from the south to the northernmost areas by alongshore sediment transport. In ad-

dition, the temporal variability in the northernmost areas was greater than that in the other areas (Fig. 2-9c).

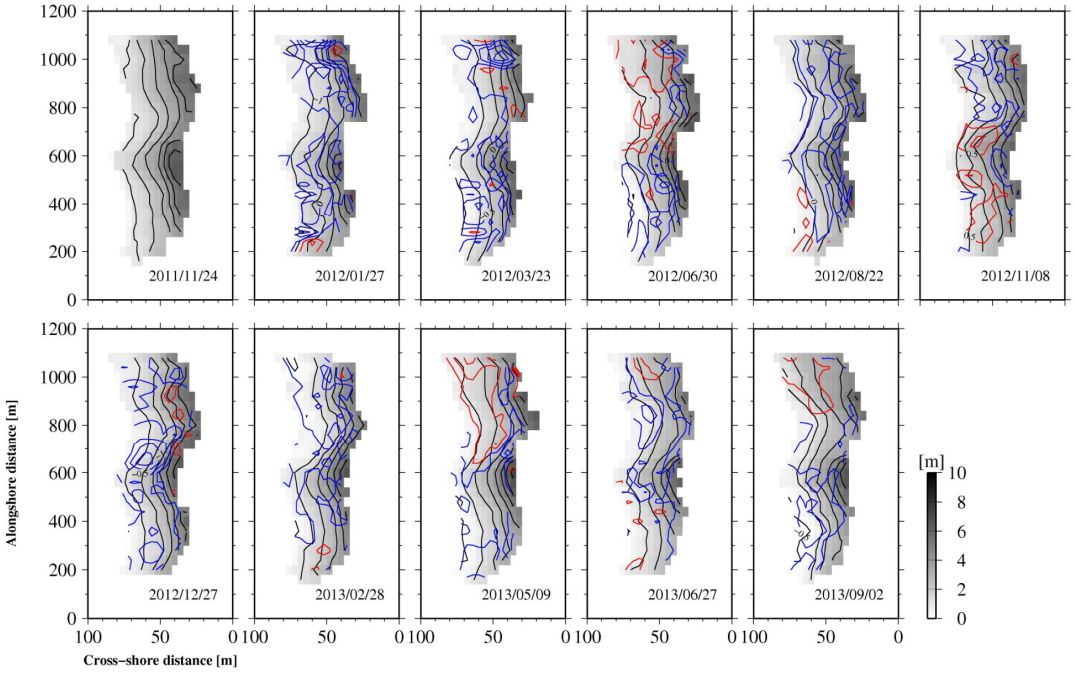

Figure 2-8. Beach topography measured by RTK-GPS (contour lines and white-gray gradation). Red and blue contour lines denote sand deposition and erosion, respectively (contour interval is 0.5 m).

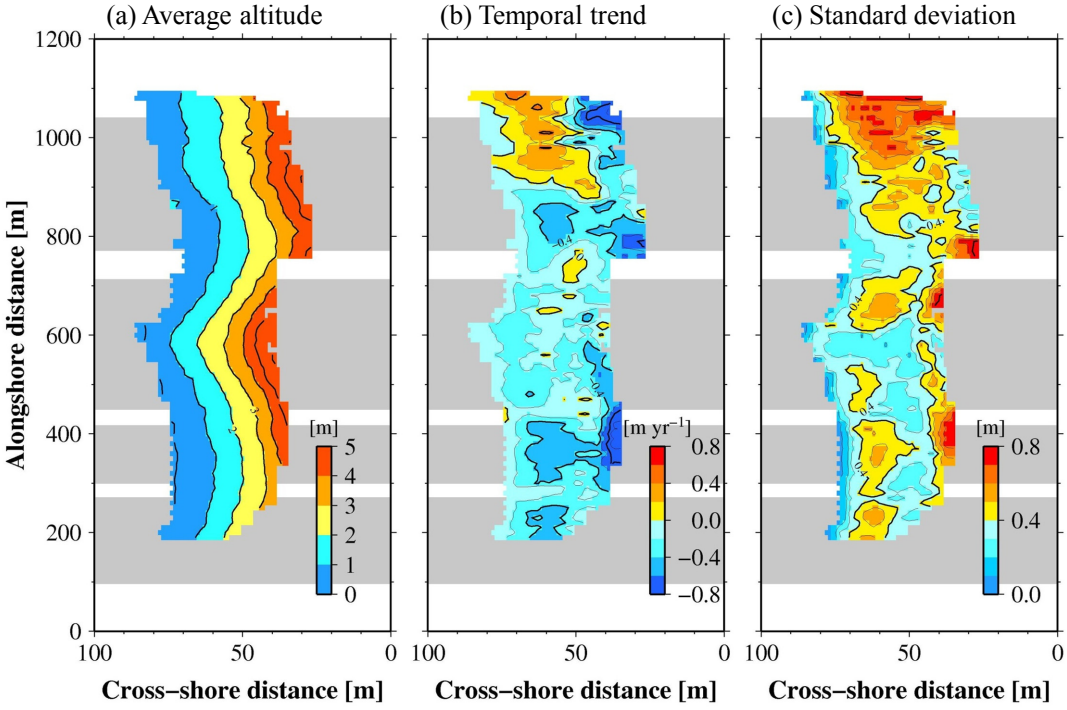

Figure 2-9. Temporal variability of beach topography showing the alongshore position of the LCSs (light gray areas).

2.4 Discussion

The residence time was fully determined by the exponential decay of cohort population revealed by the MR experiments. By understanding the factors determining the exponential decay, we might be able to estimate the residence time on other beaches without MR experiments. As the first step to understanding the factors, the temporal variation of the floats is compared with the observation data on the tides, wind and frequency of swash events. The number of floats decreases exponentially, while the remnants of floats showed large alongshore movement. Thus, the relationship between the decrease in floats and the alongshore movement of their remnants is discussed. In addition, the alongshore concentration for remnant was consistent with that for emigration. The concentration for emigration denotes the frequency of the beached position before backwashing offshore. The high concentration for remnant and emigration might be an important clue to understanding the physical mechanism of the backwash process. Thus, we discuss the backwash process by comparing the alongshore concentration for remnant and the alongshore movement.

2.4.1 Comparison of the population decay with tide, wind and swash events

To assume the factors determining the population decay of the floats, the cohort population is compared with the time series of the 30-day moving averages of the adjusted sea level (Fig. 2-3a), monthly wind velocity and direction (Fig. 2-3b) and swash events (gray line in Fig. 2-3c).

The positive sea level anomaly corresponds well with the Kuroshio path variation: the Kuroshio took the nearshore nonlarge meander path and hit Niijima Island in September 2011, May 2012, from September to November 2012, in April 2013 and from July to August 2013 (JCG, 2013). The sea level changes due to the tide (by about ±40 cm) around Niijima Island. Regarding the wind fields, weaker easterly winds dominated in summer whereas stronger westerly winds prevailed from late autumn to early spring. Corresponding to the winds, the frequency of swash events was low in summer and high from late autumn to early spring (light gray line in Fig. 2-3c).

The population decreases with a lower (higher) rate from June to August 2012, from November 2012 to February 2013 and from May to August 2013 (August to November 2012). There was no significant relationship between the temporal variability of sea level records and that of the decreasing rate. On the other hand, the local maximum of immigration in June 2012 and May 2013 (see Fig. 2-2) was preceded by the nearshore nonlarge meander path, which suggests that the Kuroshio plays an important

role in the transportation of the target items. Surprisingly, a significant relationship was not found between the temporal change in the rate and that in the monthly wind speed. In actuality, the floats on the beach might be intermittently backwashed to the sea by storms that are not represented by the monthly average wind speed. In this study, we will not examine the mechanisms of the intermittent temporal change in the decreasing rate due to the difficulty in clarifying the mechanisms based on MR experiments at one- or three-month intervals.

2.4.2 Relationship of alongshore movement of floats with decreasing rate

To compare the northward-southward movement of floats and the decrease in floats, a movement velocity and a decreasing rate were determined for each experiment period. The movement velocity was calculated by dividing the standard deviation of the alongshore movement distance by each experiment period. The movement velocity in each experiment period is shown in Table 2-2. The movement velocity for November 24–26, 2011 was much larger than that in the other experiment periods because it was two days. Thus, the movement velocity for this period was ignored in the comparison with the decreasing rate. Considering the exponential decay of the cohort population of floats (Figs. 2-3c and 2-4), the decreasing rate γ was calculated as:

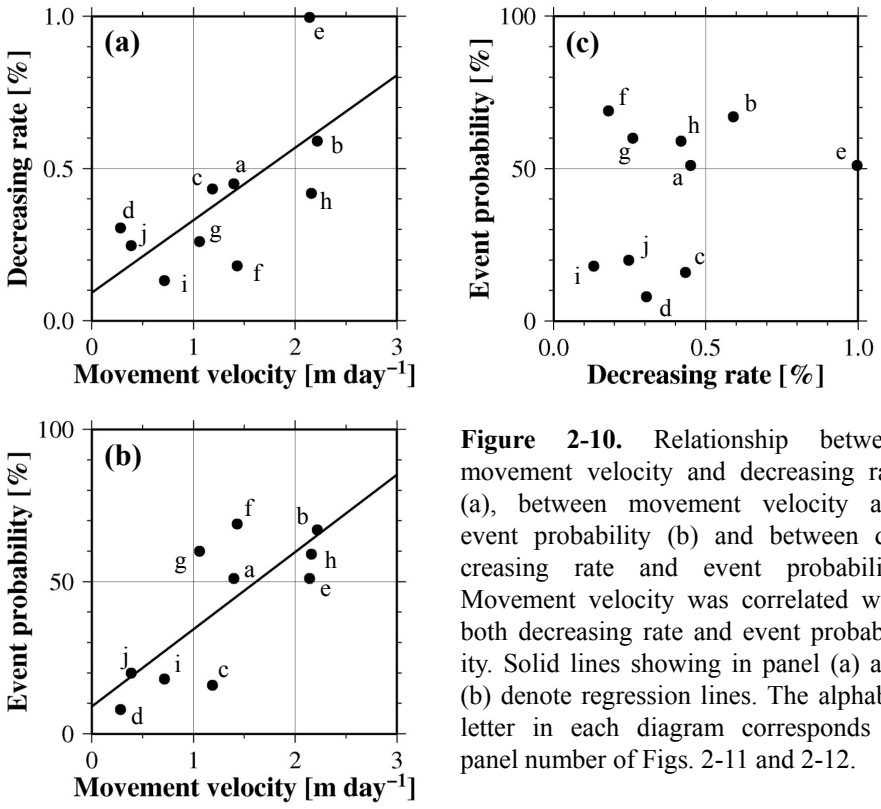

Figure 2-10. Relationship between movement velocity and decreasing rate (a), between movement velocity and event probability (b) and between decreasing rate and event probability. Movement velocity was correlated with both decreasing rate and event probability. Solid lines showing in panel (a) and (b) denote regression lines. The alphabet letter in each diagram corresponds to panel number of Figs. 2-11 and 2-12.

$$\gamma = 100 \times \left[1 - \left(\frac{y(t')}{y(t)} \right)^{\frac{1}{\Delta t}} \right] \tag{2.5}$$

where $y(t)$ shows the total population (i.e., the sum of remnant and immigration) of floats at time *t*, and $y(t')$ shows the remnants at time $t' = t + \Delta t$. Δt is the experiment period. Therefore $y(t')/y(t)$ denotes the survival ratio. The decreasing rate per day is shown in Table 2-2. The decreasing rate varied between 0.0% and 1.0%, and the mean was 0.5%, which is consistent with the decreasing rate determined using the average residence time (τ_r = 224 days) of Wadahama Beach (i.e., $1 - e^{-1/224}$).

Figure 2-10 shows the correlation between the movement velocity and the decreasing rate except for the results from September 30 to November 26, 2011. The movement velocity was significantly correlated with the decreasing rate at the 95% confidence level (n = 10, R = 0.68, P = 0.0319 < 0.05; see solid line in Fig. 2-10a). This demonstrates that the alongshore movement contributed to the exponential decrease in the number of floats.

Basically, the floats are comparatively small and show little movement from the wind pressure on the beach (see 2.2.2). The force moving the floats would be mainly swash waves. Thus the alongshore movement of the floats was compared with the frequency of swash events that run up to the backshore (i.e., event probability) because most of the floats had washed ashore on the backshore (Fig. 2-5). The event probability was also significantly correlated with the movement velocity at the 95% confidence level (n = 10, R = 0.77, P = 0.009 < 0.05; see solid line in Fig. 2-10b). Therefore, the floats would have been moved by the swash from the wind waves, and the alongshore movement of floats depends on the frequency of swash events.

The movement velocity was significantly correlated to both the decreasing rate and the event probability. However, a significant relationship was not found between the event probability and the decreasing rate (R = 0.27, P = 0.443 > 0.05). In this study, the event probability was calculated regardless of the magnitude of swash events. In actuality, the backwash of floats might depend on the magnitude of swash events.

2.4.3 Factors determining alongshore movement of floats

The northward-southward movement of floats is an important clue for clarifying the backwash process because it is significantly correlated with the decreasing rate. In this section, we investigate factors determining the alongshore movement from November 26, 2011 to August 31, 2013. Figure 2-11 shows the ratio of the number of floats in each 100-m-wide transect in the next experiment to the number in the 100-m-wide

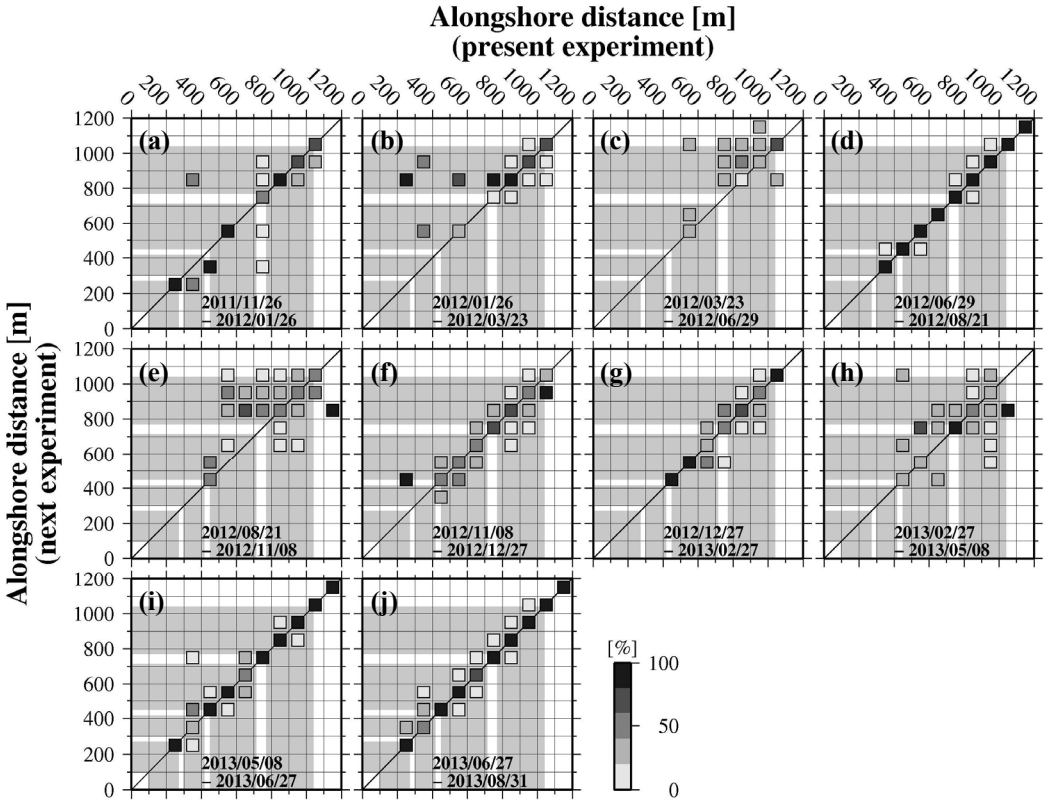

Figure 2-11. Movement ratio in each experiment period. Lateral and vertical axes are alongshore distance at the present and next experiments, respectively. Square with white-black gradation in the upper left (lower right) from the solid line denotes northward (southward) alongshore movement. White-black gradation denotes movement ratio, the scale of which is shown at the right side of panel (j). Light gray area means the alongshore position of the LCSs.

alongshore transect where they have been washed ashore in the present experiment (hereafter "movement ratio").

The floats were moved both northward and southward from where they were located in the present experiment (Figs. 2-11a, 2-11d, 2-11f, 2-11g, 2-11i and 2-11j). On the other hand, the alongshore movement in the other four experiment periods differed from that in the six experiment periods. Most floats were generally transported northward from March 23 to June 29, 2012 and from August 21 to November 8, 2012 (Figs. 2-11c and 2-11e). The floats in the southern (northern) area of the beach were transported northward (southward) by a long distance from January 26 to March 23, 2012 and from February 27 to 8 May, 2013 (Figs. 2-11b and 2-11h). Consequently, the standard deviation of the alongshore movement distance in the four experiment periods was larger than that in the other periods, which ranged from 116 m to 169 m (black arrow in Fig. 2-7 or Table 2-2). The average movement distance is around +100 m (Fig. 2-7 or Table 2-2).

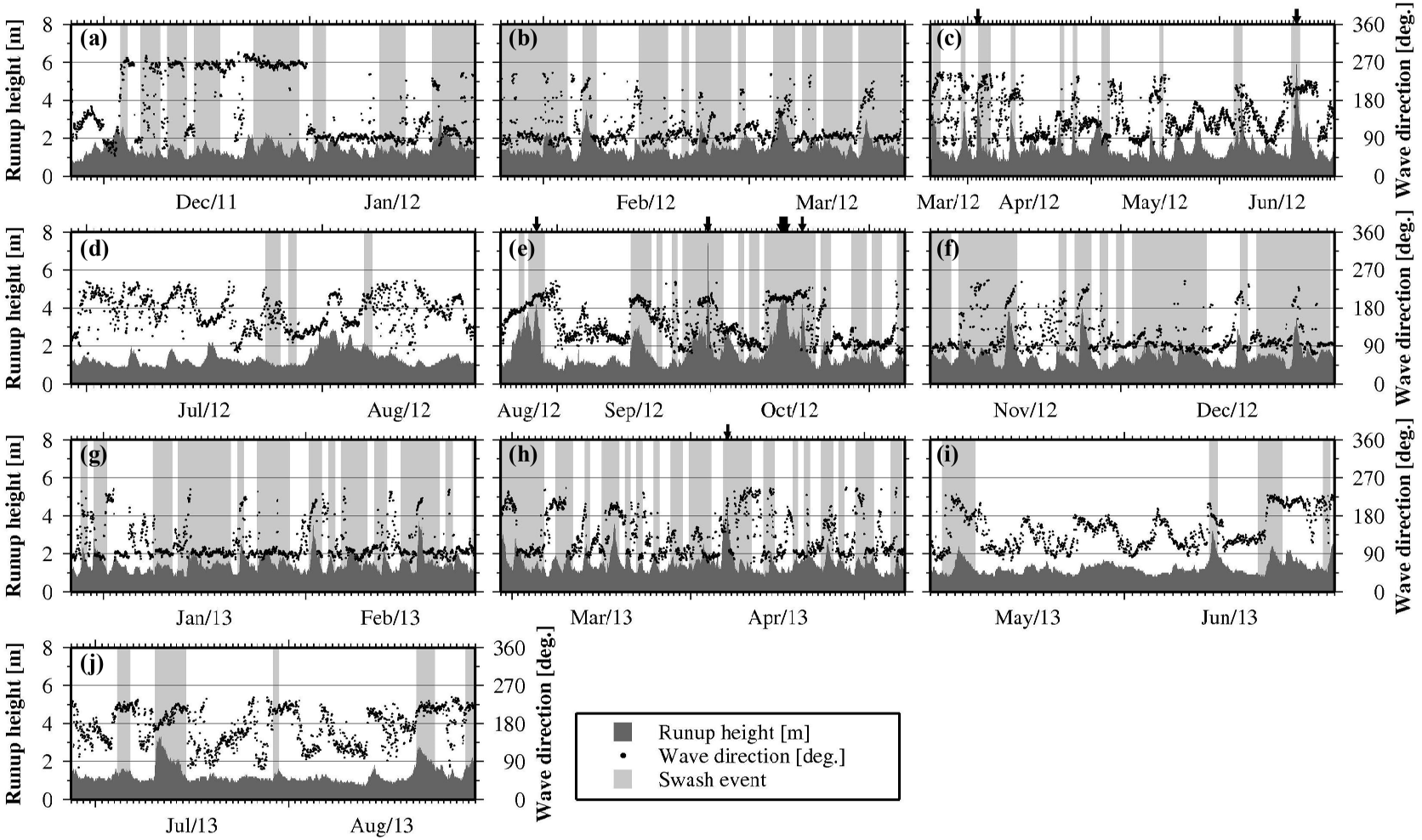

Figure 2-12. Time series of hourly runup height on Wadahama Beach and principal wave direction at 90 km offshore of the Beach (diamond in Fig. 2-1a) in each experiment period. The wave direction is expressed degrees clockwise from the north, for instance a wave coming from the south is given as 180 degrees. The meanings of areas, lines and symbols are shown in the right side box of panel (j). Light gray area denotes swash event identified by webcam monitoring (see 2.2.5). Black arrow denotes when the runup height was higher than the average beached elevation of the remnant floats in each experiment period (circle in Fig. 2-5h).

Figure 2-12 shows the time series of the hourly runup height estimated by Eq. (2.2) (gray area) and the principal wave direction (black circle) at the observation site (diamond in Fig. 2-1a). The wind-waves observed far out from Niijima Island might be different from the incoming waves on Wadahama Beach because of local effects such as wind fields. To support the estimated runup height, the swash events are shown in Fig. 2-12 (light gray area). Basically, the runup height from spring to summer is lower than that from autumn to winter corresponding to the frequency of the swash events (Fig. 2-12). When the estimated runup height was higher than 2 m, the waves whose direction ranged from 180° (northward) to 270° (eastward) could frequently come to Wadahama Beach (Fig. 2-12).

Corresponding to the low runup height during each experiment period, few floats were moved (Figs. 2-11a, 2-11d, 2-11i and 2-11j). On the other hand, when the runup height was frequently higher than 2 m during each experiment period (Figs. 2-12b, 2-12c, 2-12e, 2-12f, 2-12g and 2-12h), most of the remnant floats were moved (Figs. 2-11b, 2-11c, 2-11e, 2-11f, 2-11g and 2-11h) because they had been washed ashore in the beach elevation ranging from 2 m to 7 m (Fig. 2-5h). In particular, when the runup height is higher than the average beached elevation (black arrow in Figs. 2-12c, 2-12e, and 2-12h), many floats were moved a long distance in the alongshore direction (Figs. 2-11c, 2-11e, and 2-11h). These large events on June 19, August 28, September 30 and October 15-18, 2012 were caused by typhoons (JMA, 2012a), and those on April 3, 2012 and April 7, 2013 were caused by the unusual development of extratropical cyclones (JMA, 2012b, 2013). This indicates that the floats were largely moved due to incoming waves produced in these large events.

Interestingly, most of the floats were generally transported northward in the two experiment periods in which typhoons occurred (i.e., Figs. 2-11c and 2-11e). Corresponding to such northward movement, the decreasing rate of floats was largest in the period from August 21 to November 8, 2012 (e in Fig. 2-10c), and was relatively large in the period from March 23 to June 29, 2012 despite the low event probability (c in Fig. 2-10c). Therefore the northward movement on Wadahama Beach would be an important factor determining the backwashing of floats offshore.

2.4.4 Relationship between alongshore concentration of floats and their movement

Basically, the floats were moved both northward and southward in periods other than the four experiment periods (Fig. 2-11). Nevertheless, it is interesting that remnants of the floats were highly concentrated in the northernmost area from 700 to 1100 m of

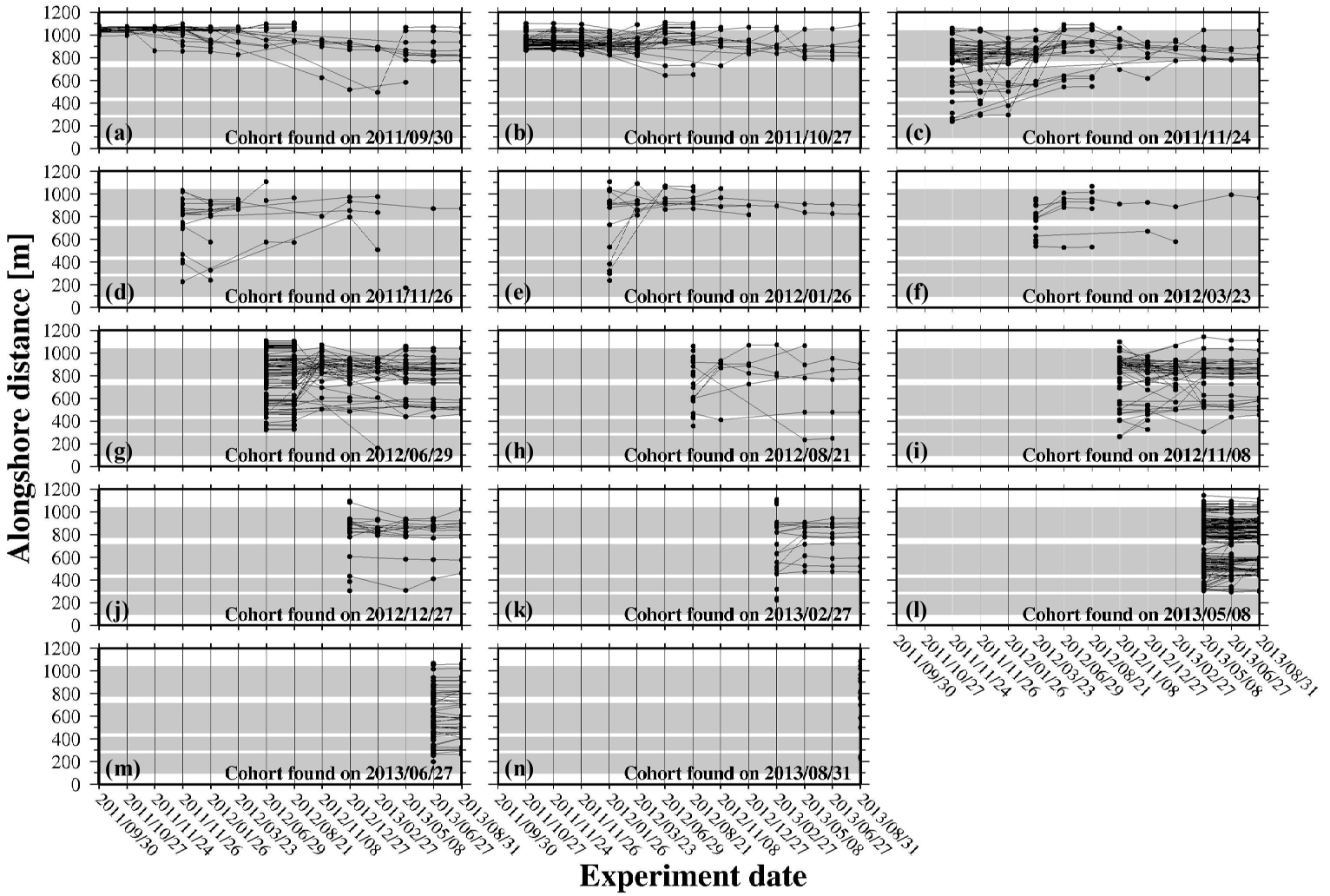

Figure 2-13. Cohort track of the three types from when new floats were found to August 31, 2013. Light gray area means the alongshore position of the LCSs.

alongshore distance through all experiment periods (Fig. 2-6). To investigate the relationship between the alongshore concentration and movement, the tracks of the three types of cohort from when the cohort was found to August 31, 2013 are shown in Fig. 2-13. The cohort track indicates that the floats tend to converge in the northern area (700–1100 m of alongshore distance), and also converge in the southern area (400–600 m of alongshore distance) (Fig. 2-13). For example, although the cohort found on June 29, 2012 was uniformly distributed, the floats gradually concentrated in these areas with both northward and southward movement (Fig. 2-13g).

To confirm the mechanism whereby the floats were concentrated in certain areas, the average alongshore remnant concentration (Fig. 2-6) was compared with the average transport velocity in each 100-m-wide alongshore transect (Fig. 2-14). The average transport velocity was calculated by the following steps: (1) the transport velocity in alongshore transects stranded at the previous experiment during the experiment period was calculated by dividing the alongshore movement distance by the experiment period; (2) the average transport velocity in each alongshore transect was calculated based on the transport velocity in the experiment periods from November 26, 2011 to August 31, 2013.

The alongshore distribution of the average transport velocity in all experiment periods (black circle in Fig. 2-14b) corresponds to the alongshore remnant concentration (black bar in Fig. 2-14a). For example, the transport velocity at 700 and 900 m of alongshore distance was 0.9 m day^{-1} and −0.4 m day^{-1}, respectively. This area ranging from 700 m to 900 m was a convergence area (i.e., $(-0.4-0.9)/200 = -0.7\times10^{-2}$ day^{-1}). Consequently, the velocity gradient indicates that the areas from 700 to 1000 m and from 300 m to 600 m were convergence areas (black outline triangle in Fig. 2-14b). Both of the alongshore remnant concentrations in the two convergence areas of the velocity gradient have a local maximum (black bar in Fig. 2-14a). The two convergence areas were located at the south of the salient part of the beach morphology (see 2.3.5 or Fig. 2-9a).

The floats in the southern areas from 800 m of alongshore distance were generally transported northward, whereas the floats in the northern areas were transported southward (black circle in Fig. 2-14b). As a result, the floats were highly concentrated in the northernmost area (i.e., 700–1100 m of alongshore distance; see Fig. 2-14a). This high concentration in the northernmost area was consistent with the temporal trend of the beach topography: the beach accretion in this area (i.e., 900–1100 m of alongshore distance; see 2.3.5 or Fig. 2-9b). This consistency between the floats and the beach topography suggests that the floats were transported by longshore currents because longshore

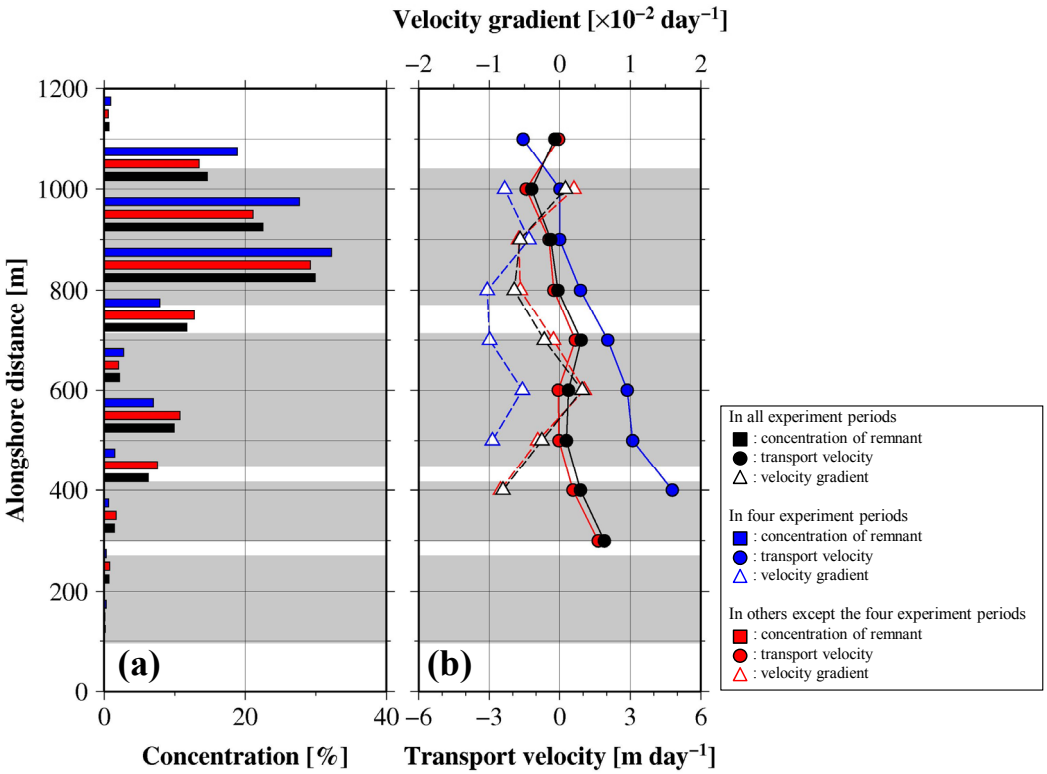

Figure 2-14. Relationship between alongshore remnant concentration (a) and transport velocity (b). Velocity gradient is also shown in panel (b). The meanings of symbols and their colors is shown in the lower right box. Four experiment periods correspond to the periods shown in Fig. 2-11b, 2-11c, 2-11e and 2-11h. Light gray area means the alongshore position of the LCSs.

currents transport sediment on the beach (e.g., Komar and Inman, 1970; Ashton et al., 2001; Bayram et al., 2007).

Wadahama Beach is located on the western side of Niijima Island, and the angle of its shoreline is approximately 7° counterclockwise from the north (Fig. 2-1a and 2-1b). The principal wave direction frequently ranged from 180° (northward) to 270° (eastward) when the runup height was higher than 2 m throughout all experiment periods (Fig. 2-12). Therefore we assume that the floats were transported northward due to the northward longshore currents that were frequently produced by the northeastward breaking waves, and were highly concentrated in the northernmost area.

On the other hand, the average transport velocity in the four experiment periods, in which the floats were widely transported from south to north (Fig. 2-11b, 2-11c, 2-11e and 2-11h), indicates the stronger northward transportation of floats all over the beach than that in all experiment periods (blue circle in Fig. 2-14b). Hence, the alongshore concentration in the northern part in the four experiment periods (blue bar in Fig. 2-14a) was higher than that in all experiments (black bar in Fig. 2-14a). On the other hand, the

average transport velocity (red circle in Fig. 2-14b) and the alongshore concentration (red bar in Fig. 2-14a) in the periods other than the four experiment periods were similar to those in all experiment periods. Several large events intermittently occurred in three experiment periods except the period from January 26 to March 23, 2012 (black arrow in Figs. 2-12c, 2-12e and 2-12h). Therefore, in particular, the floats would be strongly transported northward by intermittent large events.

2.5 Conclusion

To measure the residence time from washing ashore to backwashing offshore, two-year mark-recapture (MR) experiments using fishing floats have been conducted since September 2011 on Wadahama Beach, Niijima Island, Japan. In addition to the residence time of the fishing floats, the experiments also revealed the temporal variation in the number of floats, their spatial concentration and their movement.

The population of floats on the beach varied with the season. The population of floats newly found at each experiment (i.e., immigration) attained a local maximum in the early summer. Corresponding to the temporal variation of immigration, the population of floats that remained on the beach (i.e., remnant) also attained a local maximum in the early summer. On the other hand, the population of floats that disappeared from the beach (i.e., emigration) has a local maximum in November 2012.

Overall, the remnants of floats decreased exponentially. By approximating the decay as an exponential function, we obtained a remnant function for the floats. The residence time of the floats on the beach is estimated as $\tau_r = 1/k = 224$ days, that is, about 7.5 months, by integrating the function with respect to time. The exponential decay of the number of floats demonstrates a linear response of the beach to the input of floats, and corresponds to the unit impulse response of a linear input/output system.

In this study, spatial concentration was described according to three states (i.e., immigration, remnant and emigration). Overall, the alongshore concentration for all states was similar. The floats were highly concentrated in the northern area from 800 to 1100 m of the alongshore distance and in the southern area from 400 to 600 m of the alongshore distance. Both areas were located on the lee of the LCSs. Also, the floats were distributed in the cross-shore range from 20 to 50 m, and the width of the concentration band was approximately 30 m. The temporal variation of the vertical concentration of floats was consistent with that of the cross-shore concentration. Both the cross-shore and vertical concentration showed seasonal fluctuations.

The floats were spatially moved due to hydrodynamics in the nearshore region. In general, the floats were widely transported both northward and southward. The along-

shore movement of floats was significantly correlated with the decreasing rate of floats calculated from the ratio of the remnants of floats at each MR experiment to the total population (i.e., immigration and remnant) at the previous MR experiment. In addition, the alongshore movement of floats was significantly correlated with the frequency of swash events in which wind waves run up to the backshore of the beach. This indicates that the floats are transported by the swash from wind waves and that the alongshore movement of floats depends on the frequency of swash events.

And the alongshore movement determined the alongshore concentration of remnant floats. We found two convergence areas of transport velocity (300–600 m and 700–1000 m of alongshore distance) by calculating the average transport velocity from the alongshore movement distance. Consequently, the alongshore remnant concentration had a local maximum in the two convergence areas. In addition, the high concentration in the northern area from 700 to 1100 m agreed with the temporal linear trend of the beach elevation. This suggests that the floats were transported northward due to longshore currents driven by swash events. Therefore, we concluded that the floats would be transported northward due to longshore currents, and, in particular, the northward transportation of floats becomes strong due to intermittent storm events such as typhoons. In the transportation process, the floats concentrated in the two convergence areas (300–600 m and 700–1000 m of alongshore distance).

CHAPTER 3

Physical mechanism determining residence time of plastic litter on Wadahama Beach

3.1 Introduction

To assess the adverse impact of plastic litter on beaches, it is necessary to know the estimated residence time from washing ashore to backwashing offshore. However, the only location in the world where the residence time has been calculated is Wadahama Beach on Niijima Island, Japan (see 2.3.2). Efficient estimation requires a grasp of the physical mechanism whereby plastic litter is backwashed offshore. For example, understanding the physical mechanism of the backwash process would enable us to measure the residence time without the mark-recapture (MR) experiments described in Chapter 2.

The backwash process of plastic litter on beaches has hardly been studied despite its importance to the marine environment. Bowman et al. (1998) indicated the seasonal variation of the amount of beach litter that had washed ashore (immigration) and backwashed offshore (emigration) at six beaches along the Mediterranean Sea. They mentioned that beach litter is backwashed offshore during events in which the run-up of breaking waves reaches the position of plastic litter that had previously washed ashore (swash events).

However, the frequency of swash events was not significantly correlated with the decrease in fishing floats on Wadahama Beach, whereas the decrease in floats was significantly correlated with the alongshore movement of floats on the beach (see 2.4.2). In addition, the remnants of floats decrease according to an exponential function (Fig. 2-4). This means the remnants of floats on Wadahama Beach can be considered to have decreased at a constant rate determining by the average residence time (i.e., 0.5% per day; see 2.3.2), if a decrease in floats is seen during a period longer than one year. In the backwash process, the floats were highly concentrated in two areas: 400–600 m and 700–1100 m of alongshore distance by both northward and southward movement (see 2.4.4). Interestingly, the concentration of floats that were backwashed offshore (i.e., emigration) was also high in these concentration areas, and was consistent with that of floats newly washed ashore (i.e., immigration) and those remaining on the beach (i.e., remnant) (see Fig. 2-6). Basically, the emigration concentration denotes the frequency

of floats found before backwashing offshore, and does not denote where the floats were backwashed offshore. However, this would be an important clue for clarifying the backwash process.

The purpose of this chapter is to identify the 100-m-wide transect in the alongshore direction where the floats are most likely to be backwashed offshore (hereafter "backwash transect"), and to investigate the physical mechanism of the exponential decay of floats on Wadahama Beach. The physical mechanism of the backwash process is investigated using two calculations: (1) calculation of the residence time in the 100-m-wide alongshore transect; and (2) numerical experiments using a governing equation. Based on the possible backwash transect identified by these calculations, we discuss the physical mechanism of the backwash process on Wadahama Beach.

3.2 Materials and methods

The floats in each 100-m-wide alongshore transect have two possible fates during each experiment period: backwashing offshore or moving to other transects. Firstly, by estimating the residence time in the 100-m-wide alongshore transects, we can understand the frequency at which the floats in each transect were backwashed offshore (or moved to other transects) during each experiment period. Secondly, we identify the backwash transect by reproducing the emigration concentration and the residence time in the 100-m-wide alongshore transect using numerical experiments. In the numerical experiments, we assume that the alongshore movement of floats is governed by an advection-diffusion equation because the floats in the southern (northern) area were transported northward (southward) in two years (see 2.4.4).

3.2.1 Calculation of residence time in 100-m alongshore length

Wadahama Beach is 900 m in length (i.e., from 200 to 1100 m of alongshore distance in Fig. 2-1b). The 900-m length of the beach is divided into nine 100-m-wide alongshore transects. The residence time of the floats found in each transect was estimated using two approaches based on the position of the floats on the beach as measured in the MR experiments.

In the first approach, residence time is estimated by searching a single target transect for remnants of the floats that had been found in the target transect (hereafter "RT1"). Figure 3-1a, for instance, shows the distribution of floats at $t = t_0$, and ten floats are found in the target transect. During the first and second MR experiments, six floats remained in the target transect, two floats moved into other transects (i.e., (1) and (2) in Fig. 3-1b) and two floats were backwashed offshore from the beach (i.e., (3) and (4) in

Fig. 3-1b). During the second and third MR experiments, four floats remained in the target transect and three floats were backwashed offshore from the beach (i.e. (6), (7) and (8) in Fig. 3-1c). The floats that moved into other transects during the first and second experiments are considered to have two possible fates: returning to the target transect (i.e., (5) in Fig. 3-1c), and being backwashed offshore from the beach (i.e., (8) in Fig. 3-1c). Floats that return to the target transect are considered to remain on the beach at t_1 and are counted as remnants on the beach. As a result, the number of remnants at t_1 and t_2 is seven and five floats, respectively.

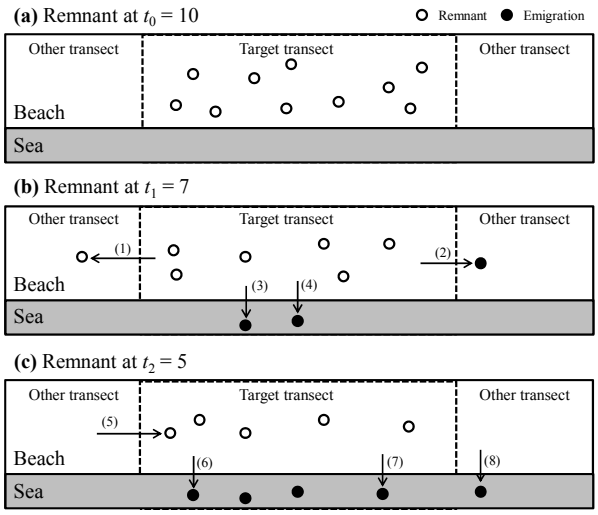

Figure 3-1. Calculation of average RT1. The meanings of the colors of circles are shown in the upper right.

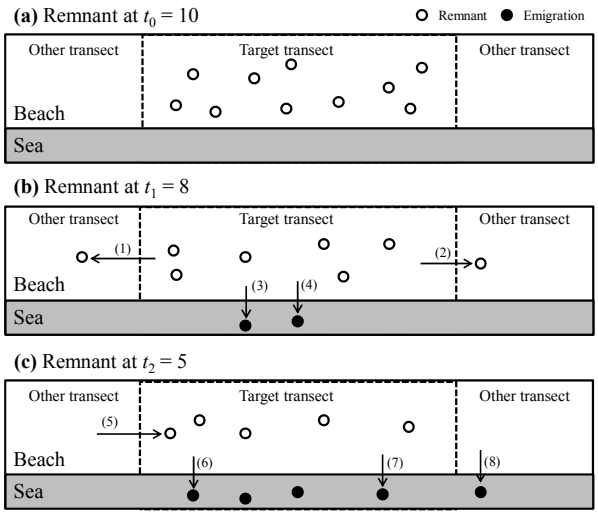

Figure 3-2. Calculation of average RT2. The meanings of the colors of circles are shown in the upper right.

In the second approach, residence time is estimated by searching the whole beach for remnants of the floats that had been found in each target transect (hereafter "RT2"). Figure 3-2 shows the concept of the second experiment. The difference between Figs. 3-1 and 3-2 is to count the floats that moved into the other transects at $t = t_1$ (i.e., (1) and (2) in Fig. 3-2b) regardless of the fate of the floats at $t = t_2$ (i.e., (5) and (8) in Fig. 3-2c). Thus, the number of remnants at $t = t_1$ is eight floats. Namely, in the second approach, the floats that moved into other transects are counted as remnants on the beach.

RT1 and RT2 are calculated by approximating the population decay of remnants as an exponential function, as shown in 2.3.2. The average of RT1 and RT2 is calculated from the coefficient k of the exponential function (i.e., $\tau_r = 1/k$). The 95% confidence interval is determined by the margin of error of the coefficient k of the exponential function.

3.2.2 Design of numerical experiments

In the numerical experiments, the 900-m-wide model domain is defined as ranging from 200 to 1100 m of alongshore distance, and is divided into nine 100-m-wide transects in the same way as described in 3.2.1. The flow chart of the numerical experiments is shown in Fig. 3-3. To identify the possible backwash transect, the emigration concentration and residence time of the floats found in the 100-m-wide alongshore transects on the whole beach (i.e., average RT2) are calculated by solving the following one-dimensional advection-diffusion equation:

$$\frac{\partial c}{\partial t} + \frac{\partial (uc)}{\partial x} = D_x \frac{\partial^2 c}{\partial x^2} + f \ , \tag{3.1}$$

where $c(x, t)$ shows the temporal change in the concentration of floats in the i-th transect. The x-axis is taken along the beach. $u(x)$ is the time-invariant velocity, and the second term of the left side of Eq. (3.1) represents the advective motion of the floats. D_x is a constant diffusion coefficient, and the first term of the right side of Eq. (3.1) represents the diffusive motion of the floats. f on the right side of Eq. (3.1) denotes the backwash of floats. At present, we have no data on how the floats were backwashed offshore, such as the offshore transport velocity. Thus, the backwash of floats is represented using a

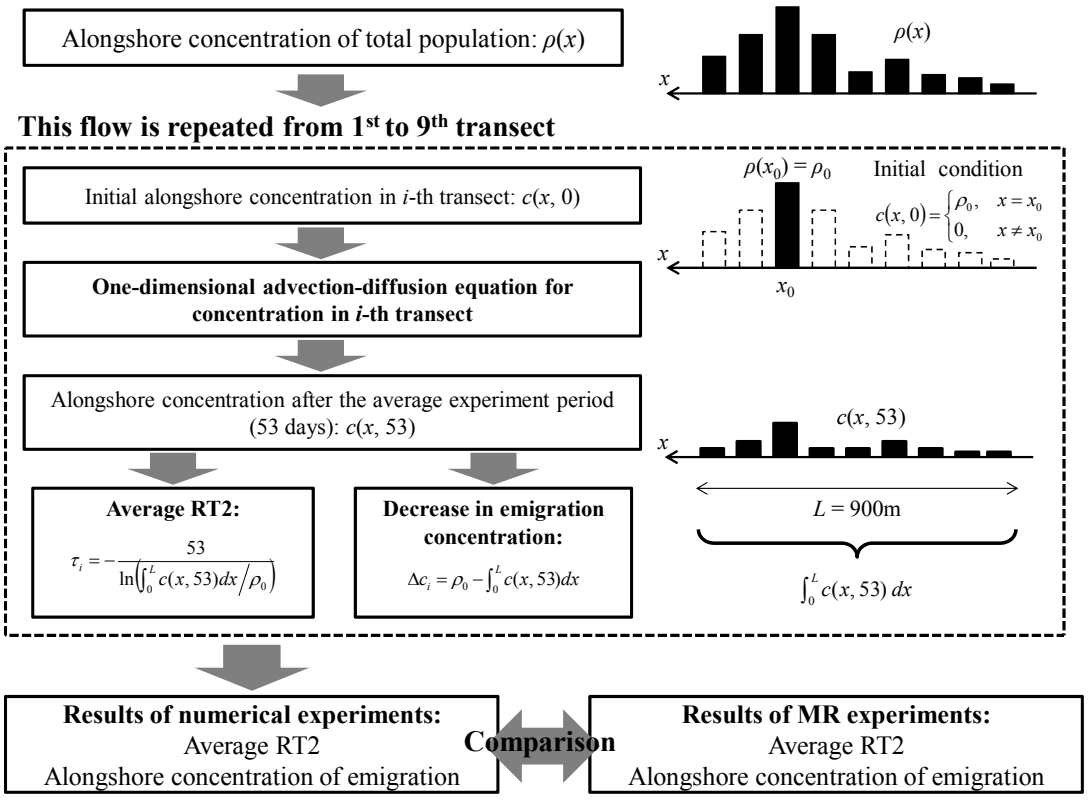

Figure 3-3. Flow chart of numerical experiments.

constant decreasing rate determining by the average residence time (i.e., 0.5% per one days; see 2.3.2). The detail of the backwash term f is described in 3.2.3.

The initial condition of this equation is defined by the average alongshore concentration of total population $\rho(x)$ (see Fig. 2-6):

$$c(x, 0) = \begin{cases} \rho_0, & x = x_0 \\ 0, & x \neq x_0 \end{cases} \tag{3.2}$$

where x_0 is the alongshore distance of the i-th transect. Also, float fluxes are assumed to be zero at x = 0 and L (= 900 m) corresponding to 200 and 1100 m of alongshore distance in Fig. 2-1b:

$$u = 0, \frac{\partial c}{\partial x} = 0 \quad \text{at } x = 0, L\,. \tag{3.3}$$

The alongshore concentration of remnants, which were located in the i-th transect at the initial time, after the average experiment period (i.e., 53 days) is calculated by solving the advection-diffusion equation using a finite-difference scheme. Details of the finite difference scheme are described in 3.2.3. The alongshore emigration concentration and the average RT2 calculated based on the solution of Eq. (3.1) are compared with that estimated based on the actual position of the floats measured in the MR experiments. Considering the exponential decay of remnants, the average RT2 in the i-th transect (τ_i) is calculated from the alongshore concentration after 53 days as follows:

$$\tau_i = -\frac{53}{\ln\left(\int_0^L c(x, 53)\,dx \Big/ \rho_0\right)}. \tag{3.4}$$

In the actual MR experiments, the emigration concentration was determined by where the backwashed floats were found in the previous experiments (see 2.2.3). Thus, the decrease in concentration (Δc_i) is determined as:

$$\Delta c_i = \rho_0 - \int_0^L c(x, 53)dx\,. \tag{3.5}$$

Thus, the average RT2 (τ_i) and decrease in emigration concentration (Δc_i) in nine transects are calculated by solving the advection-diffusion equation. To compare Δc_i with the emigration concentration shown in Fig. 2-6, the emigration concentration in the i-th transect (ϕ_i) is determined by normalizing Δc_i in each i-th transect by the summation of Δc_i in the nine transects.:

$$\phi_i = \Delta c_i \Big/ \sum_{k=1}^{n} \Delta c_k\,. \tag{3.6}$$

At present, we have no observational data to identify the backwash transects. Thus,

in each numerical experiment, candidates for backwash transect are defined by randomly selecting from the nine transects. The total number of combinations of candidates is

$$\sum_{k=1}^{9}\frac{9!}{k!(9-k)!}=511. \tag{3.7}$$

Reasonable combinations of backwash transects are determined by comparing the alongshore distribution of the emigration concentration (ϕ_i: Eq. (3.6)) and the average RT2 (τ_i: Eq. (3.4)) calculated by the numerical experiments with that observed in the MR experiments. Specifically, if both the emigration concentration and the average RT2 calculated by numerical experiment are significantly correlated to that observed in the MR experiment, the reasonable combination of backwash transects is determined.

3.2.3 Finite-difference scheme for solving the advection-diffusion equation

Based on the finite-difference formulation of the one-dimensional advection-diffusion equation (i.e., Eq. (3.1)), the remnant concentration at each time step can be computed as:

$$c_i^{k+1}=c_i^k+\frac{\Delta t}{\Delta x}\left[u_i\left(\frac{c_i^k+c_{i-1}^k}{2}\right)-u_{i+1}\left(\frac{c_{i+1}^k+c_i^k}{2}\right)\right]+\frac{D_x\Delta t}{\Delta x^2}\left(c_{i+1}^k-2c_i^k+c_{i-1}^k\right)-\frac{\alpha}{\rho_b}c_i^k \tag{3.8}$$

where Δx and Δt are the grid spacing of 100 m in size and the time interval, respectively. Figure 3-4 shows the position of variables u and c in the one-dimensional grid. c_i^k denotes the concentration in grid i at time k. i (= 1, 2, …, 9) and k (= 1, 2, …) are the x-axis grid number and the time level, respectively. u_i is the time-invariant velocity of remnants, which is the average transport velocity calculated from the alongshore movement distance in the 100-m-wide alongshore transects in each experiment period (Table 3-1). D_x is the constant diffusion coefficient for the alongshore movement of remnants. Considering that the variation of the transport velocity in each 100-m-wide transect results from the diffusive process, D_x is estimated by multiplying the grid spacing (100 m) by the average standard deviation of the transport velocity in all grids (4.84×10^{-5} m s^{-1}; see Table 3-1), which is 4.84×10^{-3} m^2 s^{-1}. In this study, Δt is deter-

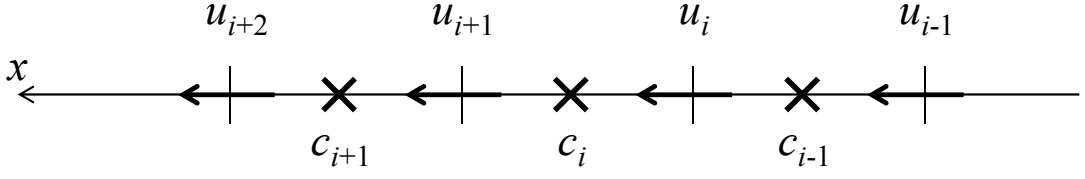

Figure 3-4. Position of variables u (arrow) and c (cross) of Eq. (4.8).

Table 3-1. Average and standard deviation of transport velocity in each grid. Average transport velocity is also described in Fig. 2-14 (black circles).

Grid number	Alongshore distance [m]	Transport velocity in each grid			
		Average		Standard deviation	
		[m s^{-1}]	[m day^{-1}]	[m s^{-1}]	[m day^{-1}]
9	1000	-1.39×10^{-5}	-1.20	2.39×10^{-6}	0.21
8	900	-4.35×10^{-6}	-0.38	2.59×10^{-6}	0.22
7	800	-8.41×10^{-7}	-0.07	1.64×10^{-6}	0.14
6	700	1.06×10^{-5}	0.91	8.48×10^{-6}	0.73
5	600	4.29×10^{-6}	0.37	3.24×10^{-6}	0.28
4	500	3.26×10^{-6}	0.28	4.32×10^{-6}	0.37
3	400	1.02×10^{-5}	0.88	2.71×10^{-6}	0.23
2	300	2.19×10^{-5}	1.89	1.33×10^{-5}	1.15
Average standard deviation				4.84×10^{-6}	0.42

mined as 3600 s (i.e., 1 hour) considering the maximum of u_i (i.e., 2.19×10^{-5} m s^{-1}) and D_x (i.e., 4.84×10^{-3} m^2 s^{-1}). This time interval satisfies the Courant-Friedrich-Levy condition: $u_i\Delta t/\Delta x = 2.19\times10^{-5}\times3600/100 = 7.88\times10^{-4} \leq 1$ and $D_x\Delta t/\Delta x^2 = 4.84\times10^{-3}\times3600/100^2 = 1.74\times10^{-3} \leq 0.5$.

α of Eq. (3.8) denotes a backwash rate of floats from the backwash transect candidates in Δt, which is calculated based on the average residence time: $1-e^{-\Delta t/\tau_r} = 1-e^{-1/(224\times24)} = 0.019\%$. ρ_b denotes the summation of the remnant concentration in backwash transect candidates at each time. If the calculating grid box is not a backwash transect candidate, the last term of the right side of Eq. (3.8) is ignored. The discretization of the boundary conditions in the model domain (i.e., Eq. (3.3)) is

$$\begin{cases} u_i = 0, \dfrac{c_i^k - c_{i-1}^k}{\Delta x} = 0 & (i=1) \\ u_{i+1} = 0, \dfrac{c_{i+1}^k - c_i^k}{\Delta x} = 0 & (i=9) \end{cases} \tag{3.9}$$

3.3 Results

3.3.1 Residence time of floats found in target transect

RT1 and RT2 of the floats found in each single transect are described in Table 3-2. The remnant concentration denotes the average alongshore concentration of remnant floats described in Fig. 2-6. R^2 in Table 3-2 denotes the coefficient of determination of the exponential function.

RT1 in the first and fifth transect could not be calculated because the temporal vari

Table 3-2. RT1 and RT2 of floats found in a single target transect.

Transect number	Alongshore distance [m]		Remnant concentration [%]	Number of found floats	RT1 of floats found in a single transect					RT2 of floats found in a single transect					Difference between RT1 and RT2 [days]
	Start	End			Average RT1 [days]	95% confidence interval [days]			R^2	Average RT2 [days]	95% confidence interval [days]			R^2	
						Minimum	Maximum	Difference			Minimum	Maximum	Difference		
9	1000	1100	15	176	136	116	163	46	0.72	260	217	325	107	0.35	125
8	900	1000	23	236	143	128	163	35	0.76	222	199	251	52	0.76	79
7	800	900	30	259	198	182	216	33	0.86	264	241	291	50	0.84	66
6	700	800	12	129	124	104	153	49	0.76	300	247	384	138	0.58	176
5	600	700	2	44	–	–	–	–	–	518	373	849	476	0	–
4	500	600	10	114	154	125	201	77	0.64	348	300	414	114	0.67	194
3	400	500	6	76	185	146	251	105	0.58	313	250	421	171	0.38	129
2	300	400	1	45	57	51	65	14	0.97	213	153	349	196	0.50	156
1	200	300	1	24	–	–	–	–	–	403	270	791	520	0	–

ation of the normalized population could not be significantly approximated as an exponential function. Overall, the average RT1 was shorter than the whole residence time of floats found on the whole beach (i.e., 224 days; see 2.3.2) because the floats that moved to other transects were not counted as remnants. The average RT1 in the seventh transect was closest to the whole residence time. In addition, the difference in 95% confidence interval was the smallest, and was similar to that of the whole residence time (i.e., 34 days; see 2.3.2). This suggests that the residence time that is close to the whole residence time can be estimated even if the MR experiments have only been conducted in the seventh transect. The methodology of the MR experiments based on this suggestion is discussed in 3.4.1.

On the other hand, the average RT2 ranged from 213 to 518 days, which was longer than the whole residence time, or close to it. The longer average RT2 indicates that it took time for the floats in the target transect to be backwashed offshore because they moved along the beach. Thus, the difference in the average between RT1 and RT2 means the frequency of floats moving to other transects because the average RT2 was calculated from the exponential decay of the remnant ratio according to backwashing offshore from the beach, while the average RT1 was calculated from the exponential decay according to both alongshore movement to other transects or backwashing offshore. The difference is shown in the last column in Table 3-2. The difference in the first and fifth transects was not calculated because the average RT1 could not be calculated. In northern transects from 700 to 1100 m of the alongshore distance, the difference in the seventh and eighth transects (800–1000 m) was significantly smaller than that in the other transects. In southern transects from 200 to 700 m of the alongshore distance, the difference in the third transect (400–500 m) was relatively smaller than that in the other transects. The small difference means that the floats found in these transects have relatively few chances to move to other transects. In addition, the concentration of remnant in these transects is significantly higher than that in the other transects in each area. On the other hand, the large difference means that the floats easily move to other transects. Therefore, this also indicates that the floats were concentrated in these transects, corresponding to the convergence area of the average transport velocity (Fig. 2-14b).

3.3.2 Advection-diffusion calculation

The numerical experiments identified twenty-eight reasonable combinations of backwash transects (Table 3-3). Table 3-3 shows the backwash transect number and the statistics (correlation coefficient, slope and intercept of regression line) of two correla-

Table 3-3. Twenty-eight combinations of the possible backwash transects identified by numerical experiment. Bold characters denote the five combinations shown in Fig. 3-5.

Combination number	Backwash transect number	Comparison of emigration concentration			Comparison of average RT2		
		Correlation coefficient	Slope	Intercept	Correlation coefficient	Slope	Intercept
1	1 9	0.86	1.37	-0.04	0.72	5.47	-1027.75
2	2 8	0.91	1.22	-0.02	0.75	2.51	-399.14
3	3 8	0.91	1.08	-0.01	0.69	1.26	-70.83
4	1 2 8	0.90	1.11	-0.01	0.69	2.29	-356.94
5	2 7 8	0.92	1.28	-0.03	0.67	1.83	-177.43
6	2 7 9	0.98	1.29	-0.03	0.69	1.89	-207.31
7	2 8 9	0.94	1.37	-0.04	0.78	3.70	-637.52
8	3 7 8	0.92	1.20	-0.02	0.69	1.40	-63.94
9	3 7 9	0.98	1.20	-0.02	0.73	1.36	-70.34
10	3 8 9	0.94	1.27	-0.03	0.77	2.09	-223.73
11	1 2 8 9	0.93	1.29	-0.03	0.72	3.38	-584.79
12	**1 3 7 8**	**0.91**	**1.13**	**-0.01**	**0.68**	**0.98**	**-13.81**
13	**2 3 7 8**	**0.91**	**1.08**	**-0.01**	**0.81**	**1.09**	**-61.39**
14	**2 3 7 9**	**0.98**	**1.06**	**-0.01**	**0.75**	**1.06**	**-60.86**
15	2 4 7 8	0.91	1.06	-0.01	0.78	0.57	91.62
16	2 4 7 9	0.98	1.04	0.00	0.69	0.51	97.88
17	3 7 8 9	0.99	1.31	-0.03	0.67	2.02	-167.94
18	1 3 7 8 9	0.99	1.25	-0.03	0.70	1.44	-103.21
19	2 3 6 7 8	0.86	0.99	0.00	0.67	0.55	93.07
20	2 3 6 7 9	0.93	0.97	0.00	0.72	0.51	91.06
21	2 3 6 8 9	0.97	1.03	0.00	0.81	0.74	29.89
22	2 3 7 8 9	0.99	1.20	-0.02	0.85	1.60	-171.42
23	**2 4 7 8 9**	**0.99**	**1.19**	**-0.02**	**0.79**	**0.95**	**15.88**
24	1 2 3 7 8 9	0.98	1.16	-0.02	0.72	1.45	-147.41
25	2 3 4 7 8 9	0.98	1.06	-0.01	0.73	0.75	36.19
26	**2 3 6 7 8 9**	**0.97**	**1.11**	**-0.01**	**0.78**	**0.91**	**12.69**
27	2 3 4 6 7 8 9	0.96	1.00	0.00	0.74	0.52	99.09
28	1 2 3 4 6 7 8 9	0.96	0.96	0.00	0.79	0.34	127.97

tions. Overall, the emigration concentration calculated from the solution of the advection-diffusion equation was in very good agreement with that observed in the MR experiments. On the other hand, the statistics of the average RT2 relatively varied among the combinations. The slope ranged from 5.47 to 0.34, and the intercept ranged from −1027.75 to 127.97. This indicates that the average RT2 depends strongly on the combinations of backwash transects.

In the identified combinations of backwash transects, we found five combinations (i.e., combination number 12, 13, 14, 23 and 24; see Table 3-3) in which the slope in two correlations is within the range from 0.8 to 1.2: the calculation error of the emigration concentration and the average RT2 are within 20%. Figure 3-5 shows the alongshore distribution of both the emigration concentration and the average RT2 (left side of each figure) and their correlations between the calculation and the observation. On the left side of each figure, the black arrows denote the backwash transects. In the five combinations, the backwash transects were distributed from 700 to 1100 m (i.e., sixth−

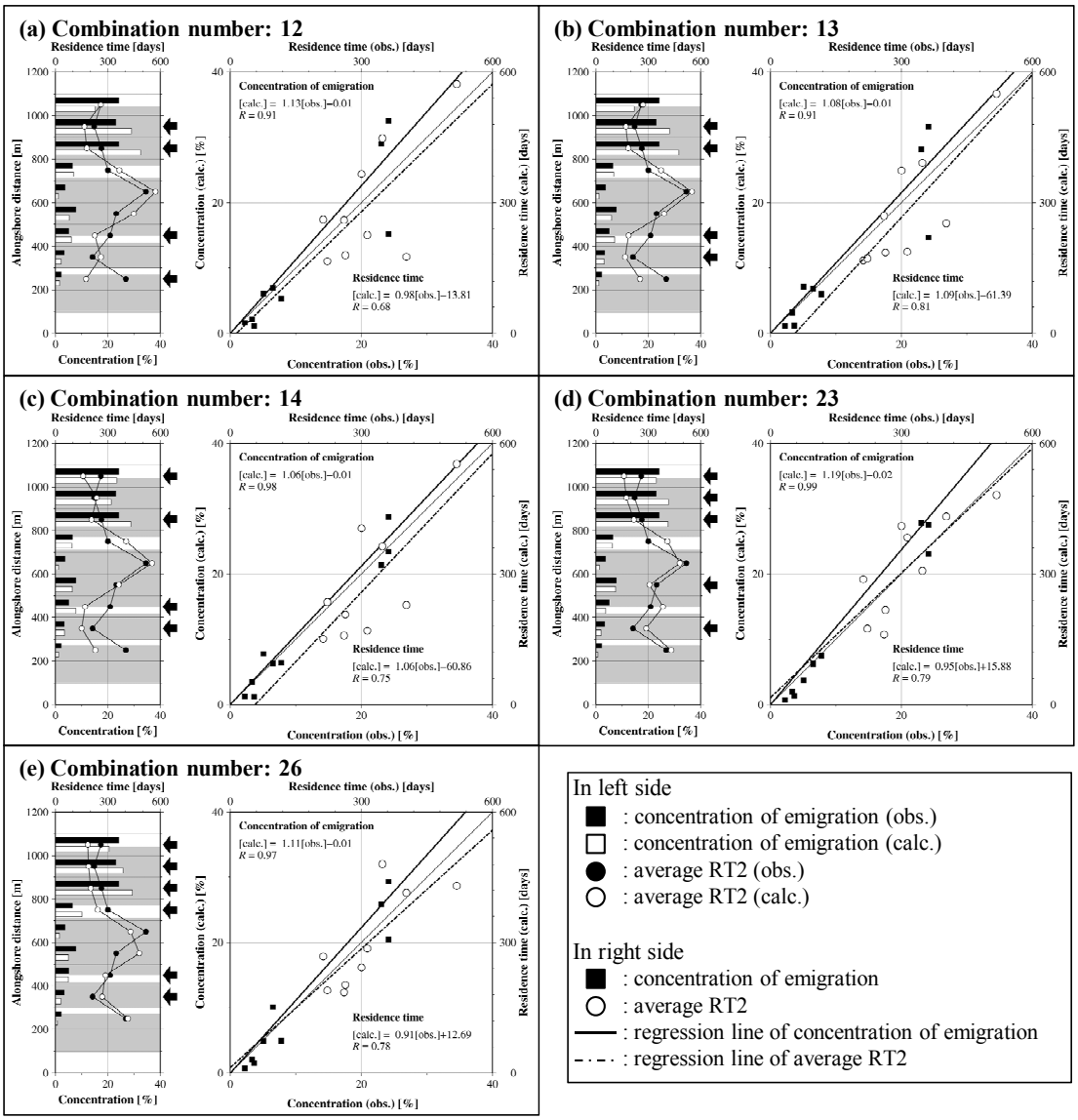

Figure 3-5. Five combinations of backwash transects identified by numerical experiments. Combination numbers correspond to those in Table 3-3. The left side in each panel shows the alongshore distribution of the emigration concentration (lower axis) and average RT2 (upper axis). On the left side, black arrows and light gray areas denote positions of backwash transects and low-crest structures, respectively. The right side in each panel shows the correlation between observation and calculation. The meanings of all symbols and lines are shown in the lower right box.

ninth transects) and from 200 to 600 m (i.e., first−fourth transects). In particular, the second, third, seventh and eighth transects were frequently identified as the backwash transects. This indicates that the floats are most likely to be backwashed offshore from both the southern (i.e., second and third) and northern (i.e., seventh and eighth) transects; conversely, they are unlikely to be backwashed offshore from the center area (i.e., fourth−sixth transects). These possible backwash transects correspond to the areas of high concentration of remnant floats (Fig. 2-6) or the convergence area of the transport velocity (Fig. 2-14). Therefore, the remnant concentration could be an indicator to iden-

tify where the floats are most likely to be backwashed offshore.

3.4 Discussion

3.4.1 Factors determining residence time

Figure 3-6 shows a schematic image of the backwash process on Wadahama Beach. The principal wave direction mostly ranged from 180° to 270° in swash events in which the runup height was higher than 2 m (Fig. 2-12). The propagating waves would normally come to Wadahama Beach from the west because of wave refraction, and could be broken on the low-crested structures (LCSs) in the nearshore zone of the beach. A number of studies confirmed that two nearshore circulations are generated in the lee of the LCSs by wave breaking on the LCSs (e.g., Martinelli et al., 2006; Kuriyama et al.,

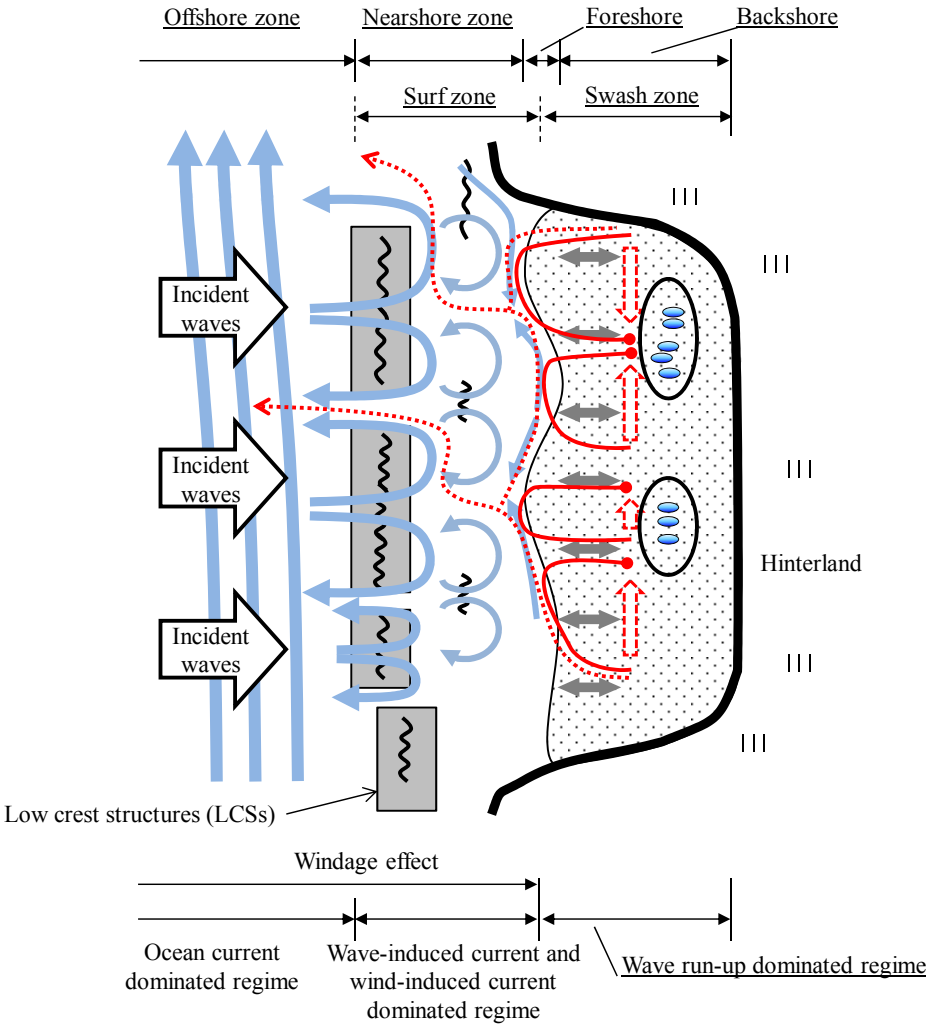

Figure 3-6. Schematic image of backwash process of floats on Wadahama Beach throughout all MR experiment periods. Blue and gray arrows denote ocean current in the offshore-nearshore region and swash of wind waves, respectively. Red arrows and lines denote the transport rate of remnants of floats and the track of floats, respectively. Ellipses denote the concentration area of floats.

2007). Basically, onshore mass transport occurs by wave breaking on the LCSs, and strong seaward current (i.e., rip current) forms around the gap between the LCSs. Conversely, near the shoreline in the lee of the LCSs, return flow is generated around the center of the LCSs and onshore current around the gap between LCSs (Kuriyama et al., 2007). Therefore the lee (gap) of the LCSs corresponds to the convergence (divergence) area of the longshore currents.

Corresponding to the longshore current pattern, possible backwash transects were identified in the lee of the LCSs (see 3.3.2). Thus we assume that the floats would be transported in the alongshore direction due to the longshore currents (see 2.4.4), and a portion of the transported floats would be backwashed offshore due to the return flow of nearshore circulation in the lee of the LCSs (e.g., red broken arrows in Fig. 3-6). On the other hand, most of the transported floats would be stranded on the beach once again. Consequently, the floats were highly concentrated in the lee of the LCSs (Fig. 2-6).

Therefore, the residence time of floats could be determined by the frequency with which the floats are transported by the nearshore circulation generated during the swash event. Even if the magnitude of the swash event is relatively small, the floats could have a high chance of reaching the backwash transects by being transported in swash events which occurred frequently during experiment periods (e.g., Figs. 2-11h and 2-12h). In addition, even if the frequency of swash events in an experiment period is relatively low, the floats could have a high chance of reaching the backwash transects by being frequently transported in a single large event (e.g., Figs. 2-11c and 2-12c).

On Wadahama Beach, the backwash transect could be determined in the lee of the LCSs. If the LCSs are not constructed in an offshore region of beaches, it might be difficult to determine the backwash transect because the position where the return flow is produced would vary depending on the formation of sand bars (e.g., Lippmann and Holman, 1990). Therefore the residence time might depend on the pattern of formation of sand bars.

From comparisons of the MR experiment results on six Israeli Mediterranean beaches, Bowman et al. (1998) concluded that swash energy to beach width and beach morphology are the dominant factors controlling the quantity of litter on the beaches. They found that the two widest beaches had the most litter. Tsouk et al. (1985) reached the same conclusion in their study on oil-polluted Israeli beaches. Their widest beach ranked lowest in self-cleaning performance. Bowman et al. (1998) also reported that high beach porosity is the most dominant physical factor, because it increases the subsurface beach drainage and diminishes the backwash of litter, thus preventing self-cleaning and encouraging litter accumulation. William and Tudor (2001) revealed

that the residence time of litter on the beach surface depended on litter size: items that were smaller than the substrate had a shorter residence time mainly due to burial of items in the beach. When we consider the residence time of litter with lower densities such as PET bottles and plastic bags, wind pressure force acting on the beached litter surface seems to be a crucial factor, since we frequently found that, for instance, plastic bags were moved down to the foreshore or up to the escarpment from the backshore of the beach by wind pressure, which appears to reduce the residence time of such litter on the beach. Therefore, the residence time would also depend on the dimensions of the particular site and the litter items.

3.4.2 Methodology of measurement of average residence time

The MR experiments enable us to understand the average residence time of plastic litter on beaches (see 2.3.2). It would be difficult to conduct the experiment on a beach where a mass of plastic litter washes ashore or on a beach that is much longer than the Wadahama. A number of beach litter surveys have been conducted on part of a beach (i.e., transect) (e.g., Garrity and Levings, 1993; Ryan et al., 2009). If the MR experiment is conducted on a single transect of the beach, the average residence time is basically underestimated (see 3.3.1). To measure the average residence time on multiple beaches by transect survey, it is essential to clarify the error of the average residence time on a beach measured in transects. Here, we discuss the measurement error of the average residence time measured by transect survey (i.e., average RT1).

The average RT1 in the seventh transect was closest to the whole residence time, while the average RT1 in the second transect differed greatly from the whole residence time (Table 3-2). In this chapter, the measurement error is evaluated by dividing the difference between the average RT1 and the whole residence time by the whole residence time. To investigate the dependence of the measurement error of the average RT1 on various selections of transects, several transects are selected from the nine transects; these selected transects are referred to as “target transects”. Namely, the number of combinations of the target transects is 511 (Eq. (3.7))

Figure 3-7 shows the relationship of the measurement error of the residence time with the ratio of the number of floats found in the target transect (hereafter “finding ratio”). The finding ratio was evaluated by dividing the number of floats found in the target transects by the total immigration number in all MR experiments (i.e., 784; see Table 2-1). If the population decay of remnants cannot be significantly approximated as an exponential function, the average RT1 was removed from Fig. 3-7. The circles denote the measurement errors of the average RT1 in target transect combinations that included

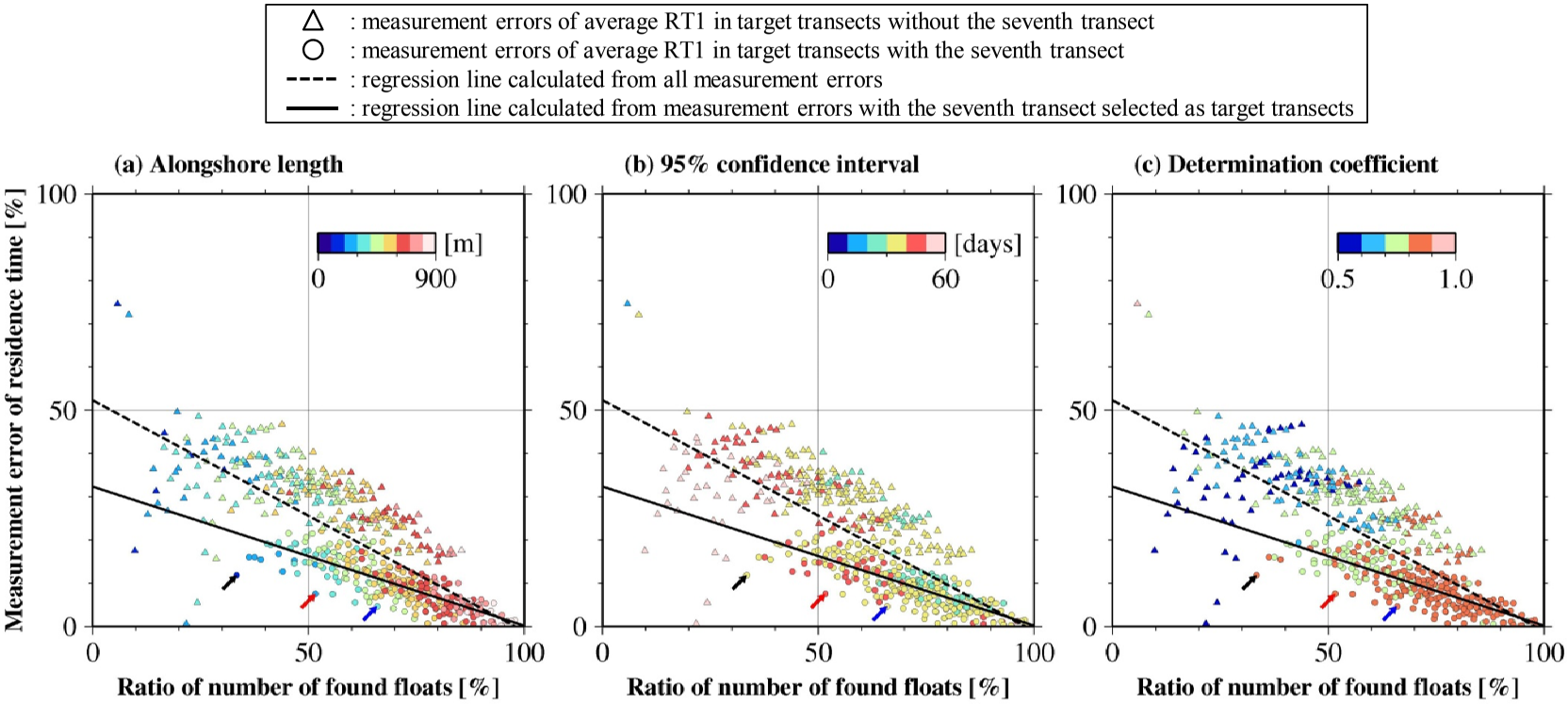

Figure 3-7. Correlation between measurement error of average RT1 and finding ratio. The meanings of all symbols and lines are shown in the upper box. The colors of symbols in (a), (b) and (c) denote total alongshore length of target transects, 95% confidence interval of average RT1 and determination coefficient for exponential function, respectively, and their scales are shown in the upper right in each panel. Black, red and blue arrows denote measurement errors of average RT1 in the seventh, seventh–eighth and seventh–ninth transects, respectively.

the seventh transect, and the triangles denote those combinations that did not include the seventh transect. The colors of the symbols in Fig. 3-7a, 3-7b and 3-7c denote the total alongshore distance of the target transect, 95% confidence interval of the RT1 and the coefficient of determination of the exponential function, respectively.

Overall, the measurement error can be reduced as the finding ratio is larger. All the measurement errors (i.e., triangles and circles in Fig. 3-7) were regressed against the finding ratio (broken line in Fig. 3-7). We found a significant negative correlation between the measurement error and the finding ratio at the 95% confidence level ($n = 505$, $R = -0.77$, $P = 6.3\times10^{-102} < 0.05$). It is interesting to note that the measurement error varies greatly, even if the finding ratio and the alongshore distance in the target transects are similar. For example, the measurement error of the average RT1 of floats found at 700 m in the alongshore distance ranged from 0% to 40%. This indicates that the selection of target transects is an important factor for measuring the whole residence time.

The measurement error of the average RT1 was generally low in target transect combinations that included the seventh transect. These measurement errors (i.e., circles in Fig. 3-7) were regressed against the finding ratio (solid line in Fig. 3-7). We found a significant negative correlation between the measurement error and the finding ratio at the 95% confidence level ($n = 255$, $R = -0.81$, $P = 2.2\times10^{-60} < 0.05$). The two regression lines demonstrate that the measurement error can be greatly reduced by selecting the seventh transect as the target transect.

The crucial transect for measuring the whole residence time can be determined by the alongshore concentration of remnant because the remnant floats were highly concentrated in the seventh transect (Table 3-2). Black, red and blue arrows in Fig. 3-7 show the measurement errors of the average RT1 that were measured in the seventh (concentration: 30%), seventh and eighth (concentration: 53%) and seventh to ninth (concentration: 68%) transects, respectively. Clearly, the measurement error is reduced as the remnant concentration increases. Thus, when determining the target transects for measuring the residence time, the remnant concentration should be taken into consideration.

3.5 Conclusions

We investigated the physical mechanism of the backwash of fishing floats found on Wadahama Beach in Niijima Island, Japan using two calculations. First, we estimated the residence time of floats that were found in 100-m-wide transects in the alongshore direction based on the beached position of floats revealed by two-year mark-recapture

(MR) experiments. Second, we identified the backwash transects by solving the one-dimensional advection-diffusion equation using a finite-difference scheme.

The residence time of floats found in 100-m-wide alongshore transects was calculated by two approaches. In the first approach, residence time (RT1) was estimated by searching a single 100-m-wide transect for remnants of the floats. In the second approach, residence time (RT2) was estimated by searching the whole beach for remnants of the floats.

Overall, the average RT1 in each transect was underestimated in comparison with the residence time of floats found on the whole beach: 224 days (whole residence time). The average RT1 in the seventh transect was closest to the whole residence time. This indicates that the seventh transect is an important transect for measuring the whole residence time. The important transect for measuring the whole residence time can be determined by the alongshore concentration of remnant. Even if MR experiments are conducted on only part of the whole beach to measure the whole residence time, the residence time can be more accurately measured by selecting the transect where plastic litter is highly concentrated.

On the other hand, the average RT2 tends to be overestimated in comparison with the whole residence time because of the alongshore movement of the floats (Table 3-2). The large difference between the average RT1 and RT2 implies that the floats frequently move to other transects. The difference in some transects (third, seventh and eighth transects) with a relatively higher concentration of remnant was smaller than that in the other transects. This demonstrates that the floats are unlikely to move to other transects until the next experiment, and are frequently backwashed offshore.

The advection-diffusion calculation using the finite-difference scheme frequently identified four transects (i.e., transect number 2–3 and 7–8) in which the floats were most likely to be backwashed offshore (backwash transects). These transects were consistent with those in which the difference between the average RT1 and RT2 was relatively smaller. Therefore, we concluded that the floats were most likely to be backwashed offshore from the high concentration area of remnant floats because the identified transects correspond to the high concentration areas.

Throughout all experiment periods, the floats in the southern (northern) part of the beach tended to be transported northward (southward), and to be highly concentrated in some transects. The concentration transects were located in the lee of the LCSs. Consequently, we assume that the physical mechanism of backwash is that the floats are transported in the alongshore direction due to longshore currents, and are backwashed offshore due to the return flow generated in the lee of the LCSs. Therefore, the resi-

dence time of floats on Wadahama Beach would be determined by the frequency with which the floats are transported by the nearshore circulation generated during the swash event.

CHAPTER 4

Application of residence time of plastic litter to beach cleanup

4.1 Introduction

Beach cleanup is a key approach to reducing two adverse effects on marine and coastal environments: fragmentation of plastic litter (Andrady, 2011) and beach pollution from toxic metals contained in plastic litter (Nakashima et al., 2012). Usually, beach cleanup is conducted at individual beaches around the world. Ocean Conservancy, for instance, organizes international coastal cleanups (Ocean Conservancy, 2012), as well as waterway and ocean cleanups every year involving many volunteers. However, since the effects of these beach cleanups are not well understood, it is necessary to identify how best to organize them, and where and when to carry them out. In response, we attempt to quantify the effects of beach cleanup. Generally, beach cleanup is conducted to improve the landscape of the beach. In addition to this, we focus on environmental improvement effects in terms of reducing plastic fragmentation and beach pollution by toxic metals.

When exposed to solar ultraviolet (UV) radiation, plastics undergo photo-oxidative degradation and gradual fragmentation. Plastics degrade much more quickly when lying on the beach compared to floating on the sea because of relatively higher temperatures and the higher oxygen concentration in air environments (Andrady, 2011). Thus, degradation on beaches is the predominant process in the fragmentation of plastics. On the other hand, fragments of plastic litter, referred to as microplastics, pick up persistent organic pollutants (POPs) in the sea and develop high concentrations of POPs (Andrady, 2011; Cole et al., 2011). Microplastics are defined as particle fragments smaller than 5 mm (Barnes et al., 2009) and are ingested by fish, seabirds and plankton in the ocean (e.g., Shaw and Day, 1994; Derraik, 2002; Boerger et al., 2010). Thus, microplastics may be important agents in the transport of toxic chemicals and contaminants, adversely affecting the ocean food web (Mato et al., 2001; Andrady, 2011).

Nakashima et al. (2012) recently suggested that toxic metals, which are often used in the production of plastics, leach into the water surrounding plastics (e.g., rain water). They found high concentrations of lead stearate ($Pb(C_{18}H_{35}O_2)_2$), which is toxic to biota (Nordic Council of Ministers, 2003), in polyvinyl chloride (PVC) plastic litter. They computed the flux leaching into the surrounding water and the resultant concentration of Pb in the beach, and concluded that Pb leaching from PVC plastic litter is a potential

future risk of such litter on beaches.

These environmental risks would depend on the residence time from washing ashore to backwashing offshore; thus, the residence time is crucial for evaluating the beach cleanup effects (BCEs). On Wadahama Beach, Niijima Island, the residence time was obtained based on the exponential decay of the remnant plastic litter revealed by two-year mark-recapture (MR) experiments (see 2.3.2). The exponential decay can be considered as a linear response of the beach to the input flux of plastic litter. Here, we show the amplitude and phase characteristics of the beach as a time-invariant linear input/output system. Furthermore, to demonstrate the importance of measuring the residence time, we suggest the quantification of BCEs based on the linear system analysis, and investigate the dependence of BCEs on the residence time. In this study, we consider three BCEs: (1) improvement of beach landscape, (2) decrease of total mass of toxic metals that could leach into the beach from plastics, and (3) prevention of plastic fragmentation.

4.2 Materials and Methods

4.2.1 Time-invariant linear input/output system of plastic litter

Assuming the beach as a time-invariant linear system of plastic litter, the cohort population of plastic litter exponentially decreases as follows:

$$h(t) = \begin{cases} \exp\left(-t/\tau_r\right), & \text{for} \quad t \geq 0 \\ 0, & \text{for} \quad t < 0 \end{cases} \tag{4.1}$$

where t and τ_r are the elapsed time and the average residence time, respectively (see 2.3.2). $h(t)$ denotes the unit impulse response (UIR) in the linear system analysis. Specifically, in the time domain of the linear system, the output $y(t)$ is described by the convolution integral of the input $x(t)$ and UIR $h(t)$ as follows:

$$y(t) = \int_0^t x(\tau)h(t-\tau)d\tau\,. \tag{4.2}$$

Based on the definition in Section 2.2.3, $x(t)$ and $y(t)$ correspond to immigration (litter input flux) and remnant, respectively. The Fourier transformation of Eq. (4.2) yields

$$Y(\omega) = H(\omega)X(\omega), \tag{4.3}$$

where $\omega\left(=2\pi/T\right)$ is the angular frequency and T is the period of temporal variability of litter input flux. Equation (4.3) describes the system in the frequency domain. Hereafter, the frequency response of the system is expressed as a function of the dimensionless residence time (ζ) normalized as the residence time (τ_r) by the litter input period (T): $\zeta = \tau_r/T$.

The frequency response of the UIR represents the system function $H(\zeta)$:

$$H(\zeta) = \frac{\tau_r}{1+(2\pi\zeta)^2}(1 - i2\pi\zeta). \tag{4.4}$$

The amplitude and phase characteristics of the system are expressed as:

$$A(\zeta) = \frac{|H(\zeta)|}{\tau_r} = \frac{1}{\sqrt{1+(2\pi\zeta)^2}}. \tag{4.5}$$

$$\theta(\zeta) = \tan^{-1}\frac{\mathrm{Im}(H(\zeta))}{\mathrm{Re}(H(\zeta))} = \tan^{-1}(-2\pi\zeta). \tag{4.6}$$

where $A(\zeta)$ is the normalized amplification factor, which is defined as the ratio of the absolute value of $H(\zeta)$ to the residence time (τ_r). In this study, $\theta(\zeta)$ is the phase lag of the output with respect to the input. Note that θ is a negative phase lag (i.e., $\theta < 0$). Thus, the system characteristics (i.e., Eqs. (4.5) and (4.6)) are fully described by the UIR.

4.2.2 Beach cleanup effect 1 (BCE1): Improvement of beach landscape

Figure 4-1 shows a schematic image of the beach cleanup effect in relation to improvement of the beach landscape (hereafter "BCE1"). The beach cleanup temporarily reduced the remnant plastic litter at one time, after which it started accumulating again.

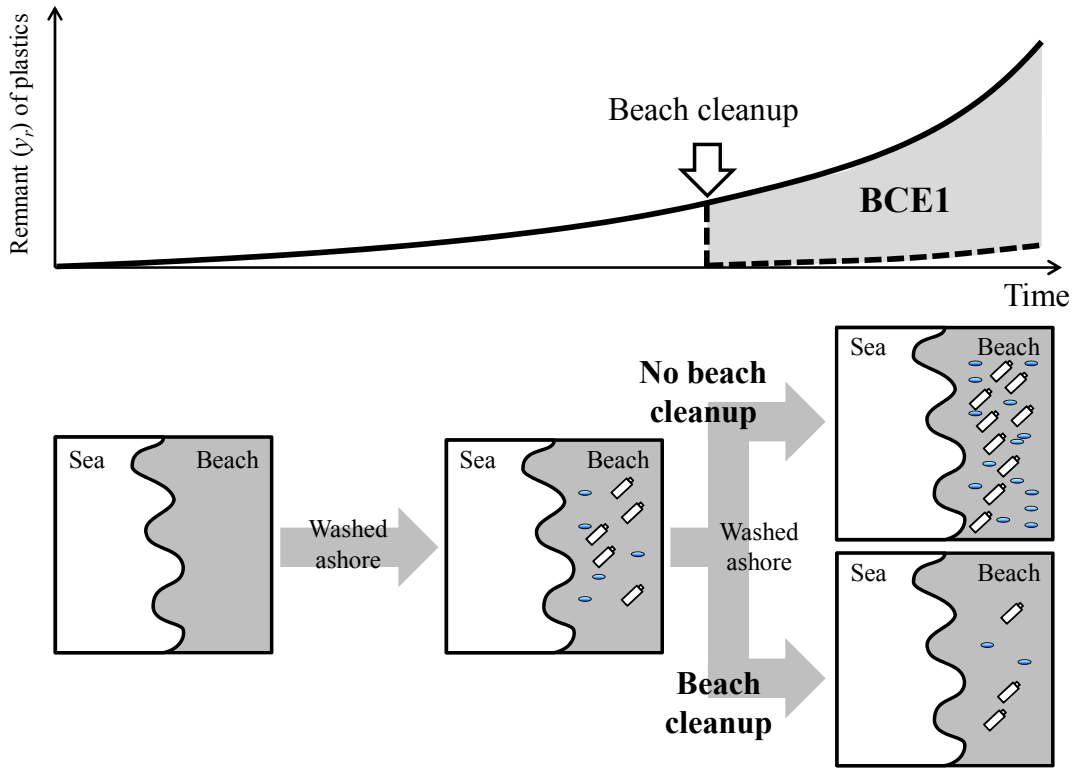

Figure 4-1. Schematic image of a beach cleanup effect in relation to improvement of the beach landscape (BCE1).

Finally, the remnant amount approached that without a beach cleanup.

Therefore, BCE1 is evaluated based on the difference between the cumulative remnant with and without beach cleanup. In the time-invariant linear system, the remnant ($y_r(t)$) on the beach is defined by Eq. (4.2): $y_r(t) = y(t)$. The cumulative remnant $Y_r(t)$ is evaluated by the integral of Eq. (4.2):

$$Y_r(t) = \int_0^t \int_0^{\tau'} x(\tau) h(t-\tau) d\tau d\tau' = \int_0^t y_r(\tau) d\tau \,. \tag{4.7}$$

4.2.3 Beach cleanup effect 2 (BCE2): Decrease in total mass of toxic metals

Figure 4-2 shows a schematic image of the beach cleanup effect in relation to toxic metals that could leach into the beach from plastics (hereafter "BCE2"). Based on Nakashima et al. (2012), toxic metals leach into the beach via surrounding water (e.g., rainwater). Most beach litter would have washed ashore after being transported in the ocean. Toxic metals might have leached from the surface of plastics via seawater when the plastics are washed ashore. However, toxic metals are likely to leach into the beach by mechanical weathering on the beach.

Considering a time-invariant linear system, the leaching flux ($y_m(t)$) of toxic metals from the remnant is estimated as follows:

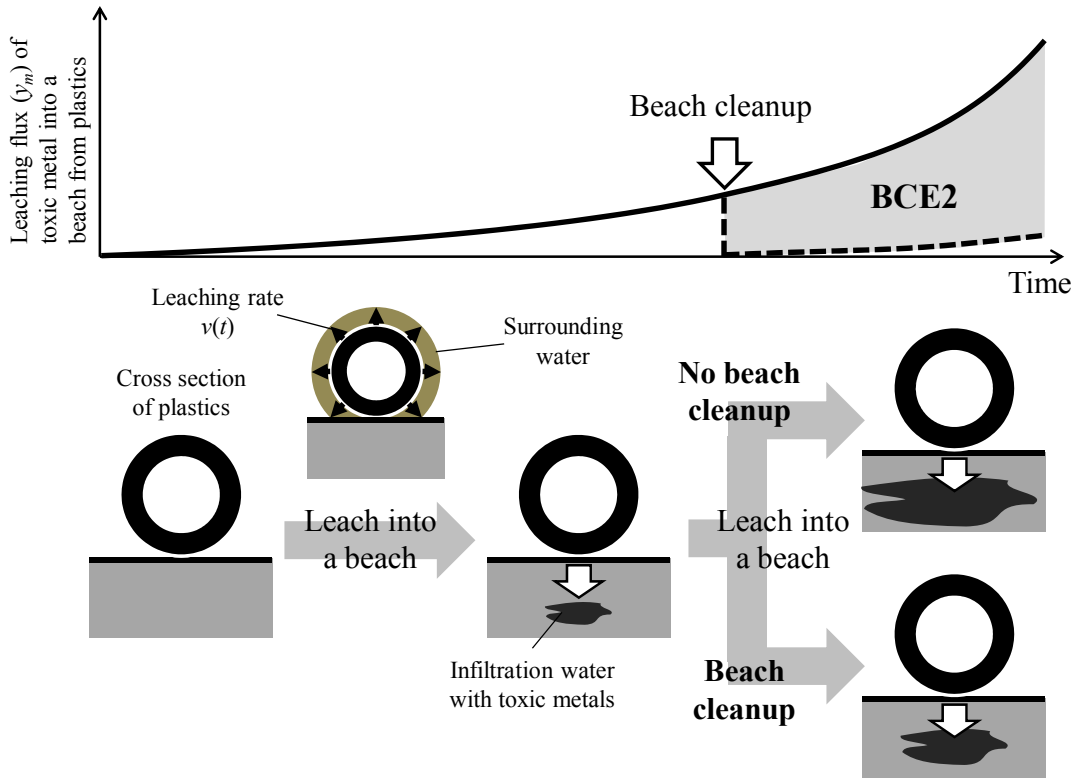

Figure 4-2. Schematic image of a beach cleanup effect in relation to toxic metals that could leach into the beach from plastics (BCE2).

$$y_m(t) = \int_0^t v(t-\tau)(t-\tau)x(\tau)h(t-\tau)d\tau \,. \tag{4.8}$$

where $t-\tau$ denotes the age from when the plastic litter washed ashore to time t. $v(t)$ is the leaching rate of toxic metals from one plastic object. The total mass ($Y_m(t)$) of toxic metals leached into the beach is estimated by the integral of Eq. (4.8):

$$Y_m(t) = \int_0^t \int_0^{\tau'} v(t-\tau)(t-\tau)x(\tau)h(t-\tau)d\tau d\tau' = \int_0^t y_m(\tau)d\tau \,. \tag{4.9}$$

Therefore, BCE2 is evaluated based on the difference between the total mass with and without conducting beach cleanup.

4.2.4 Beach cleanup effect 3 (BCE3): Prevention of plastic fragment generation

Figure 4-3 shows a schematic image of the beach cleanup effect in relation to fragmentation of plastics (hereafter "BCE3"). Plastics could eventually break down due to exposure to solar UV radiation and beach temperature (Andrady, 2011). Portions of the plastic surface could exfoliate in the breakdown process as the result of a chemical change that drastically reduces the average molecular weight of the polymer (Andrady, 2011). We assume the generation of plastic fragments by the breakdown and exfoliation

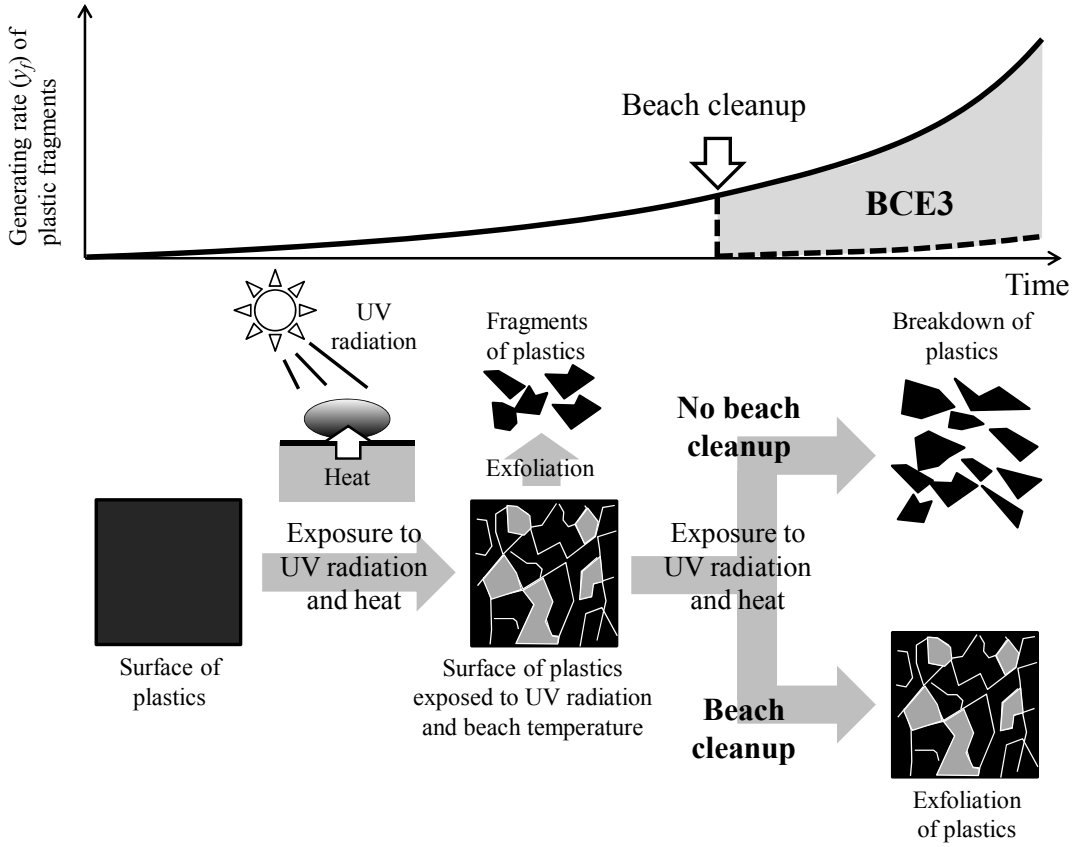

Figure 4-3. Schematic image of a beach cleanup effect in relation to plastic fragmentation (BCE3).

of plastics.

Considering the time-invariant linear system, the generating rate ($y_f(t)$) of plastic fragments is estimated as follows:

$$y_f(t) = \int_0^t p(t-\tau)x(\tau)h(t-\tau)d\tau \,. \tag{4.10}$$

where $p(t)$ is the probability that plastic fragments are generated from the remnant per unit time (hereafter "generating probability"). The amount of fragments ($Y_f(t)$) generated from the remnant on the beach is estimated by the integral of Eq. (4.10):

$$Y_f(t) = \int_0^t \int_0^{\tau'} p(t-\tau)x(\tau)h(t-\tau)d\tau d\tau' = \int_0^t y_f(\tau)d\tau \,. \tag{4.11}$$

Therefore, BCE3 is evaluated based on the difference between the amount of plastic fragments with and without conducting beach cleanup.

4.2.5 Evaluation of three beach cleanup effects

To evaluate the three beach cleanup effects, it is necessary to define the litter input flux $x(t)$. The litter input flux usually shows seasonal variation due to oceanic and/or weather conditions (e.g., Bowman et al., 1998; Kako et al., 2010; Fig. 2-2 in Chapter 2). For example, immigration has local maximums on Wadahama Beach, Niijima Island in early summer (see 2.3.1) when the Kuroshio Current approaches the island (see 2.4.1). Accordingly, the idealized litter input flux is expressed as the combination of constant input and sinusoidal input:

$$x(t) = x_0 + a\sin(2\pi t/T). \tag{4.12}$$

where x_0, T and a are the average, period and amplitude of the idealized input flux, respectively. Basically, the output $y(t)$ depends on three combinations of x_0 and a (i.e., $x_0 > a$; $x_0 = a$; $x_0 < a$). In this chapter, to simply investigate the dependence of beach cleanup effects on the residence time, we assume that x_0 is equal to a (i.e., $x_0 = a$).

By defining the periodic litter input flux, BCE1 can be evaluated based on the cumulative remnant ($Y_r(t)$). On the other hand, to evaluate BCE2 and BCE3, the leaching rate ($v(t)$ in Eqs. (4.8) and (4.9)) and the generating probability ($p(t)$ in Eqs. (4.10) and (4.11)) must be determined, respectively.

In general, the leaching rate of toxic metals from one plastic object would depend on various factors, such as the chemical elements, polymer type and depth from the plastic surface to the concentration of toxic metals. Precipitation would also determine the leaching flux (Nakashima et al. (2012)). On the other hand, fragmentation of plastics might occur more rapidly in the summer season due to stronger UV radiation and higher beach temperature. The generating rate of plastic fragments would also depend on vari-

ous factors, such as the polymer type (e.g., Gregory and Andrady, 2003; Andrady, 2011). In addition, the breakdown of plastics could quickly generate more plastic fragments than exfoliation of the plastic surface. In this chapter, to simply investigate the dependence of BCE2 and BCE3 on the residence time, we assume that the leaching rate of toxic metals from one plastic remnant is a constant value (i.e., $v(t) = v_0$) and that the generating probability $p(t)$ is proportional to the age of the remnant ($t-\tau$) (i.e., $p(t) = p_0(t-\tau)$).

Assuming a constant leaching rate (v_0) and proportional generating probability ($p_0(t-\tau)$), the leaching flux ($y_m(t)$) and the generating rate ($y_f(t)$) depend on the total age ($y_a(t)$):

$$y_a(t) = \int_0^t (t-\tau)x(\tau)h(t-\tau)d\tau . \tag{4.13}$$

Using $y_a(t)$, $y_m(t)$ and $y_f(t)$ are expressed as:

$$\begin{cases} y_m(t) = v_0 y_a(t), \\ y_f(t) = p_0 y_a(t). \end{cases} \tag{4.14}$$

Both the total mass of toxic metals leached into the beach ($Y_m(t)$) and the amount of plastic fragments ($Y_f(t)$) depend on the cumulative age ($Y_a(t)$):

$$Y_a(t) = \int_0^t \int_0^{\tau'} (t-\tau)x(\tau)h(t-\tau)d\tau d\tau' = \int_0^t y_a(\tau)d\tau . \tag{4.15}$$

Using $Y_a(t)$, $Y_m(t)$ and $Y_f(t)$ are expressed as:

$$\begin{cases} Y_m(t) = v_0 Y_a(t), \\ Y_f(t) = p_0 Y_a(t). \end{cases} \tag{4.16}$$

Therefore, in this chapter, BCE1 is evaluated based on the difference between the cumulative remnant with and without conducting beach cleanup, and BCE2 and BCE3 are evaluated based on the difference between the cumulative age with and without beach cleanup.

4.3 Results

4.3.1 System characteristics of exponential decay type UIR

Figure 4-4 shows the system characteristics of exponential decay type UIR. The system characteristics depend on the dimensionless residence time (i.e., $\zeta = \tau_r/T$). The amplification factor A and the phase lag θ (not time lag) respectively approach 1 and 0 as $\zeta \to 0$. For $\zeta \gg 1$, $A \approx 0$ and $\theta \approx 90°$ (= $\pi/2$). If the litter input period T is 365 days, the system characteristics of a beach with one month, one year and ten years of residence

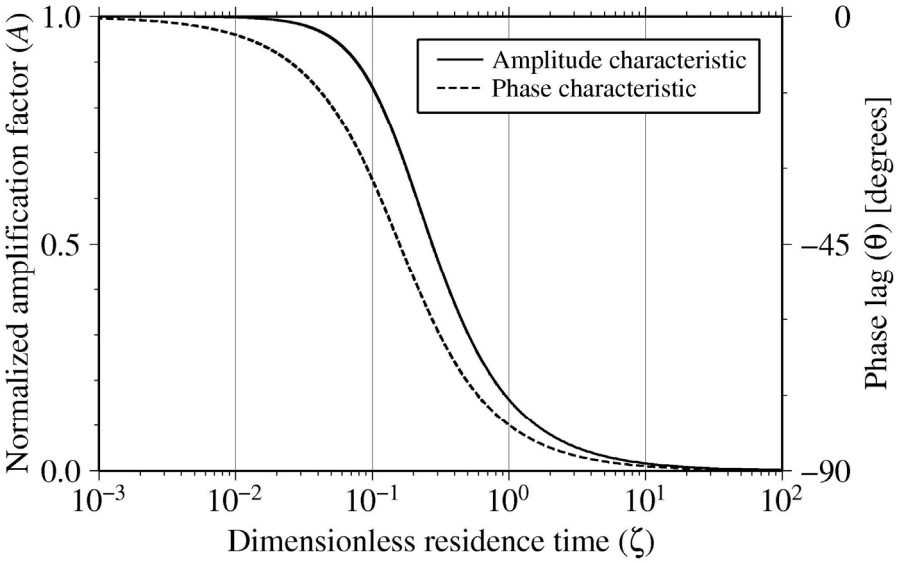

Figure 4-4. System characteristics as functions of ζ. The meaning of lines is shown in the upper right box.

time are determined by 10^{-1}, 10^{0} and 10^{1} of ζ. Table 4-1 shows A and θ (degrees) for $\zeta = 10^{-1}$, 10^{0} and 10^{1}. The amplification factor A (phase lag θ) in the case of $\zeta = 10^{1}$ is smaller (larger) than that of $\zeta = 10^{-1}$, and the time-variant float input in the case of $\zeta = 10^{1}$ would have a lower impact on the beach environment than that of $\zeta = 10^{-1}$.

Table 4-1. Normalized amplification factor A and phase lag θ in the case of $\zeta = 10^{1}$, 10^{0} and 10^{-1}.

Dimensionless residence time ζ	Normalized amplification factor A	Phase lag θ [degrees]
10^{1}	1.59×10^{-2}	-89.09
10^{0}	1.57×10^{-1}	-80.96
10^{-1}	8.47×10^{-1}	-32.14

4.3.2 Dependence of temporal evolution of remnant and total age on the residence time

Substituting the UIR (Eq. (4.1)) and the idealized input flux (Eq. (4.12)) into Eq. (4.2), the remnant ($y_r(t)$) is given by:

$$y_r(t) = x_0 \int_0^t \exp\left[-(t-\tau)/\tau_r\right] d\tau + a \int_0^t \sin(2\pi t/T) \exp\left[-(t-\tau)/\tau_r\right] d\tau$$

$$= x_0 \tau_r \left[1 - \exp(-t/\tau_r)\right] + a\,\tau_r A\left[\sin(2\pi t/T + \theta) - \sin\theta \exp(-t/\tau_r)\right]. \quad (4.17)$$

Normalizing $y_r(t)$ by $x_0 \tau_r$, the dimensionless remnant (y'_r) is considered as a function of ζ and the dimensionless time ξ normalized as the elapsed time (t) by the litter input period (T) (i.e., $\xi = t/T$):

$$y'_r(\xi,\zeta)=\frac{y_r}{x_0\tau_r}=y'^{const}_r+y'^{\sin}_r. \tag{4.18}$$

where y'^{const}_r and $y'^{\sin}_r$ are the constant and sinusoidal components of the dimensionless remnant calculated from the constant and sinusoidal components of $x(t)$, respectively:

$$\begin{cases} y'^{const}_r = 1-\exp(-\xi/\zeta), \\ y'^{\sin}_r = \dfrac{a}{x_0}A\left[\sin(2\pi\xi+\theta)-\sin\theta\exp(-\xi/\zeta)\right]. \end{cases} \tag{4.19}$$

where A and θ of Eq. (4.19) are the normalized amplification factor (Eq. (4.5)) and the phase lag (Eq. (4.6)), respectively. In this study, we assume that $a/x_0 = 1$ (see 4.2.5). On the other hand, substituting the UIR (Eq. (4.1)) and idealized input flux (Eq. (4.12)) into Eq. (4.13), the total age ($y_a(t)$) is given by:

$$\begin{aligned} y_a(t) &= x_0\int_0^t (t-\tau)\exp\left[-(t-\tau)/\tau_r\right]d\tau + a\int_0^t (t-\tau)\sin(2\pi t/T)\exp\left[-(t-\tau)/\tau_r\right]d\tau \\ &= x_0\tau_r^2\left[1-(1+t/\tau_r)\exp(-t/\tau_r)\right] \\ &\quad + a\tau_r^2 A\left[A\sin(2\pi t/T+2\theta)-(t/\tau_r)\sin\theta\exp(-t/\tau_r)-A\sin 2\theta\exp(-t/\tau_r)\right]. \end{aligned} \tag{4.20}$$

Normalizing $y_a(t)$ by $x_0\tau_r^2$ in the same way as in Eqs. (4.18) and (4.19), the dimensionless total age y'_a is also considered as a function of ζ and ξ:

$$y'_a(\xi,\zeta)=\frac{y_a}{x_0\tau_r^2}=y'^{const}_a+y'^{\sin}_a. \tag{4.21}$$

where y'^{const}_a and $y'^{\sin}_a$ are the constant and sinusoidal components of the dimensionless total age calculated from the constant and sinusoidal components of $x(t)$, respectively:

$$\begin{cases} y'^{const}_a = 1-(1+\xi/\zeta)\exp(-\xi/\zeta), \\ y'^{\sin}_a = \dfrac{a}{x_0}A\left[A\sin(2\pi\xi+2\theta)-(\xi/\zeta)\sin\theta\exp(-\xi/\zeta)-A\sin 2\theta\exp(-\xi/\zeta)\right]. \end{cases} \tag{4.22}$$

Figures 4-5c and 4-5d show the dependence of the dimensionless remnant (y'_r) and the total age (y'_a) on the dimensionless residence time (ζ), respectively. Both y'_r and y'_a completely depend on ζ. If the residence time (τ_r) is shorter than the input period (T) (e.g., $\zeta = 10^{-1}$), both constant components (i.e., y'^{const}_r and y'^{const}_a) of y'_r and y'_a quickly increase (gray dash-dotted line in Figs. 4-5a and 4-5b). Conversely, if τ_r is longer than T (e.g., $\zeta = 10^{1}$), both y'^{const}_r and y'^{const}_a slowly increase (gray solid line in Figs. 4-5a and 4-5b). If $\xi \to \infty$, y'_r and y'_a finally approach:

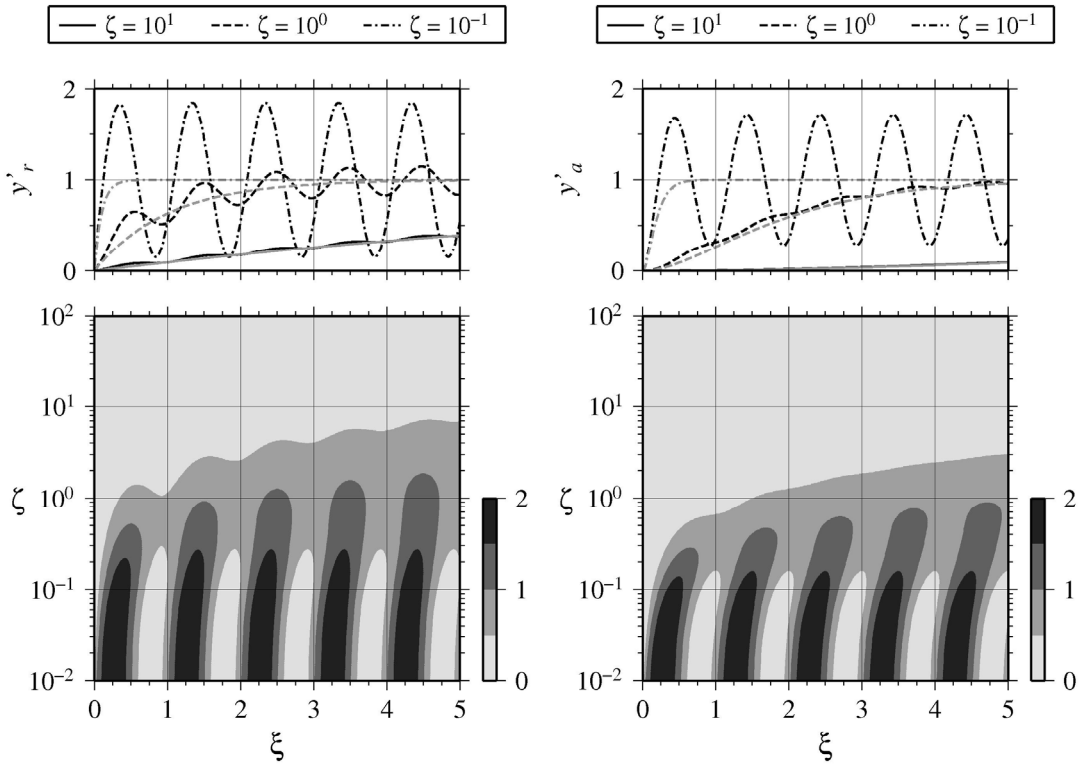

Figure 4-5. Dependence of the temporal evolution of dimensionless remnant y'_r and total age y'_a on the dimensionless residence time ζ. Panels (a) and (b) show the temporal evolution of y'_r and y'_a of $\zeta = 10^1$ (solid line), 10^0 (broken line) and 10^{-1} (dash-dotted line), respectively. In (a) and (b), the black line denotes y'_r and y'_a, and the gray line denotes the constant components of y'_r and y'_a. Panels (c) and (d) show the temporal evolution of y'_r and y'_a in the range from 10^{-2} to 10^2 of ζ, respectively. The white-black gradation of (c) and (d) denotes y'_r and y'_a, respectively. The gradation scale is shown on the right side of (c) and (d).

$$y'_r \to 1 + \frac{a}{x_0} A \sin\left(2\pi\xi + \theta\right) \ , \tag{4.23}$$

$$y'_a \to 1 + \frac{a}{x_0} A^2 \sin\left(2\pi\xi + 2\theta\right) \tag{4.24}$$

as predicted by Eq. (4.19) and Eq. (4.22), respectively. The dimensionless remnant y'_r (dimensionless total age y'_a) fluctuates with the amplitude A (A^2) at around $x_0\tau_r$ ($x_0\tau_r^2$), and has a phase delay of θ (2θ) compared with the litter input flux. The relaxation time t_{90} until y'_r and y'_a reach 90% of $x_0\tau_r$ and $x_0\tau_r^2$ are respectively determined by the constant components of y'_r ($y_r'^{const} = 0.9$) and y'_a ($y_a'^{const} = 0.9$), which are 2.3ζ and 3.9ζ. Thus, the relaxation time is proportional to the dimensionless residence time ζ.

Overall, the constant components ($y_r'^{const}$ and $y_a'^{const}$) dominate the temporal evolution. The contribution of the sinusoidal components ($y_r'^{\sin}$ and $y_a'^{\sin}$) to the temporal evolution is determined by the amplitude of the sinusoidal components (A and A^2). The normalized amplification factor A depends on the dimensionless residence time (ζ) (Fig.

4-4). For instance, A of $\zeta = 10^{-1}$ is much larger than that of $\zeta = 10^{1}$ (Table 4-1).

4.3.3 Dependence of temporal evolution of cumulative remnant and age on the residence time

The cumulative remnant ($Y_r(t)$) and age ($Y_a(t)$) are calculated by the integral of the remnant (y_r(t)) and the total age (y_a(t)), respectively. Substituting the remnant (Eq. (4.17)) into Eq. (4.7), the cumulative remnant ($Y_r(t)$) is given by:

$$\begin{aligned} Y_r(t) &= x_0\tau_r\int_0^t\left[1-\exp\left(-t/\tau_r\right)\right]d\tau + a\tau_r\int_0^t\left[A\sin\left(2\pi t/T+\theta\right)-A\sin\theta\exp\left(-t/\tau_r\right)\right]d\tau \\ &= x_0\tau_r^2\left[t/\tau_r-1+\exp\left(-t/\tau_r\right)\right] \\ &\quad + a\tau_r^2 A\left\{-\frac{1}{2\pi\tau_r/T}\left[\cos\left(2\pi t/T+\theta\right)+\cos\theta\right]+\sin\theta\left[\exp\left(-t/\tau_r\right)-1\right]\right\}. \end{aligned} \tag{4.25}$$

Normalizing $Y_r(t)$ by $x_0\tau_r^2$, the dimensionless cumulative remnant Y'_r is considered as a function of the dimensionless residence time (ζ) and the dimensionless time (ξ):

$$Y'_r(\xi,\zeta) = \frac{Y_r}{x_0\tau_r^2} = Y_r'^{const} + Y_r'^{\sin}. \tag{4.26}$$

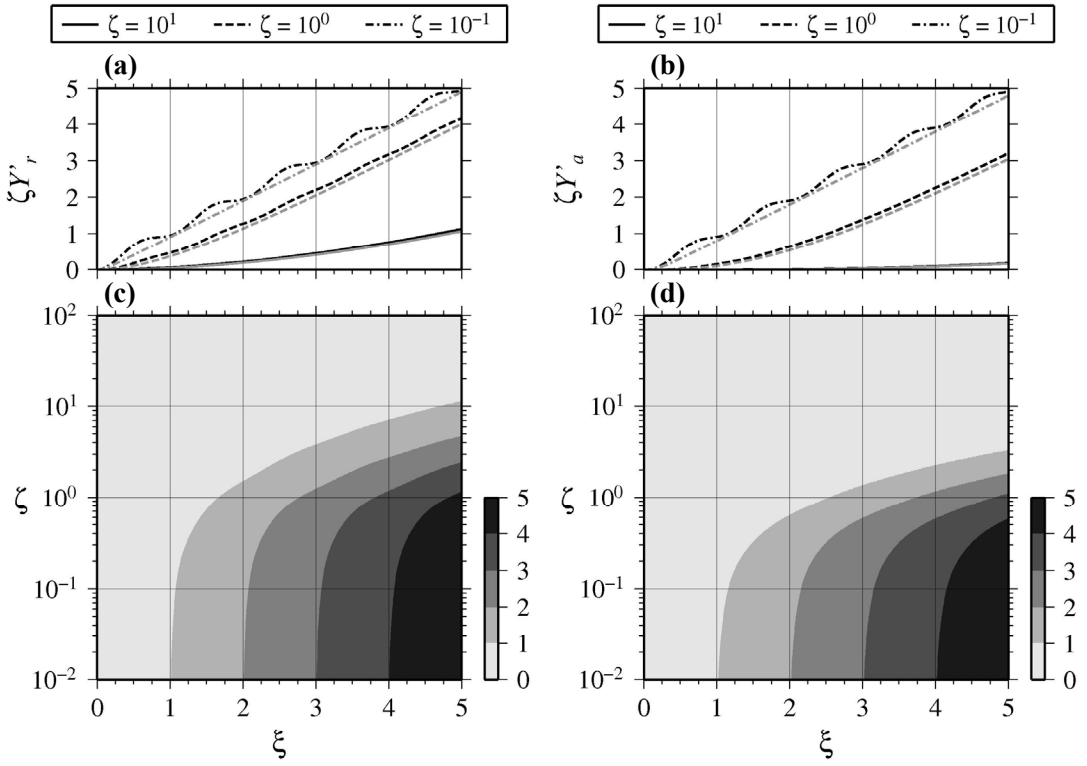

Figure 4-6. Dependence of the temporal evolution of the dimensionless cumulative remnant Y'_r and age Y'_a on the dimensionless residence time ζ. Note that Y'_r and Y'_a are multiplied by ζ. (i.e., $\zeta Y'_r$ and $\zeta Y'_a$). The format is the same as that of Fig. 4-5.

where $Y_r'^{const}$ and $Y_r'^{\sin}$ are the constant and sinusoidal components of the dimensionless remnant calculated from the constant and sinusoidal components of $x(t)$, respectively:

$$\begin{cases} Y_r'^{const} = \xi/\zeta - 1 + \exp(-\xi/\zeta), \\ Y_r'^{\sin} = \dfrac{a}{x_0} A\left[-\dfrac{1}{2\pi\zeta}\left[\cos(2\pi\xi + \theta) + \cos\theta\right] + \sin\theta\left[\exp(-\xi/\zeta) - 1\right]\right]. \end{cases} \quad (4.27)$$

where A and θ of Eq. (4.19) are the normalized amplification factor (Eq. (4.5)) and the phase lag (Eq. (4.6)), respectively. In this study, we assume that $a/x_0 = 1$ (see 4.2.5).

On the other hand, substituting the total age (Eq. (4.20)) into Eq. (4.15), the cumulative age ($Y_a(t)$) is given by:

$$\begin{aligned} Y_a(t) &= x_0\tau_r^2 \int_0^t \left[1 - (1 + t/\tau_r)\exp(-t/\tau_r)\right] d\tau \\ &\quad + a\tau_r^2 \int_0^t \left[A^2 \sin(2\pi t/T + 2\theta) - A(t/\tau_r)\sin\theta\exp(-t/\tau_r) - A^2 \sin 2\theta \exp(-t/\tau_r)\right] d\tau \\ &= x_0\tau_r^3\left[t/\tau_r - 2 + (t/\tau_r + 2)\exp(-t/\tau_r)\right] \\ &\quad + a\tau_r^3 A\left\{ \frac{A}{2\pi\tau_r/T}\left[\cos 2\theta - \cos(2\pi t/T + 2\theta)\right] - (\sin\theta + A\sin 2\theta)\left[1 - \exp(-t/\tau_r)\right] \right. \\ &\qquad \left. + (t/\tau_r)\sin\theta\exp(-t/\tau_r)\right\}. \end{aligned} \quad (4.28)$$

Normalizing $Y_a(t)$ by $x_0\tau_r^3$, the dimensionless cumulative age Y'_a is also considered as a function of ζ and ξ:

$$Y_a'(\xi, \zeta) = \frac{Y_a}{x_0\tau_r^3} = Y_a'^{const} + Y_a'^{\sin}. \quad (4.29)$$

$$\begin{cases} Y_a'^{const} = \xi/\zeta - 2 + (\xi/\zeta + 2)\exp(-\xi/\zeta), \\ Y_a'^{\sin} = \dfrac{a}{x_0} A\left\{ \dfrac{A}{2\pi\zeta}\left[\cos 2\theta - \cos(2\pi\xi + 2\theta)\right] - (\sin\theta + A\sin 2\theta)\left[1 - \exp(-\xi/\zeta)\right] \right. \\ \qquad \left. + (\xi/\zeta)\sin\theta\exp(-\xi/\zeta)\right\}. \end{cases} \quad (4.30)$$

Figures 4-6c and 4-6d show the dependence of the dimensionless cumulative remnant (Y'_r) and age (Y'_a) on the dimensionless residence time (ζ), respectively. Both Y'_r and Y'_a completely depend on ζ, namely, Y'_r and Y'_a become much smaller as ζ becomes larger. To simply describe the dependence of Y'_r and Y'_a on ζ, Y'_r and Y'_a are multiplied by ζ in Fig. 4-6. If the residence time (τ_r) is shorter than the input period (T) (e.g., $\zeta = 10^{-1}$), both constant components (i.e., $Y_r'^{const}$ and $Y_a'^{const}$) of Y'_r and Y'_a quickly increase corresponding to the temporal variation of y'_r and y'_a (gray dash-dotted line in Figs. 4-6a and 4-6b). Conversely, if τ_r is longer than T (e.g., $\zeta = 10^1$), the constant components slowly increase (gray solid line in Figs. 4-6a and 4-6b). If $\xi \to \infty$, Y'_r and Y'_a become:

$$Y_r' \to \xi/\zeta - 1 + \frac{a}{x_0} A\left[-\frac{1}{2\pi\zeta}\left[\cos(2\pi\xi + \theta) + \cos\theta\right] - \sin\theta \right] \text{ and} \tag{4.31}$$

$$Y_a' \to \xi/\zeta - 2 + \frac{a}{x_0} A\left\{ \frac{A}{2\pi\zeta}\left[\cos 2\theta - \cos(2\pi\xi + 2\theta)\right] - \sin\theta - A\sin 2\theta \right\}. \tag{4.32}$$

Clearly, both Y'_r and Y'_a are proportional to the dimensionless time (ξ) because the first term of Eqs. (4.31) and (4.32) is significantly larger than the other terms of these equations. Therefore, the constant components dominate the temporal evolution of Y'_r and Y'_a compared with the sinusoidal components. Furthermore, corresponding to the temporal variation of y'_r and y'_a, the temporal evolution of Y'_r and Y'_a is also determined by the amplitude of the sinusoidal components. If ζ is smaller, the amplitude is larger (see Table 4-1). This suggests that the beach cleanup effects depend on the time duration of the beach cleanup (hereafter "cleaning time").

4.3.4 Example of beach cleanup effects on Wadahama Beach

The average residence time on Wadahama Beach was 224 days (see 2.3.2). Also, the litter input period (T) is considered to be 365 days due to the seasonal variation of immigration. Thus, the dimensionless residence time ζ becomes 0.61. As mentioned in

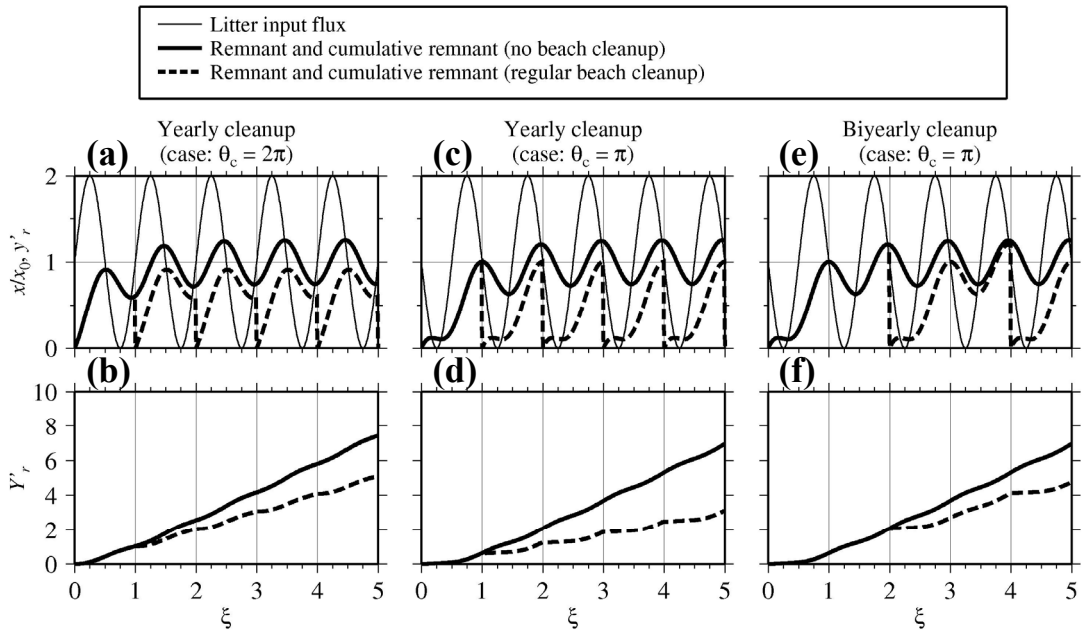

Figure 4-7. Temporal evolution of the dimensionless remnant y'_r and cumulative remnant Y'_r during the five periods in the case of 0.61 of dimensionless residence time ζ. Panels (a), (c) and (e) show the temporal evolution of y'_r in the case of yearly cleanup at 2π of the cleaning phase θ_c, yearly cleanup at $\theta_c = \pi$ and biyearly cleanup at $\theta_c = \pi$, respectively. Panels (b), (d) and (f) show the temporal evolution of Y'_r in these three patterns of regular cleanups. The meaning of lines is shown in the upper box.

4.1, beach clearance is basically conducted yearly, such as in the International Coastal Cleanups (Ocean Conservancy, 2012). Here, we show an example of the beach cleanup effects (hereafter "BCEs") on Wadahama Beach in a case where beach cleanup is conducted yearly or biyearly.

The temporal evolution of four dimensionless responses (i.e., remnant (y'_r), cumulative remnant (Y'_r), total age (y'_a) and cumulative age (Y'_a)) after a beach cleanup can be represented by shifting the time from the start of the temporal evolution to the cleaning time t_c (i.e., $t \to t - t_c$) and delaying the phase of all sinusoidal and cosinusoidal components of Eqs. (4.19), (4.22), (4.27) and (4.30) because the temporal evolution of four responses should be described from the phase of the litter input period at the cleaning time (hereafter "cleaning phase θ_c"), such as $\sin\theta \to \sin(\theta + \theta_c)$; $\cos\theta \to \cos(\theta + \theta_c)$. Thus, the BCEs are evaluated by dividing the difference between the cumulative responses (i.e., Y'_r and Y'_a) with and without conducting beach cleanup.

Figures 4-7a and 4-7b show the temporal variation of y'_r and Y'_r in a case where beach cleanups are conducted yearly at 2π of the cleaning phase θ_c, respectively (bold solid line: no cleanup; bold broken line: regular cleanup). Figures 4-8a and 4-8b show the temporal variation of y'_a and Y'_a in the same case (i.e., $\theta_c = 2\pi$). If the cleanups are conducted yearly at 2π of the cleaning phase θ_c (Figs. 4-7a and 4-8a), the cumulative remnant (Fig. 4-7b) and age (Fig. 4-8b) can be reduced by 31% and 63%, respectively, compared with that with no beach cleanups after five periods (i.e., $\xi = 5$) (Table 4-2).

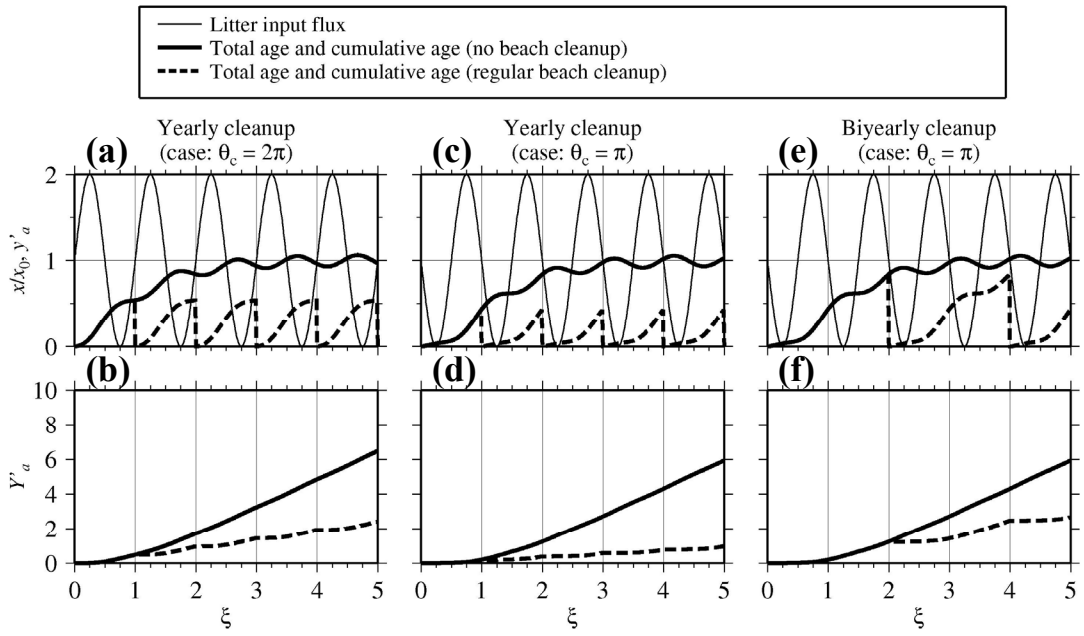

Figure 4-8. Temporal evolution of the dimensionless total age y'_a and cumulative age Y'_a during the five periods in the case of 0.61 of dimensionless residence time ζ. The format is the same as that of Fig. 4-7.

Table 4-2. Beach cleanup effects (BCEs) calculated from the dimensionless cumulative remnant Y'_r and age Y'_a after the five periods in the case of yearly cleanup at 2π of the cleaning phase θ_c, yearly cleanup at $\theta_c = \pi$ and biyearly cleanup at $\theta_c = \pi$.

		Yearly cleanup (case: $\theta_c = 2\pi$)	Yearly cleanup (case: $\theta_c = \pi$)	Biyearly cleanup (case: $\theta_c = \pi$)
Dimensionless cumulative remnant Y'_r	No cleanup	7.44	6.95	6.95
	Cleanup	5.10	3.10	4.76
	BCE (%)	31	55	32
Dimensionless cumulative age Y'_a	No cleanup	6.47	5.92	5.92
	Cleanup	2.41	0.97	2.66
	BCE (%)	63	84	55

On the other hand, regular cleanups conducted at $\theta_c = \pi$ (Figs. 4-7c and 4-8c) can greatly reduce the cumulative remnant (Fig. 4-7d) and age (Fig. 4-8d). The BCEs of the cumulative remnant and age in this case are 55% and 84%, respectively (Table 4-2). Therefore, the BCEs depend on the timing of the regular cleanups (i.e., cleaning phase θ_c). Regular cleanups at $\theta_c = \pi$ are more effective than that at $\theta_c = 2\pi$. On Wadahama Beach (or $\zeta = 0.61$), the remnant at $\theta_c = \pi$ mostly corresponds to the peak of the remnant because the phase lag θ is 81° (Table 4-1). This demonstrates that beach cleanup at the time of the remnant peak is the most effective.

Generally, beach clearance involves high labor costs. If it is conducted every two years, it should be timed to coincide with the remnant peak. Even if beach cleanup is conducted only once every two years, it is as effective as regular cleanup at $\theta_c = 2\pi$ (Figs. 4-7e, 4-8e and Table 4-2). This indicates that the cleaning phase is an important factor for conducting effective beach cleanups.

4.3.5 Dependence of the effect of beach clearance on the residence time

Figures 4-9a and 4-10a describe the dependence of BCEs for the remnant and total age by yearly cleanups during the five input periods on both the dimensionless residence time (ζ) and the cleaning phase (θ_c), respectively. The horizontal axes of Figs. 4-9a and 4-10a denote the phase lag ($d\theta$) between the phase of the input flux at the remnant peak determined by Eq. (4.6) (e.g., $\pi/2-\theta$ because the phase at the remnant peak is defined by $2\pi\xi + \theta = \pi/2$; see Eq. (4.19)) and the cleaning phase (θ_c): $d\theta = (\pi/2 - \theta) - \theta_c$. Note that θ is a negative phase lag (Eq. (4.6)). The vertical axes of Figs. 4-9a, and 4-10a denote the dimensionless residence time (ζ). The white-black gradation of Figs. 4-9a and 4-10a represents the BCEs calculated from the cumulative remnant (Y'_r) and age (Y'_a), respectively (see 4.3.4). The BCEs clearly increase as ζ

becomes longer. Conversely, regular cleanup on a beach with shorter ζ has little effect on the beach environment. Therefore, cleanups on a beach with longer ζ are more effective than that with shorter ζ.

Figures 4-9b and 4-10b show the dependence of BCEs of $\zeta = 10^{-1}$, 10^{0} and 10^{1} on the phase lag (dθ). At all levels of ζ, the BCEs for the remnant are fully maximized at d$\theta = 0$ (Figs. 4-9a and 4-9b). Thus, the most effective time for the remnant matches the time of the remnant peak (Figs. 4-9a and 4-9b). Furthermore, regular cleanups at around the remnant peak can also effectively reduce the cumulative age, although the maximum BCEs for the total age occur shortly after the time of the remnant peak (Figs. 4-10a and 4-10b). Therefore, beach cleanups conducted at around the remnant peak would become the most effective considering BCE1 (see 4.2.2), BCE2 (see 4.2.3) and BCE3 (see 4.2.4).

The maximum difference in BCEs (i.e., the difference between the maximum and minimum BCEs) also depends on the dimensionless residence time (ζ) (Figs. 4-9c and 4-10c). The maximum difference in $10^{-1} < \zeta < 10^{0}$ is larger than that in $\zeta > 10^{0}$. As mentioned in 4.3.3, the amplitude A of the cumulative remnant (Y'_r) and age (Y'_a) becomes

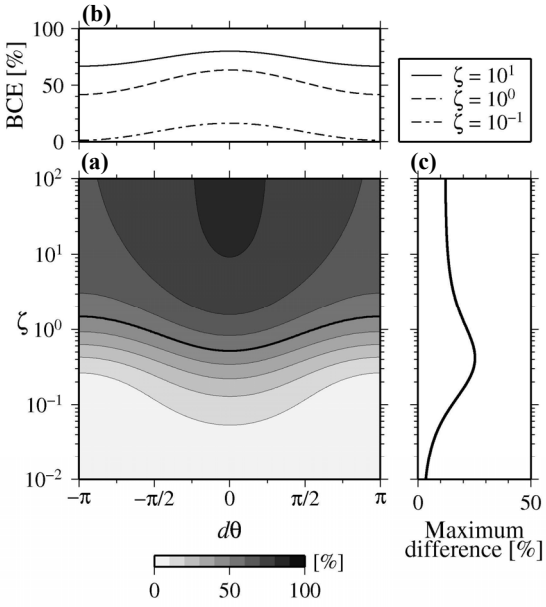

Figure 4-9. (a) Dependence of the beach cleanup effect (BCE) for the remnant on the normalized residence time ζ and the cleaning phase θ_c. The horizontal axis represents the phase lag dθ between the phase of input flux at the remnant peak and θ_c. The contour line and white-black gradation of (a) denotes the BCE; its scale is shown under panel (a). (b) Dependence of the BCE of $\zeta = 10^{1}$ (solid line), 10^{0} (broken line) and 10^{-1} (dash-dotted line) on θ_c. (c) Dependence of the maximum difference (i.e., difference between maximum and minimum BCE) on ζ.

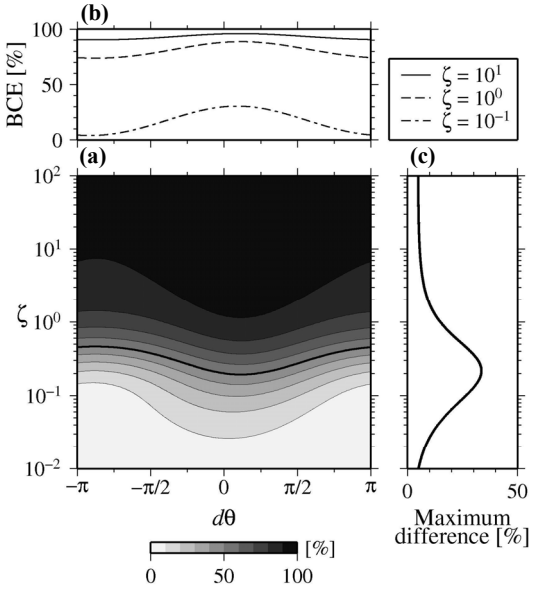

Figure 4-10. (a) Dependence of the beach cleanup effect (BCE) for total age on the normalized residence time ζ and the cleaning phase θ_c. The format is the same as that of Fig. 4-9.

smaller as ζ becomes longer (Fig. 4-4 and Table 4-1). If ζ is shorter than 10^{-1}, the maximum difference is small because the BCEs are very low (Figs. 4-9a and 4-10a). Therefore, the BCEs on beaches with longer residence time (τ_r) than the input period (T) ($\zeta > 10^0$) are weakly dependent on the clearing phase (θ_c). On the other hand, the BCEs on beaches with $10^{-1} < \zeta < 10^0$ are strongly dependent on θ_c.

4.4 Discussion

4.4.1 Efficacy of the time-invariant linear system in plastic pollution

To simply investigate the dependence of beach cleanup effects (BCEs) on the residence time, several assumptions are employed for evaluating the total mass of toxic metals leached into the beach and the amount of plastic fragments: the leaching rate ($v(t)$) of toxic metals from plastics is a constant and the generating probability ($p(t)$) is proportional to the remnant age ($t-\tau$). In actuality, $v(t)$ and $p(t)$ would depend on the local precipitation and UV radiation (and/or temperature). Thus, these functions should be determined according to the local site. In any case, if these reasonable functions can be obtained, we can evaluate the total mass of toxic metals and the amount of plastic fragments by applying the time-invariant linear system.

For example, Nakashima et al. (2012) estimated the leaching rate of lead stearate ($Pb(C_{18}H_{35}O_2)_2$) from PVC floats by laboratory experiment. The Fickian diffusion process has been applied to the estimation of the leaching rate. If $v(t)$ follows the diffusion process as applied in Nakashima et al. (2012), it can be approximated as an exponential function:

$$v(t) = v_0 \exp(-t/\tau_m). \tag{4.33}$$

where v_0 and τ_m denote the initial leaching rate and average time of toxic metal until leaching into the beach (hereafter "leaching time"). Substituting Eqs. (4.33) and (4.12) into Eq. (4.8), the leaching flux ($y_m(t)$) can be expressed as:

$$\begin{aligned} y_m(t) &= v_0 x_0 \int_0^t (t-\tau)\exp\left[-(t-\tau)/\beta\right]d\tau + a\int_0^t (t-\tau)\sin(2\pi t/T)\exp\left[-(t-\tau)/\beta\right]d\tau \\ &= v_0 x_0 \beta^2 \left[1-(1+t/\beta)\exp(-t/\beta)\right] \\ &\quad + v_0 a\beta^2 A'\left[A'\sin(2\pi t/T+2\theta') - (t/\beta)\sin\theta'\exp(-t/\beta) - A'\sin 2\theta'\exp(-t/\beta)\right]. \end{aligned} \tag{4.34}$$

where β denotes the coefficient determined by the residence time (τ_r) and the leaching time (τ_m):

$$\beta = \frac{\tau_r \tau_m}{\tau_r + \tau_m}. \tag{4.35}$$

Also, A' and θ' denote the normalized amplification factors and phase lag replacing τ_r of

Eq. (4.5) with β. Thus, the system characteristics of the leaching flux $y_m(t)$ (i.e., A' and θ') fully depend on β. In addition, $y_m(t)$ can be determined by β, and the total mass $Y_m(t)$ can also be evaluated by Eq. (4.9). Therefore, based on the exponential type of leaching rate, the beach cleanups depend on the ratio of β to the litter input period T corresponding to the dimensionless residence time ζ.

4.4.2 Suggestion for effective beach cleanup

Assuming that the remnant decreases exponentially, we can devise a plan for effective beach cleanup. This chapter demonstrated that beach cleanup is more effective at beaches with a residence time longer than the input period (i.e., $\zeta > 10^0$) for two reasons: (1) the beach cleanup effects (BCEs) are very high, and (2) the BCEs are weakly dependent on the clearing phase (Figs. 4-9a and 4-10a). Here, we discuss effective beach cleanup strategies based on the dependence of BCEs on the residence time.

Our suggestion is to conduct cleanup on beaches with a residence time of longer than one year because the amount of plastic litter on beaches has shown a seasonal variation (e.g., at six beaches along the Mediterranean Sea in Israel: Bowman et al. (1998); New Jersey beach in the US: Ribic (1998); Ookushi Beach in Japan: Kako et al. (2010); Wadahama Beach in Japan: see Fig. 2-2). The seasonal variation indicates that the predominant input period at these beaches is less than one year. Even if the litter input period (T) is shorter than the residence time (τ_r), the BCEs become relatively high because $\zeta > 10^0$ (Figs. 4-9a and 4-10a). Therefore, beach cleanup on these beaches would be more effective.

Moreover, cleanup on these beaches ($\zeta > 10^0$) has an advantage in terms of the weak dependence of the BCEs on the clearance time. Generally, beach cleanup is most effective when conducted at the time of the remnant peak (hereafter "effective time"). The time for conducting beach cleanups would be determined by various factors, such as weather conditions, availability of labor, and cost. In particular, the weather conditions are important for the safety of beach cleanups. If the remnant peak is during the stormy season, cleanup will be difficult. However, cleanup on beaches with a longer dimensionless residence time will likely have a sufficient effect even if it cannot be conducted at the most effective time.

To plan effective beach clearance, it is necessary to understand the residence time, input period and effective time. The residence time is not yet well understood except at Wadahama Beach in Japan (see 2.3.2). The residence time can be measured by the MR experiments described in 2.2.3. In addition, the residence time can be measured with relatively little labor by applying the transectional MR experiment that includes high

concentration areas (see 3.4.1). We also investigated the physical mechanism of the backwash of plastic litter, and demonstrated its relationship to nearshore circulation (see 3.4.1). Understanding the physical mechanism of the backwash of plastic litter enables us to estimate the residence time on multiple beaches, such as by establishing a model using hydrodynamic parameters (e.g., wave statistics).

Understanding the litter input period and the effective time has been difficult because there was no way to sequentially monitor the amount of beach litter on multiple beaches in order to obtain the input period and effective time. For example, the input period is consistent with the remnant period based on the time-invariant linear system (Eq. (4.17)). Thus, the predominant input period can be calculated by applying Fourier transformation to the temporal variability of the remnant. Furthermore, the effective time can be directly obtained as the time of the remnant peak through long-term monitoring. This would be an issue for conducting effective beach cleanups.

4.5 Conclusions

To demonstrate the advantage of the exponential decay of the amount of plastic litter, we suggested the quantification of beach cleanup effects (BCEs) assuming a time-invariant linear system for the remnant plastic litter, and investigated the dependence of BCEs on the residence time. This study focused on three BCEs: improvement of beach landscape (BCE1), decrease of the total mass of toxic metals (BCE2) and prevention of the generation of plastic fragments (BCE3).

In the time-invariant linear system, the exponential decay of the remnant corresponds to the unit impulse response (UIR), which enables us to understand the system characteristics. The system characteristics are fully determined by the residence time (τ_r) on the beach, and can be described as functions of the dimensionless residence time (ζ), which is defined as the ratio of τ_r to the periods of litter input variability (T). Considering a litter input flux expressed as a combination of constant and sinusoidal input, the temporal evolution of the remnant and total age depend on ζ.

Assuming the time-invariant linear system, evaluation of the three BCEs has been suggested in this chapter. BCE1 can be evaluated based on the remnant plastic litter on the beach (see 4.2.5). On the other hand, some assumptions are applied to the evaluation of BCE2 and BCE3: the leaching rate ($v(t)$) of toxic metals from plastics is a constant and the generating probability ($p(t)$) is proportional to the remnant age ($t-\tau$). By applying these assumptions, BCE2 and BCE3 can be evaluated based on the total age of plastic litter on the beach. Thus, in this study, the BCEs are evaluated based on the remnant and total age.

The residence time on Wadahama Beach, Niijima Island, Japan was successfully estimated by this study (see 2.3.2). At present, the residence time is not yet well understood except at Wadahama Beach. Thus, we investigated the BCEs after five years in the three patterns in which regular beach cleanups are conducted: yearly cleanup at 2π of the phase of litter input flux (hereafter "cleaning phase (θ_c)"), yearly cleanup at $\theta_c = \pi$ and biyearly cleanup at $\theta_c = \pi$. The BCEs depend on θ_c, and the yearly cleanup at $\theta_c = \pi$ is more effective than that at $\theta_c = 2\pi$. Also, the BCEs by biyearly cleanup at $\theta_c = \pi$ are almost the same as that by yearly cleanup at $\theta_c = 2\pi$. This indicates that the cleaning phase is an important factor for conducting effective beach cleanups.

Finally, we investigated the dependence of the BCEs on the dimensionless residence time (ζ) and the cleaning phase (θ_c). Generally, the BCEs clearly increase as ζ becomes longer. At all levels of ζ, the BCEs for both the remnant and total age are maximized by conducting the beach cleanups at around the phase of the remnant peak. This indicates that beach cleanups at the remnant peak are effective considering the three BCEs. The maximum difference of BCEs (i.e., the difference between the maximum and minimum BCEs) indicates that the dependence of θ_c differs according to ζ. The maximum difference in $10^{-1} < \zeta < 10^{0}$ is larger than that in $\zeta > 10^{0}$. This indicates that BCEs on beaches of $10^{-1} < \zeta < 10^{0}$ are strongly dependent on θ_c.

Beach cleanup is an important way to remove plastic litter from marine and coastal environments. To plan effective beach cleanups, we need to understand the residence time (τ_r), input period (T) and effective cleaning phase (θ_c). The residence time can be measured by MR experiments, but it is difficult to understand the input period and effective cleaning phase because there is no way to sequentially monitor the amount of beach litter on multiple beaches. This would be an issue for conducting effective beach cleanups.

CHAPTER 5

A new technique using a webcam for sequential monitoring of the amount of plastic litter on beaches

5.1 Introduction

Quantification of the amount of plastic litter on beaches depends on beach surveys conducted at a monthly or yearly time scale (e.g., Sheavly, 2007; Ryan et al., 2009; Seino et al., 2009; Ribic et al., 2010). Although these beach surveys can be used to investigate the amount, primary materials and type of beach litter, it is difficult to sequentially monitor the amount of plastic litter and understand its temporal variability at multiple sites because this requires immense manpower and cost. Moreover, to conduct effective beach cleanup, it is crucial to understand the remnant peak and predominant period for the input flux of plastic litter (see 4.4.2), which cannot be identified by monthly or yearly beach surveys. Thus, we developed a new technique for the sequential monitoring of plastic litter.

In fact, Kako et al. (2010) have already established a sequential monitoring system using webcams placed on Ookushi Beach on the Goto Islands, Japan, and computed the temporal variability in the amount of beach litter over a period of one and a half years. They considered the covered area as an index of the amount of beach litter and computed the covered area by counting the photograph pixels with lightness values that were higher than the established threshold value. In their study, the amount of beach litter generally fluctuated on a monthly or shorter time scale. Sequential monitoring by webcam would allow us to understand the remnant peak and predominant input period on multiple beaches at low operating and labor costs.

However, Kako et al. (2010) applied the lightness values to detect photograph pixels of plastic litter (hereafter “plastic pixels”) because of the prevalence of white polystyrene buoys in the beach litter on Ookushi Beach. As shown in their report, light-colored plastic pixels (e.g., white polystyrene) were detected by using the lightness values. However, dark-colored plastic pixels (e.g., blue or red plastics) were not detected. Generally, plastic litter on beaches consists of both light and dark colors. Thus, to obtain the temporal variability in the amount of plastic litter at multiple sites, it is necessary to develop a new technique for detecting plastic pixels with both light and dark colors.

Here, we describe a new technique for detecting plastic pixels of various colors and computing an area that is covered with plastic litter by using images taken by a webcam installed on Sodenohama Beach, Tobishima Island, Japan.

5.2 Materials and Methods

5.2.1 Study site

Tobishima Island is one of the more remote islands in the Sea of Japan where the majority of plastic litter washes ashore (NPEC, 2007). The Tsushima Current passes nearby, impacting the western shores of the island. Most plastic litter transported by the Tsushima Current is washed ashore on beaches facing the Sea of Japan compared with those facing the North Pacific coast (NPEC, 2007). Thus, the Sea of Japan would be a major route for plastic litter around Japan. In addition, large plastic items are washed ashore (e.g., fishing buoys, polythene tanks and polystyrene buoys) compared with the plastic litter found along the North Pacific coast.

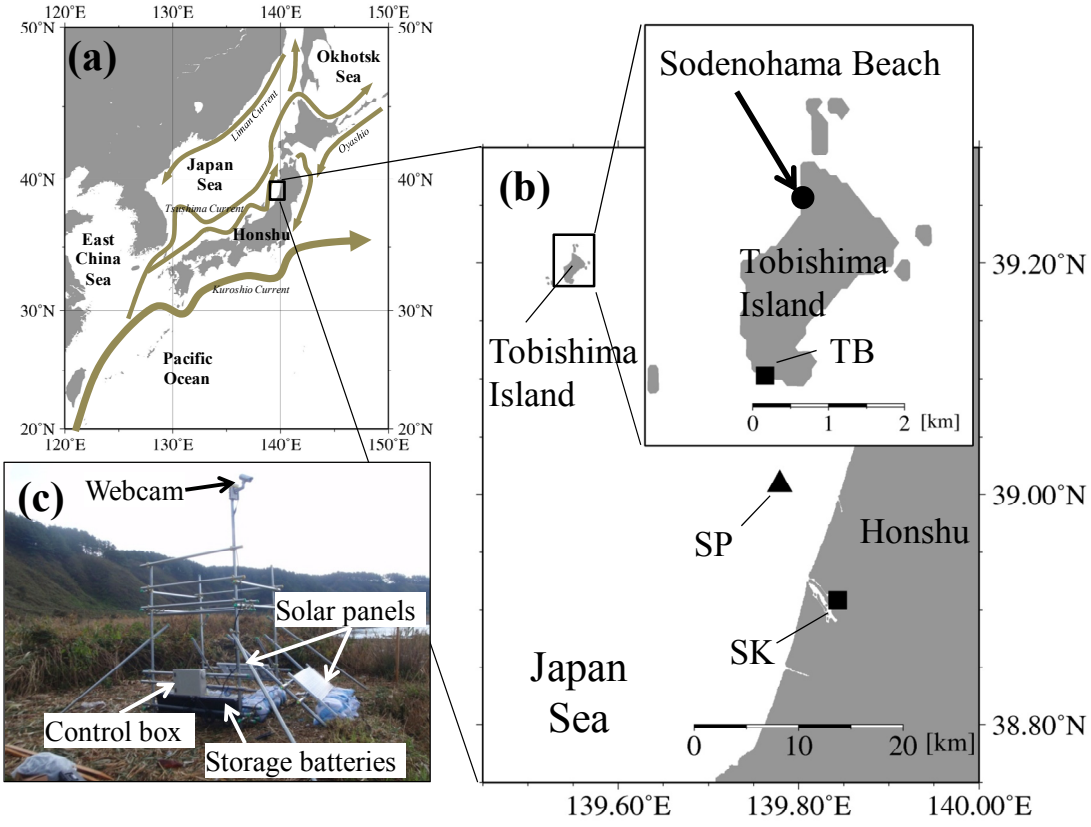

Figure 5-1. (a) Map showing sea currents around Japan, and (b) enlarged map of the area around Tobishima Island. Map (b) indicates the location of the webcam placed on Sodenohama Beach on Tobishima Island, the meteorological observatories (SK and TB) of the Japan Meteorological Agency (solid squares) and the seabed wave gauges (SP) of the Port and Airport Research Institute (solid triangles). (c) Photograph of the webcam system.

Sodenohama Beach is a rocky area about 20 m wide (Fig. 5-1). The beach is not a public bathing site and thus sees hardly any visitors. There is a mountain behind the beach and a gentle slope from the shoreline to 100 m offshore. The Sea of Japan generally has low tides; however, during the autumn and winter, high wind waves are produced by the northeasterly monsoon. Thus, plastic litter on the beach frequently moves during the autumn and winter due to wind waves induced by the northeasterly monsoon, while it hardly moves during the spring and summer.

5.2.2 Webcam monitoring system

The monitoring system consists of a webcam (IP7361, Vivotek), two solar panels (DC080-12, Denryo), two storage batteries (DC-31, ACDelco), a solar charge controller (SS-20L, Denryo), a timer (H2F-31, Omron), a mobile router (DCR-G54/U, I-O Data Device) and a mobile card (L-05A, LG Electronics). Electric power to operate the system is charged by the two storage batteries using the two solar panels. The webcam is controlled by the timer and operates every two hours from 07:00 to 15:00 (JST) (five times every day). Five photographs are taken at intervals of three minutes during each operation, resulting in 25 photographs daily. The photographs are transmitted to our laboratory via the Internet. They are also backed up on an SDHC card installed in the webcam.

5.2.3 Generation of color references to detect plastic pixels

Generally, plastic litter in the photographs is visually recognized from the shape or color. However, shape recognition is difficult to achieve in image processing since the shape of the plastic litter depends on its orientation to the webcam. Also, beached plastic litter has fragmented into smaller litter of various shapes by chemical and/or mechanical weathering. Thus, we attempted to detect plastic pixels by image processing based on the color. The color of plastic litter changes within a specific range of a certain color space due to the amount and angle of sunlight (Fig. 5-2a). To detect plastic pixels in images, the particular color range of the plastic litter in the color space, that is, a color reference, must be defined, and then each pixel can be identified as a plastic pixel or not according to its position in the color space. In order to define the color reference, the color difference is used. The color difference is measured as the Euclidean distance between two colorimetric values in the color space. The Commission Internationale de l'Éclairage (CIE) recommended the CIELUV color space, which attempts to achieve perceptual uniformity, to measure the color difference (CIE, 1986). The CIELUV color space is three-dimensional and has the following components: lightness L^*,

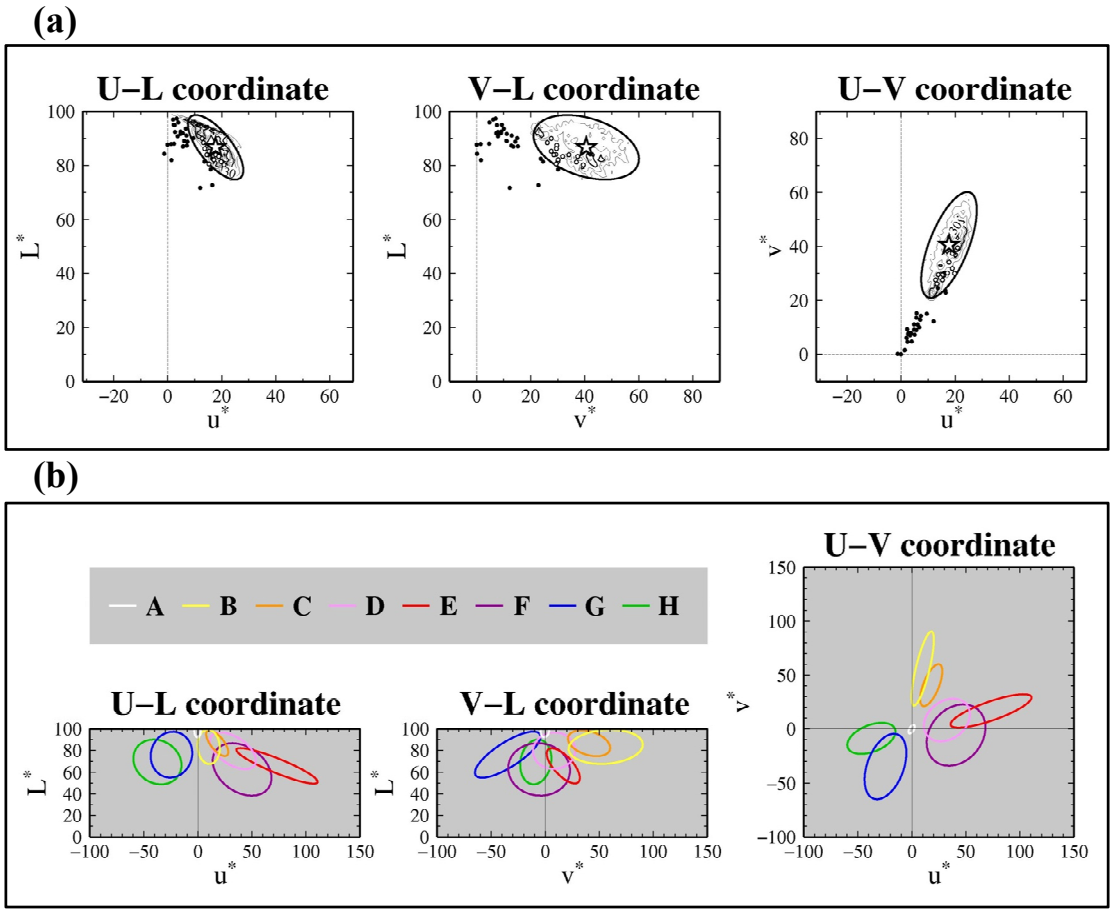

Figure 5-2. (a) Distribution of CIELUV values of color C, the generated ellipsoid body and scatter plots of CIELUV values of driftwood pixels on three diagrams in CIELUV color space. The open (solid) circles indicate that CIELUV values are included within (excluded from) the ellipsoid body in the CIELUV color space. (b) The eight ellipsoid bodies generated using the original photographs from November 2010 to May 2011. The color of each ellipsoid body is the average color. Details of the data for generating the ellipsoid bodies are shown in Table 5-1.

redness-greenness u^*, and yellowness-blueness v^* (CIELUV value). In this study, the CIELUV color space is used to define the color reference.

The original photographs are in JPEG format, and each pixel has a red (R), green (G) and blue (B) value (RGB value). However, the RGB color space is not perceptually uniform. The RGB value of each pixel in the photographs can be converted to the CIELUV value (L^*, u^* and v^*) (Fairchild, 2005). The color references are generated using the original photographs taken during certain periods. These periods are determined by considering the condition that most of the plastic litter is not moved by winds and/or waves during the period. The images taken during the five periods (p1–p5) from November 2010 to May 2011 were used to generate the color references in this study (Table 5-1). At least one plastic item is selected for each color from the images taken during

each period. Due to the heterogeneous distribution of the CIELUV values on each item, we visually selected fifty pixels as color-sample points from among the pixels of each item.

Table 5-1. Typical colors, periods and numbers of pixels used for generating ellipsoid bodies and threshold values during two periods.

Typical color	Ellipsoid body	Periods[a]	Number of selected pixels	Threshold values	
				Nov/10-Mar/11	Apr/11-Aug
white	A	p1, p2, p3, p4, p5	41755	0.6	0.8
yellow	B	p2, p3, p4, p5	23491	0.5	0.5
	C	p1	8712	0.6	0.6
red	D	p1, p3, p4, p5	19100	0.5	0.6
	E	p1	5000	0.5	0.5
	F	p1, p2, p3, p4, p5	24000	0.5	0.5
green	G	p1, p2, p3, p4, p5	62000	0.5	0.5
blue	H	p1, p3, p4, p5	33200	0.5	0.5

[a]Periods: p1, November 21-27, 2010; p2, December 14-21, 2010; p3, February 16-2 2011; p4, April 1-7, 2011; p5, May 18-24, 2011

The CIELUV values for each color, to which the RGB values of sample pixels are converted, are dispersed on three coordinates (U-L, V-L and U-V) in the CIELUV color space (Fig. 5-2). Basically, the distribution of CIELUV values is elongated in a particular direction due to the variability in the amount and angle of sunlight for each period. The distribution on each coordinate is approximated as an ellipse. The center of the ellipse is the average CIELUV value (hereafter, the color of the average CIELUV value is referred to as the "average color") (stars in Fig. 5-2a). The length of the major axis of the three ellipses represents twice the standard deviation of the color difference from the average CIELUV value in a certain direction. The standard deviation is obtained by the solution of an eigenvalue problem on a variance-covariance matrix, and is the square root of the eigenvalue of the first mode. The direction of the major axis corresponds with that of the eigenvector of the first mode. Similarly, the length of the minor axis and the direction of these ellipses are obtained from the eigenvalue and vector of the second mode, respectively. The three ellipses form the ellipsoid body in the CIELUV color space. In this technique, the ellipsoid bodies are used as the color reference.

Basically, the distribution of the CIELUV values of selected pixels was categorized into five colors (white, yellow, red, green and blue) according to the direction of the main axis of the three ellipses. If necessary, the distribution in each color was subdivided according to the average color, length of the axes and direction of the ellipses. The eight ellipsoid bodies were generated using the original images taken at Sodenohama Beach obtained for the five periods from November 2010 to May 2011 (Fig. 5-2b and Table 5-1). However, an ellipsoid body was not generated for the black plastic pixels because they could not be distinguished from the dark-colored pixels of the ground. This is discussed in further detail in 5.4.2.

5.2.4 Detection of plastic pixels using color reference

In this technique, a pixel having a color located within any of the ellipsoid bodies in

the CIELUV color space is determined to be a plastic pixel. However, it is possible for a pixel corresponding to sea water, driftwood, grass or ground to be partially detected as a plastic pixel from the ellipsoid bodies. For example, the pixel color of wet driftwood is frequently located within ellipsoid body "C" in the CIELUV color space (Fig. 5-2a).

To reduce the chance of misdetection, we prepared a composite of images obtained during a certain period. The composite period should be determined according to the movement of plastic litter because the pixels cannot be detected as plastic pixels if the plastic litter is moved by wind and/or waves during the composite period. At each pixel location in the images during the composite period, the frequency of the color location within each ellipsoid body (hereafter "frequency value") is calculated, and the most frequent color and the frequency value are determined. Then, the pixels having a frequency value that is greater than the threshold value of the most frequent color are judged to be plastic pixels.

The composite period and the threshold value are important parameters for detecting plastic pixels in the composite method. For example, if the composite period is too long, the frequency of misdetection could be reduced, but the accuracy of detection of plastic litter could also be reduced. In this study, the most appropriate composite period was determined by investigating the accuracy of detection and the frequency of misdetection in various composite periods (i.e., from one day to seven days). As a result, a three-day composite period was applied in the detection of plastic litter from webcam images.

The threshold value was determined by considering the sunlight conditions (e.g.,

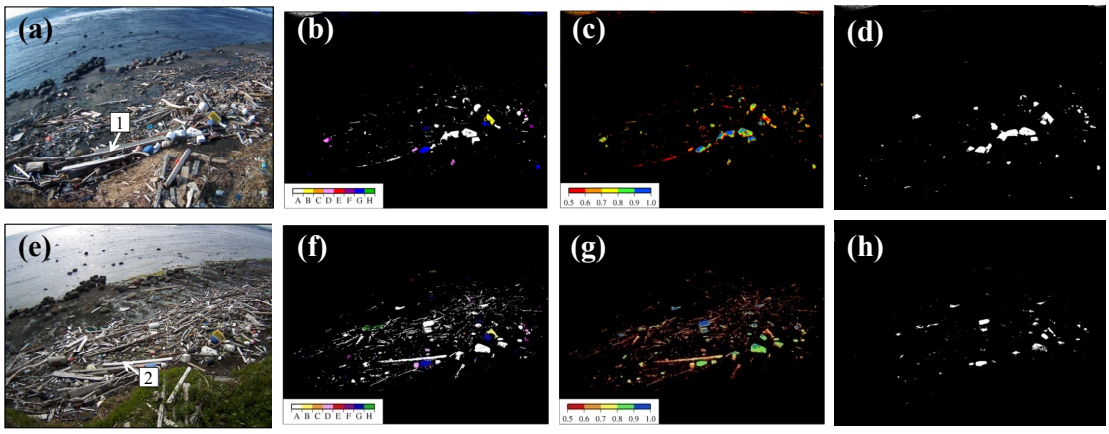

Figure 5-3. Photographs (a) and (e) are original photographs taken on December 20, 2010 and May 8, 2011, respectively. Maps (b) and (c) indicate the most frequent color and the frequency value of each pixel exceeding 0.5 during December 19–21, 2010. Maps (f) and (g) indicate the most frequent color and the frequency value during May 7–9, 2011. Images (d) and (h) are composite images, on which pixels with a frequency value exceeding the threshold values (shown in Table 5-1) are colored white, during December 19–21, 2010 and May 7–9, 2011.

amount of sunshine). In the detection of plastic litter, different threshold values are used for two periods: from November 2010 to March 2011 and from April 2011 to August 2011 (Table 5-1). During spring to summer (April 2011 – August 2011), the CIELUV values of the driftwood pixels (e.g., "2" in Fig. 5-3e) were frequently located within ellipsoid body "A" in the CIELUV color space because the driftwood dried out in the sunshine (Figs. 5-3f and 5-3g). On the other hand, during autumn to winter (November 2010 – March 2011), the frequency value of the color of the driftwood pixels located within ellipsoid body "A" (e.g., "1" in Fig. 5-3a) was less than 0.6 (Figs. 5-3b and 5-3c). Thus, plastic pixels of any color except black or transparent were successfully detected by determining the appropriate threshold values every season (Figs. 5-3d and 5-3h).

5.2.5 Projective transformation method

Following Kako et al. (2010), an area of the beach covered with plastic litter was used as an index of the amount of plastic litter. In order to compute the covered area, a projective transformation was applied because the covered areas are distorted in the original photographs. The projective transformation is based on the method developed by Magome et al. (2007). First, using real-time kinematic (RTK) GPS (Trimble 5800 II, Trimble), we measured the geographic coordinates of the center of ten panels (1×1 m) placed randomly in the coverage area of the image. The RTK-GPS consists of a base and a rover station. The base station is placed in an arbitrary location because the absolute geographic coordinates of the panels are not necessary for the projective transformation. The relative geographic coordinates of the center of the ten panels were measured using the rover station. Thereafter, using the geometrical relationship between the geographic coordinates of the panel locations and the photographic coordinates of the panels in the image as suggested by Magome et al. (2007), the planes in the photographs are rotated in both the horizontal and vertical directions to the plane viewed perpendicularly. Figures 5-4d and 5-4e are the images converted from Figs. 5-4a and 5-4c, respectively, using this method.

The error in covered area computed by this method using the Tobishima webcam images is confirmed to be within 5.0% by comparing the area of the pentagon in Fig. 5-4d as computed from the projective transformation method (121.20 m^2) and directly measured by the RTK-GPS (115.43 m^2). The covered area is computed by multiplying the number of plastic pixels in the converted image by the area of a single pixel (16 cm^2). The area of a single pixel signifies that the recognizable plastic litter of the webcam system is macro plastic litter (> 2.0 cm diameter) (Ryan et al., 2009).

5.3 Results

5.3.1 Comparison with previous method

Although dark-colored plastic pixels were not detected in the previous study (Kako et al., 2010), they can be detected by applying a lower lightness threshold value than the threshold values (85 and 90) established by Kako et al. (2010). Therefore, the applicability of the detection method using ellipsoid bodies (hereafter "DMEB") in detecting plastic pixels was investigated through comparison with the detection method using lightness values (hereafter "DML"). The period from February 4 to February 15 was selected for the comparison. A threshold value for the lightness needed to be determined in the DML. In the experiment, lightness values of 80 (L80) and 90 (L90) were used as the threshold values. In addition, for the comparison with DMEB, the three-day composite method was applied in the DML. Frequency values of 0.7 (C07), 0.8 (C08) and 0.9 (C09) were used as the threshold values for the composite method. Thus, the ability to detect plastic pixels in the DMEB was compared with that in six cases (hereafter, L80-C07, L80-C08, L80-C09, L90-C07, L90-C08 and L90-C09) of the DML.

The composite image in the DMEB and the DML is shown in Figs. 5-4c and 5-4f, respectively. Plastic pixels of any color except black were detected in the DMEB (Fig. 5-4c). In addition, the driftwood pixels were rejected by the composite method (Fig. 5-4c), even if they were detected in image processing using a single photograph (Fig. 5-4b). On the other hand, although white plastic pixels were successfully detected

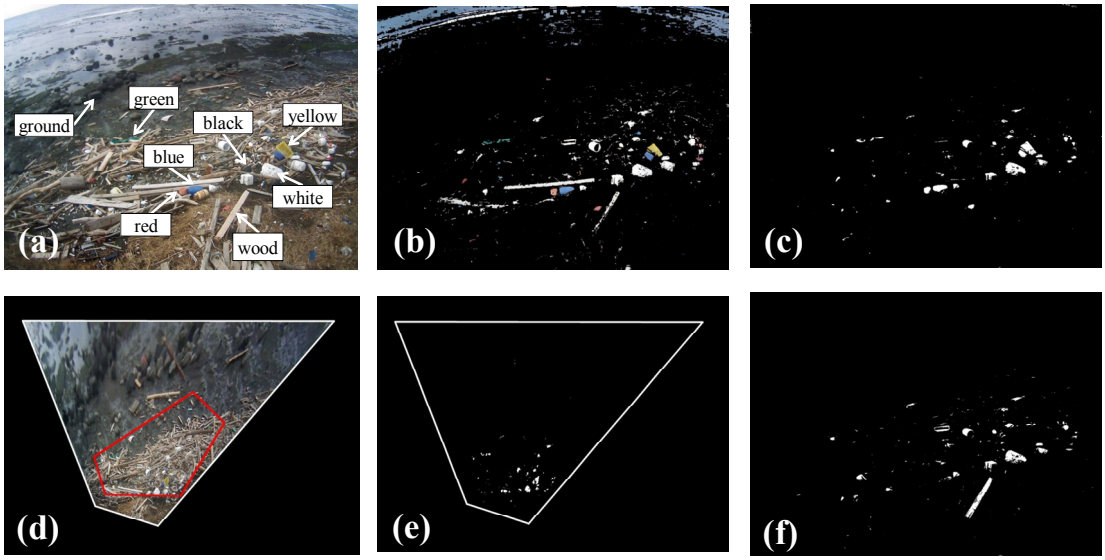

Figure 5-4. (a) Photograph taken on February 7, 2011, and (b) image in which plastic pixels are detected using any of the ellipsoid bodies in (a). (c) and (f) are images in which plastic pixels are identified by DMEB and DML, respectively. (d) and (e) are images after applying the projective transformation to (a) and (c), respectively. Pentagon in panel (d) is the area used to confirm the accuracy of the projective transformation method.

in the DML, plastic pixels of other colors were rejected (Fig. 5-4f). Furthermore, the driftwood pixels were misdetected.

In order to compare the "detection ratio" of plastic pixels of each typical color and the "misdetection ratio" of driftwood pixels by the DMEB with those ratios by the DML, certain plastic pixels and driftwood pixels were selected from the images obtained during the experiment period. The number of selected pixels is shown in Fig. 5-5. The detection ratio of the plastic pixels and the misdetection ratio of the driftwood pixels were applied as the ratio of the number of pixels detected by each method to the number of selected pixels. In both the DMEB and the DML, these ratios calculated from the composite image were determined as the mid-period ratios. For example, the detection ratio on February 5 is the ratio calculated from the composite image for February 4–6. The time series of each ratio is shown in Fig. 5-5.

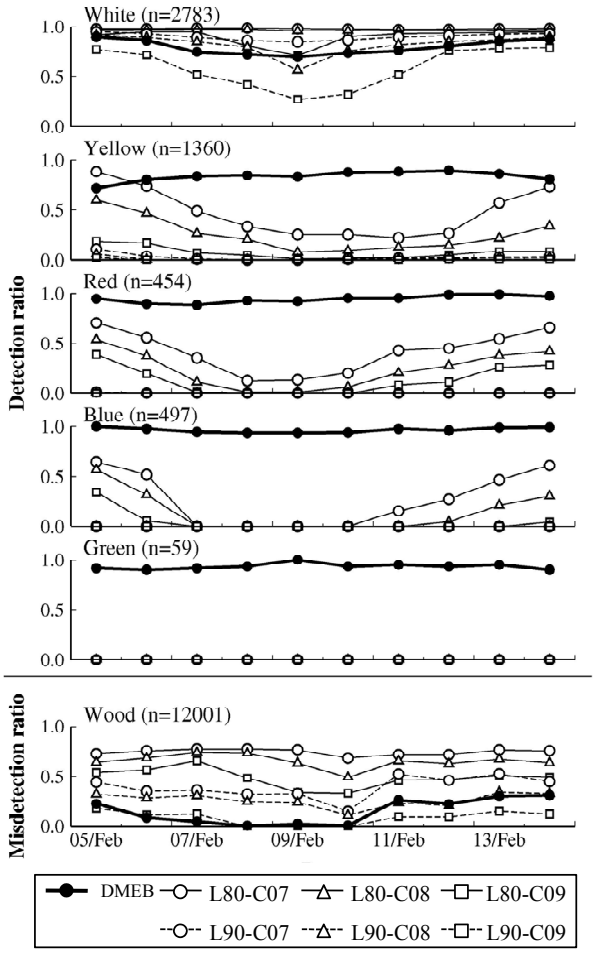

Figure 5-5. Detection ratio of plastic pixels of each color and misdetection ratio of driftwood pixels. The number of selected pixels of each color is shown in the upper left of each graph. The meaning of each line pattern is shown below the figure.

In the DMEB, the detection ratio was higher than 0.70 for any color. The average detection ratio for white, yellow, red, blue and green was 0.79, 0.83, 0.94, 0.97 and 0.93, respectively. The maximum misdetection ratio was 0.31, and the average misdetection ratio was 0.15. On the other hand, in the DML, the average detection ratio for white was greater than 0.80 in all cases except L90-C09 (L80-C07: 0.98, L80-C08: 0.96, L80-C09: 0.90, L90-C07: 0.90, L90-C08: 0.82, L90-L09: 0.59). The detection ratios for the other colors in all cases for the DML were mostly smaller than the ratios in the DMEB. In particular, most of the colored plastic pixels except white were not detected in the cases using L90. In all cases using L80, although the plastic pixels of yellow, red and blue

were partially detected, the green plastic pixels were not detected in the DML. The average detection ratio of all colors in the DMEB (0.83) was higher than that in any of the cases for the DML (L80-C07: 0.70, L80-C08: 0.62, L80-C09: 0.51, L90-C07: 0.49, L90-C08: 0.44, L90-L09: 0.31). The misdetection ratios in all cases except L90-C09 of the DML were higher than the ratios in the DMEB, and the white color detection ratio in L90-C09 was the minimum.

5.3.2 Time series

The DMEB was sequentially applied to all the original photographs except those with poor image quality (due to halation from reflected sunlight or snow/water covering the webcam lens) taken from November 7, 2010 to August 31, 2011, and a time series of daily covered areas was obtained (Fig. 5-6). A separate time series for each of the five typical colors was obtained. The covered area of all the colors fluctuated sharply but only temporarily (periods 1, 2 and 3 in Fig. 5-6). To investigate the mechanism of these fluctuations, the time series was compared with those of winds, waves and snowfall (Fig. 5-7) observed at TB, SP and SK (Fig. 5-1b), respectively. These fluctuations were due to a seasonal storm. Eastward winds of 10 m s^{-1} or more and waves of 5 m or more were recorded during these periods (Figs. 5-7a and 5-7b). Observation of the

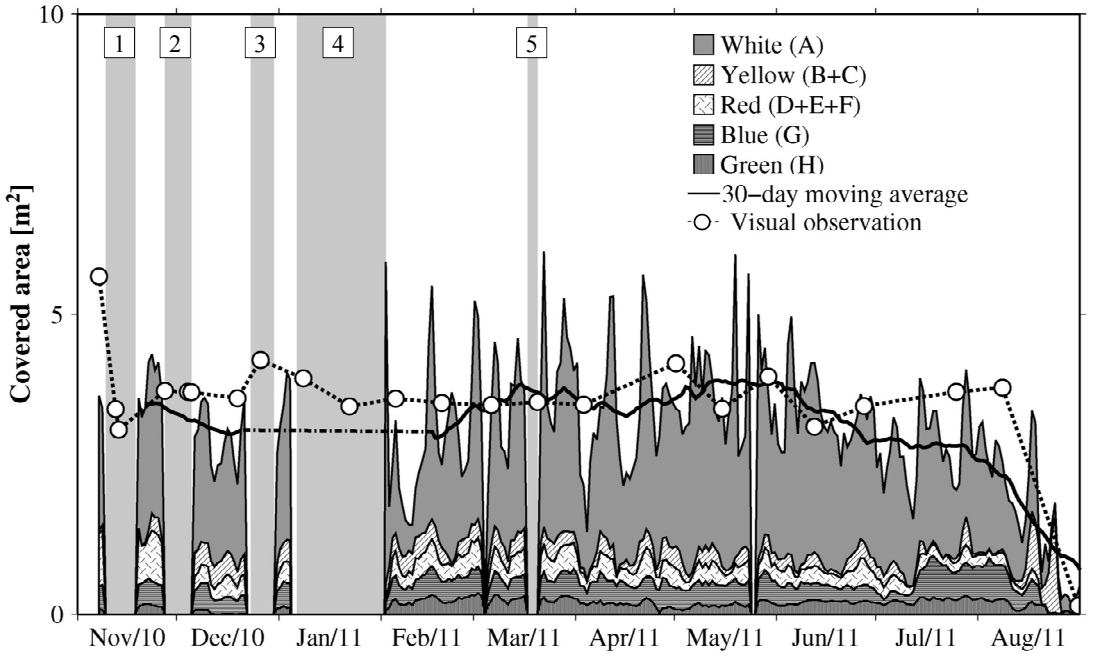

Figure 5-6. Time series of the covered area of plastic litter. The time series is separated by each color of plastic litter. The meaning of each curve is explained in the upper right corner. Light gray bars indicate periods in which computed covered areas have missing or abnormal values. The covered areas during these periods except period 4 are linearly interpolated.

original photographs taken during these periods confirmed that most of the plastic litter was moved by strong winds and high waves. As mentioned earlier, if the plastic litter moves during the composite period, the plastic pixels cannot be detected in the DMEB. Also, the covered areas could not be computed during periods 4 and 5 in Fig. 5-6 because the beach was covered with snow (Fig. 5-7c). The covered areas during these periods except period 4 in Fig. 5-6 were linearly interpolated. The covered areas decreased toward the end of August 2011 as a result of a beach cleanup conducted by islanders on August 20, 2011. White plastic litter was predominant in the color composition of the average amount of plastic litter during the analyzed period on Sodenohama Beach (white: 0.66, yellow: 0.08, red: 0.09, blue: 0.11, green: 0.06). Most of the white plastic litter was polystyrene buoys (e.g., Fig. 5-3a). The average covered area was 3.20 m^2.

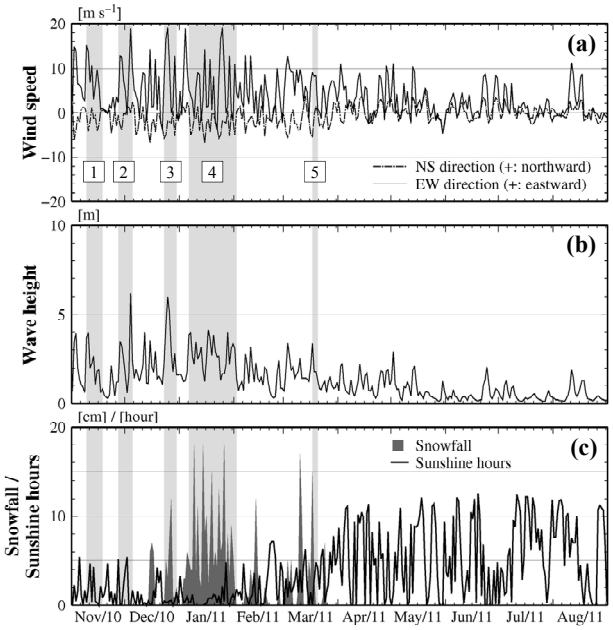

Figure 5-7. Wind speed at TB (a), wave height at SP (b), snowfall at SK and sunshine hours at TB (c) measured from November 2010 to August 2011. Light gray bars indicate periods in which computed covered areas have missing or abnormal values.

The variability in covered areas depended partially on changes in the weather conditions, especially in the amount of sunlight. Covered areas of white plastic litter were particularly affected by the amount of sunlight because ellipsoid body "A" was much smaller than the other ellipsoid bodies (Fig. 5-2b). Therefore, with even a slight change in the color of white plastic litter, the CIELUV values were excluded from the spatial area of ellipsoid body "A". For example, when the ground shadow from behind the webcam covers the white plastic litter, the plastic pixels cannot be detected by ellipsoid body "A". Also, short-term fluctuations are caused by the misdetection of driftwood as white plastic litter because the pixels of dried-out driftwood under the sunshine are partially identified by the DMEB (Fig. 5-5). In addition, variability was caused by strong winds during the period from November 2010 to March 2011 (Fig. 5-7a) because white polystyrene buoys are prevalent in the white plastic litter and are moved by gentler winds compared to those required to move dense plastics such as polyethylene or poly-

propylene.

To remove these short-term fluctuations caused mainly by over- and underestimation of the covered area due to the weather conditions, a time series of the 30-day moving average was used in subsequent analyses (bold line in Fig. 5-6). To validate this time series, a comparison was made with a time series of visual covered areas (dotted line in Fig. 5-6). The visual covered areas were computed from the number of plastic pixels detected by visual observation in the original photographs taken every two weeks from November 7, 2010 to August 31, 2011 (white circles in Fig. 5-6). In the visual observation, black litter (e.g., fishing buoy) and transparent litter (e.g., PET bottles) were removed from the calculation of the covered area because of the limits of detection using only colors (see 5.2.3). The error of the detection of plastic pixels was described by the rate of the root mean square error (RMSE) to the visual covered area.

The rate of the RMSE was 12%, while the covered areas calculated by the DMEB were significantly correlated with the visual covered area at the 95% confidence level ($n = 16$, $R = 0.81$, $P = 1.6\times10^{-4} < 0.05$). Therefore, the temporal variability of the covered area was successfully calculated based on the DMEB. This suggests that the DMEB is the applicable technique for webcam images taken at various sites.

5.4 Discussion

5.4.1 Methodology of webcam monitoring to reduce measurement errors

Measurement error of the amount of plastic litter (covered area) occurs for two reasons: (1) non-plastic pixels (e.g., driftwood) are misdetected, and (2) plastic pixels are not detected due to color change by sunlight conditions. Reason (1) results in overestimation, while reason (2) results in underestimation. The measurement error corresponds to the difference between overestimation and underestimation because the moving average cannot completely remove the difference. In this section, we focus on reason (2), and investigate the cause of measurement errors. In addition, we discuss the methodology of webcam monitoring.

Specifically, the detection of white plastic pixels depends strongly on the sunlight conditions and the shape of plastic litter (see 5.3.2). For example, convex parts of the plastic surface and the top plane of plastic litter are lighter than the concave parts and side plane. Thus, changes in the CIELUV values (L^*, u^* and v^*) at the top and side planes due to sunlight conditions are investigated using blue tanks, white cubes (polystyrene buoy) and white cylinders (polystyrene buoy) as the types of plastic litter in webcam images (Fig. 5-8) taken for one month (April 2011). In a comparison of color change, the monthly average and monthly standard deviation of the CIELUV values are

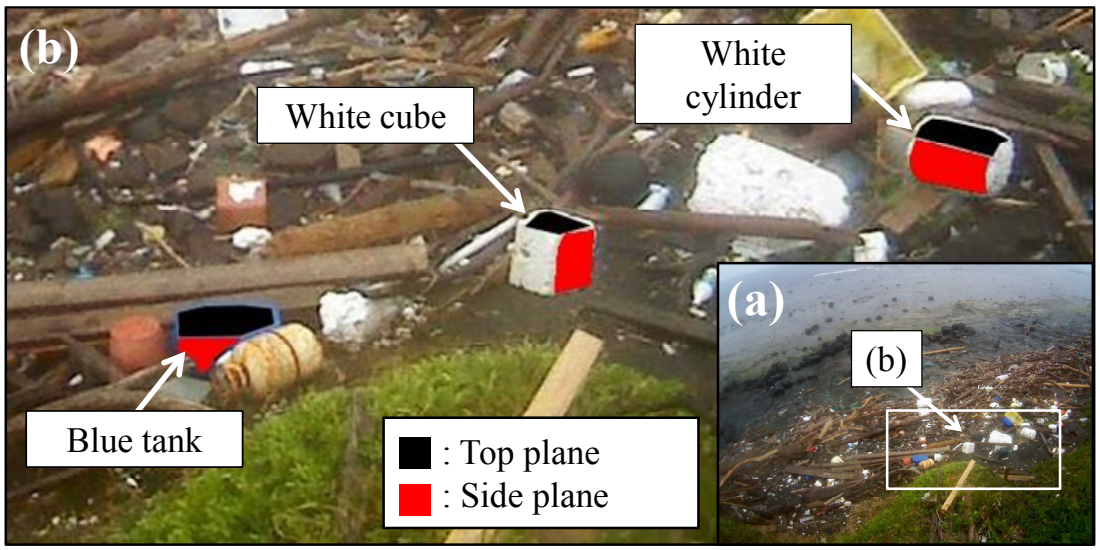

Figure 5-8. (a) Original webcam image. (b) Plastic litter used to investigate the cause of measurement error.

calculated every time the webcam images are taken (i.e., 07:00, 09:00, 11:00, 13:00 and 15:00). The color change due to the sunlight angle can be understood by calculating the average and standard deviation of the CIELUV values every time.

Figure 5-9 shows the variability of color at the top plane for the three types of plas-

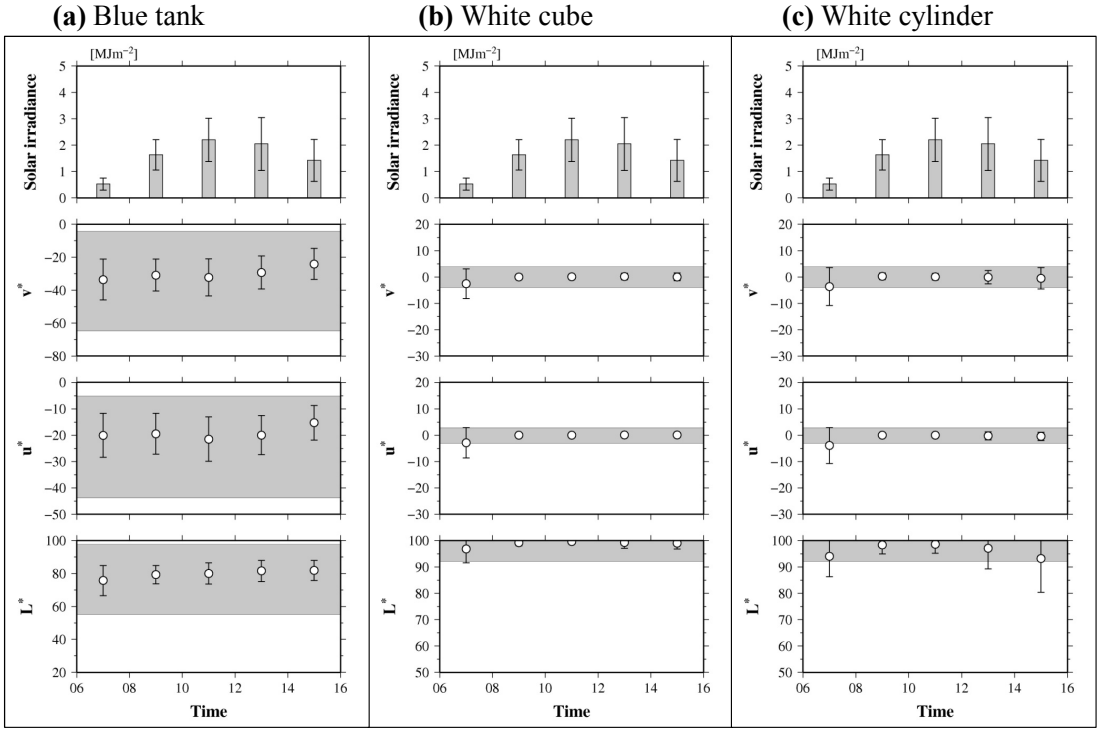

Figure 5-9. Color variability (circle: average, error bar: standard deviation) of the top plane of three types of plastic litter at each time and solar irradiance observed at TB (see Fig. 5-1b). (a) Blue tank, (b) white cube = polystyrene buoy and (c) white cylinder = polystyrene buoy. Gray area shows the color references of each CIELUV value.

tic litter. The gray area denotes the area of color reference for each value. Thus, if the CIELUV values are within the gray area, we can recognize this as detected plastic pixels. In the color change of the blue tank and white cube, the average and standard deviation of three CIELUV values are within the gray area regardless of the time the images were taken (Figs. 5-9a and 5-9b). In the color variability of the white cylinder, although the standard deviation of three CIELUV values at 7:00, L^* at 13:00 and L^* at 15:00 extends outside the gray area, overall, the averages are within the gray area regardless of the time the images were taken (Fig. 5-9c). On the other hand, the color variability of all litter is smaller than the variability of solar irradiance, and a significant relationship between the variability of litter color and solar irradiance is not found. This indicates that detection of the top plane of the three types of plastic litter does not quite depend on the sunlight angle and solar irradiance.

Figure 5-10 shows the color variability of the side plane of the three types. The plastic pixels of the blue tank are detected at almost every time the images were taken, but the plastic pixels of the white cube and white cylinder are not detected except at 09:00 and 11:00. This is the reason for the underestimation of amount of plastic litter. If the covered area on Sodenohama Beach in April 2011 is calculated based on the DMEB, the measurement error can be reduced by detecting plastic pixels using the webcam im-

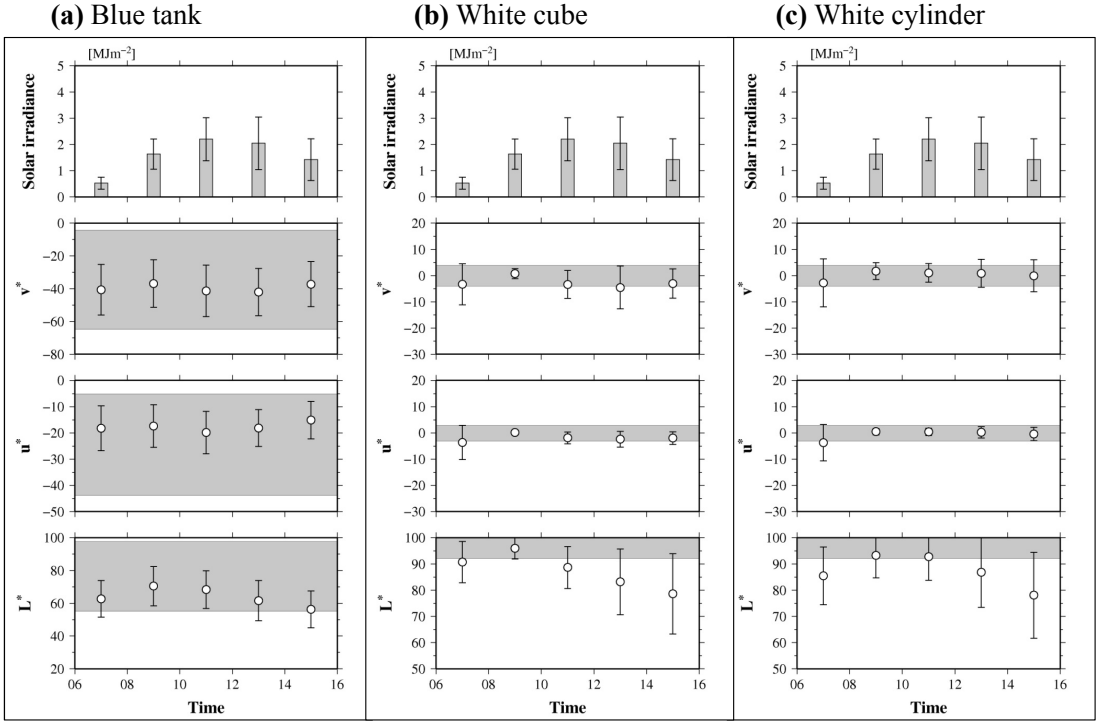

Figure 5-10. Color variability (circle: average, error bar: standard deviation) of the side plane of three types of plastic litter at each time and solar irradiance observed at TB (see Fig. 5-1b). The format is the same as for Fig. 5-9.

ages taken at 09:00 and 11:00. Figure 5-11 shows a schematic image of the cause of the measurement error. Basically, in the morning, both the top and side planes of the plastic litter are a clear color (not transparent) because the camera direction is westward. On the other hand, in the afternoon, the side plane of the plastic litter becomes dark while the opposite plane is exposed to the sunlight. Therefore, it is important to consider the sunlight angle in sequential webcam monitoring of the amount of plastic litter.

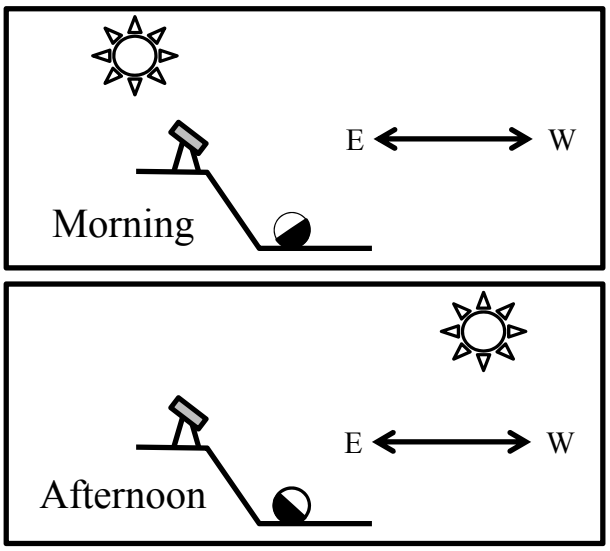

Figure 5-11. Schematic image of cause for measurement error on Sodenohama Beach.

5.4.2 Technical issues of webcam monitoring

This study presented a new technique for detecting plastic pixels of various colors from images taken by a webcam. The technique had three issues: black plastic pixels could not be detected, driftwood pixels could not be completely removed, and some plastic pixels were rejected in the composite method when plastic litter moved due to winds and/or waves within a short time scale in the composite period (three days).

In this study, plastic litter with black or transparent areas was neglected because the plastic pixels with these colors were remarkably similar to the color of the beach ground and/or shadows (e.g., Fig. 5-4a). Neglecting these plastic pixels was not a critical issue for calculating the covered area from webcam images because relatively little litter with these colors washed ashore (e.g., Fig. 5-4a). However, if black or transparent plastic litter predominantly washed ashore, it would be necessary to take measures to add black and transparent pixels. One measure is to estimate the covered area of all plastic litter by investigating the ratio of black and transparent plastic litter to all litter.

To reduce the chance of driftwood pixels being misdetected as plastic pixels, the composite method is used in the DMEB. As a result, driftwood pixels that are misdetected using ellipsoid bodies on a single image (Fig. 5-4b) are successfully removed by the composite method (Fig. 5-4c). Thus, the composite method is effective against misdetection of driftwood pixels. However, the pixels corresponding to driftwood are partially identified as plastic litter (Fig. 5-5). It is difficult to completely dis-

tinguish between plastic pixels and driftwood pixels because the color of driftwood that has dried out under the sunshine is very close to the color of white plastic litter ("2" in Fig. 5-3e). Even if most of the driftwood pixels are removed by the composite method, a portion is identified as white plastic pixels on a continuously sunny day, and the covered area is overestimated. On the other hand, to completely remove the driftwood pixels, a longer composite period should not be used because the plastic litter could move during the period due to winds and/or waves. Nevertheless, if the primary objective of webcam monitoring is to obtain the temporal variability of the amount of plastic litter, neglecting short-term movements would not be a critical issue because the temporal variability in the 30-day moving average was consistent with that of the visual covered areas.

5.4.3 Application of webcam monitoring to beach cleanup

Generally, the covered area would not be used as an index to measure the amount of plastic litter. In addition, areas covered with plastic litter under objects (e.g., driftwood and sand) cannot be estimated by this method. Thus, the precise covered areas cannot be estimated using this technique. However, we consider that the covered area would be useful as an index for planning beach cleanup campaigns. For example, white plastic litter was predominant on Sodenohama Beach, and most of the white litter was polystyrene buoys (see 5.3.2). Considering the height of white litter as the average height of the predominant litter, the volume of white plastic litter can be estimated. For example, the volume of white litter is approximately 0.422 m^3 because the average covered area of white plastic litter from November 2010 to August 2011 and the average height of white plastic litter were, respectively, 2.11 m^2 and 0.2 m (i.e., 2.11 m^2 × 0.2 m = 0.422 m^3). Although this is a rough estimation, it is possible to determine the manpower required by estimating the work volume before implementing a beach cleanup.

Nakashima et al. (2011) presented an efficient method for quantifying the amount of litter on a beach surface based on the covered area. They obtained the total mass of plastic litter on Ookushi Beach on the Goto Islands, Japan, by combining the estimation of the covered area by balloon-assisted aerial photography with in situ measurement of the litter mass per unit area. Thus, it is possible to accurately estimate the amount of plastic litter from webcam images through the combination of monitoring of the covered area and in situ measurement of plastic litter mass per unit area.

The new technique for sequential monitoring enables us to conduct effective beach cleanup (i.e., to understand the remnant peak and predominant period of litter input; see 4.4.2). Furthermore, Isobe et al. (2012) simulated the reduction effect on litter amount

by cleanup projects using the variation in covered area that Kako et al. (2010) computed using webcam images on Ookushi Beach. Thus, the monitoring of litter amount would be a potential tool for systematic planning of beach cleanup.

5.5 Conclusion

This study presented a new technique for sequential monitoring of the amount of colored plastic litter (plastic pixels) using photographs taken by webcam on Sodenohama Beach on Tobishima Island, Japan. The new technique is described as following three steps: (1) Color references (ellipsoid bodies in CIELUV color space) to detect plastic pixels are generated by converting RGB values obtained from the original photographs into CIELUV values. (2) The plastic pixels are detected using the color reference and a composite image method. (3) The area covered by plastic litter (covered area) is calculated by applying a projective transformation to the webcam images.

To confirm the applicability of the detection method using ellipsoid bodies in CIELUV color space (DMEB), we compared the detection ratio of five typical colors of plastic pixels and the misdetection ratio of driftwood pixels based on the DMEB with those based on a detection method of plastic pixels using lightness values (DML), which was developed by Kako et al. (2010). The DMEB was superior to the DML in that the detection ratio of all five typical colors was higher and the misdetection ratio of driftwood was lower.

Next, the amount of plastic litter (covered areas) calculated from webcam images fluctuated at a short time scale. The short-time fluctuation in covered areas was due to sunlight conditions (e.g., amount of sunlight). To remove the short-term fluctuation, the 30-day moving average was calculated. The time series of the 30-day moving average was compared with that of the visual covered area computed from the number of plastic pixels selected by human perception. The variability in moving average covered area was consistent with that of the visual covered area, although the average error was 12%.

The cause of measurement error was investigated based on the color change of three types of litter (blue tanks, white cubes and white cylinders) on webcam images taken in April 2011. The variability of color at the side plane of plastic litter depends strongly on the sunlight angle. Therefore, it is important to consider the sunlight angle in sequential webcam monitoring of the amount of plastic litter.

The new technique for webcam monitoring would enable us to sequentially measure the amount of plastic litter on multiple beaches. By applying the webcam monitoring, we can systematically plan more effective beach cleanups.

CHAPTER 6

Conclusions

This research focused on the residence time of plastic litter from washing ashore to backwashing offshore. There are three major reasons why the residence time is important information for reducing the environmental risk of plastic pollution on beaches: the degradation of plastics, which is one of the most serious problems in plastic pollution, is most likely to proceed on beaches; plastic litter is transported via oceans and repeatedly washes ashore and backwashes offshore at multiple beaches; and the collection of plastic litter from the marine environment is mainly conducted on beaches. Thus, we measured the residence time on the beach, and proposed the application of residence time to beach cleanups.

In Chapter 2, we described our two-year mark-recapture (MR) experiments using fishing floats to measure the residence time from washing ashore to backwashing offshore. The experiments were conducted at one- or three-month intervals starting in September 2011 on Wadahama Beach, Niijima Island, Japan. In addition, we investigated the movement of floats to clarify the physical mechanism of the process determining the residence time. The cohort population of floats decreased according to an exponential function (Fig. 2-4). The average residence time of floats was calculated based on the exponential decay, which was 224 days. Therefore, the floats on Wadahama Beach were backwashed offshore 224 days after washing ashore, on average.

The floats on Wadahama Beach moved both northward and southward by the swash of wind waves (Fig. 2-7), and the movement depended on the frequency of swash events (Fig. 2-10). The floats were highly concentrated in the northernmost areas through alongshore movement (i.e., 800–1100 m of alongshore distance; see Fig. 2-6). These areas correspond to the convergence areas of the average transport velocity that was calculated from the alongshore movement distance during each experiment period (Fig. 2-14). In addition, the high concentration area of floats corresponds to the deposition area of sediment (Fig. 2-9). Therefore, we assume that the floats were transported northward by longshore currents along the shoreline at swash events, and were concentrated in the northernmost area. In the process, a portion was backwashed offshore.

In Chapter 3, to demonstrate the assumption for the backwash process, we investigated the physical mechanism of the backwash of fishing floats found on Wadahama Beach on Niijima Island, Japan through the two-year MR experiments in situ and nu-

merical experiments based on a one-dimensional advection-diffusion equation. Firstly, the residence time of floats found in a 100-m-wide alongshore transect was calculated by two approaches based on the beached position of the floats measured by the two-year MR experiments. In the first approach, the residence time (RT1) was estimated by searching only the 100-m-wide transect for remnants of the floats. In the second approach, the residence time (RT2) was estimated by searching the whole beach for remnants of the floats. Secondly, we identified backwash transects by solving the advection-diffusion equation using a finite-difference scheme.

The average RT1 was shorter than the whole residence time of floats found on the whole beach (224 days) because the floats that moved to other transects were not counted. Conversely, the average RT2 was longer than the whole residence time. Wadahama Beach has some 100-m-wide transects where the difference between RT1 and RT2 was relatively small compared to that at the other transects. This means that the floats converge in these transects. In actuality, these transects were consistent with the high concentration areas of floats. In addition, the backwash transects were frequently identified as these transects by the numerical experiments. These findings demonstrated our assumption that the floats on Wadahama Beach were concentrated in some transects after being transported by longshore currents, and then were backwashed offshore in the transport process.

In Chapter 4, to demonstrate the meaning of the measurement of residence time, we attempted to quantify three effects of beach cleanups (i.e., improvement of the beach landscape; decrease of total mass of toxic metals; and prevention of the generation of plastic fragments) based on the linear system analysis, and then the dependence of these beach cleanup effects (BCEs) on the residence time was clarified.

The BCEs depend strongly on the dimensionless residence time normalized as the residence time by the period of litter input flux (litter input period), and the BCEs increase as the dimensionless residence time becomes longer. Also, the BCEs depend on the time when the beach cleanups are conducted, and the beach cleanups are more effective when the remnants of floats reach a peak (effective cleaning time). Therefore, it is crucial to understand the residence time, the predominant litter input period and the effective cleaning time.

In Chapter 5, to understand the predominant litter input period and the effective cleaning time, we attempted to develop a new technique for sequential monitoring of remnants of plastic litter of various colors on Sodenohama Beach on Tobishima Island, Japan. The new technique is as follows: (1) Color references (ellipsoid bodies in CIELUV color space) to detect plastic pixels from images are generated by converting

RGB values obtained from the original photographs into CIELUV values. (2) The plastic pixels are detected using the color reference and a composite image method. (3) The area covered by plastic litter (covered area) is calculated by applying a projective transformation to webcam images.

The detection method for plastic pixels using ellipsoid bodies (DMEB) was superior in that the detection ratio of all five typical colors was higher and the misdetection ratio of driftwood was lower in a comparison with the detection method using the lightness value (DML). The DMEB enables us to measure the covered area on sites where plastic litter of various colors has washed ashore. In addition, we successfully monitored the temporal variability of the covered areas with a 12% measurement error. The measurement error depends strongly on the sunlight angle. Therefore, it is important to consider the sunlight angle in sequential webcam monitoring of the amount of plastic litter. The new technique for webcam monitoring would enable us to sequentially measure the amount of plastic litter on multiple beaches. By applying the webcam monitoring, we can systematically plan more effective beach cleanups.

At present, the residence time of plastic litter on the world's beaches is hardly understood. However, the residence time is crucial information for taking measures against pollution because plastics on beaches rapidly undergo fragmentation, and it is much more difficult to remove plastic fragments from the marine environment. Therefore, understanding the residence time would enable the removal of plastic litter through effective beach cleanups around the world.

REFERENCES

Andrady, A.L., 2011. Microplastics in the marine environment. Mar. Pollut. Bull. 62(8), 1596–1605.

Ashton, A., Murray, A. B., Arnoult, O., 2001. Formation of coastline features by large-scale instabilities induced by high-angle waves. Nature, 414(6861), 296–300.

Barnes, D.K.A., Galgani, F., Thompson, R.C., Barlaz, M., 2009. Accumulation and fragmentation of plastic debris in global environments. Phil. Trans. R. Soc. B 364, 1985–1998.

Battjes, J. A., 1974. Surf similarity. Proc. 14th Conf. Coastal Eng., Am. Soc. Civ. Eng., 466–479.

Bayram, A., Larson, M., Hanson, H., 2007. A new formula for the total longshore sediment transport rate. Coastal Eng. 54(9), 700–710.

Boerger, C.M., Lattin, G.L., Moore, S.L., Moore, C.J., 2010. Plastic ingestion by planktivorous fishes in the North Pacific Central Gyre. Mar. Pollut. Bull. 60(12), 2275–2278.

Bowman, D., Manor-Samsonov, N., Golik, A., 1998. Dynamics of litter pollution on Israeli Mediterranean beaches: a budgetary, litter flux approach. J. Coast. Res. 14(2), 418–432.

CIE, 1986. Colorimetry, CIE Publication 15.2, CIE, Vienna, Austria.

Cole, M., Lindeque, P., Halsband, C., Galloway, T. S., 2011. Microplastics as contaminants in the marine environment: A review. Mar. Pollut. Bull. 62(12), 2588–2597.

Cooper, D. A., Corcoran, P. L., 2010. Effects of mechanical and chemical processes on the degradation of plastic beach debris on the island of Kauai, Hawaii. Mar. Pollut. Bull. 60(5), 650–654.

Derraik, J.G.B., 2002. The pollution of the marine environmental by plastic debris: a review. Mar. Pollut. Bull. 44(9), 842–852.

Fairchild, M.D., 2005. Color Appearance Models, second ed. John Wiley, New York.

Garrity, S. D., Levings, S. C., 1993. Marine debris along the Caribbean coast of Panama. Mar. Pollut. Bull. 26(6), 317–324.

Gregory, M. R., Andrady, A. L., 2003. Plastics in the marine environment. In: Andrady, A.L. (Ed.), Plastics and the environment, John Wiley & Sons, Inc., New York, 379–401.

Gregory, M. R., 2009. Environmental implications of plastic debris in marine settings entanglement, ingestion, smothering, hangers-on, hitch-hiking and alien invasions.

Phil. Trans. R. Soc. B 364, 2013–2025.

Hinata, H., Yanagi, T., Takao, T., Kawamura, H., 2005. Wind-induced Kuroshio warm water intrusion into Sagami Bay. J. Geophys. Res. 110(C3), C03023.

Hunt, I. A., 1959. Design of seawalls and breakwaters. Proc. Am. Soc. Civ. Eng. 85, 123–152.

Isobe, A., Hinata, H., Seino, S., Magome, S., Kako, S., Nakashima, E., Kojima, A., Kaneko, H., 2012. Beach litter and oceanography – our research outcomes and future perspective. Bull. Coast. Oceanogr. 49(2), 139–151 (in Japanese).

Ivar do Sul, J. A., Costa, M. F., 2007. Marine debris review for Latin America and the Wider Caribbean Region: From the 1970s until now, and where do we go from here?. Mar. Pollut. Bull. 54(8), 1087–1104.

Japan Coast Guard (JCG), 2013. Quick bulletin of ocean conditions. WWW page: http://www1.kaiho.mlit.go.jp/KANKYO/KAIYO/qboc/index_E.html.

Japan Meteorological Agency (JMA), 2012a. Tropical cyclone tracks. WWW page: http://www.data.jma.go.jp/fcd/yoho/typhoon/route_map/bstv2012.html

Japan Meteorological Agency (JMA), 2012b. Tropical cyclone tracks. Available at: http://www.data.jma.go.jp/fcd/yoho/data/hibiten/2012/1204.pdf

Japan Meteorological Agency (JMA), 2013. Weather maps. Available at: http://www.data.jma.go.jp/fcd/yoho/data/hibiten/2013/1304.pdf

Kako, S., Isobe, A., Magome, S., 2010. Sequential monitoring of beach litter using webcams. Mar. Pollut. Bull. 60(5), 775–779.

Kako, S., Isobe, A., Magome, S., Hinata, H., Seino, S., Kojima, A., 2011a. Establishment of numerical beach-litter hindcast/forecast models: An application to Goto Islands, Japan. Mar. Pollut. Bull. 62(2), 293–302.

Kako, S., Isobe, A., Kubota, M., 2011b. High‐resolution ASCAT wind vector data set gridded by applying an optimum interpolation method to the global ocean. J. Geophys. Res. 116, D23107.

Kataoka, T., Hinata, H., Nihei, Y., 2013. Numerical estimation of inflow flux of floating natural macro-debris into Tokyo Bay. Estuar., Coast. and Shelf Sci. 134(1), 69–79

Komar, P. D., Inman, D. L., 1970. Longshore sand transport on beaches. J. Geophys. Res. 75(30), 5914-5927.

Kubota, M., 1994. A mechanism for the accumulation of floating marine debris north of Hawaii. J. Phys. Oceanogr. 24(5), 1059–1064.

Kuriyama, Y., Yamaguchi, S., Ikegami, M., Ito, A., Takano, S., Tanaka, J., Tomoda, N. 2007. Bathymetry changes around large-scale submerged breakwater on the Niigata coast. Journal of the Japan Society of Civil Engineers B 63(4), 255–271. (in

Japanease)

Kusui, T., Noda, M., 2003. International survey on the distribution of stranded and buried litter on beaches along the Sea of Japan. Mar. Pollut. Bull. 47(1), 175–179.

Law, K. L., Moret-Ferguson, S., Maximenko, N. A., Proskurowski, G., Peacock, E. E., Hafner, J., Reddy, C. M., 2010. Plastic accumulation in the North Atlantic subtropical gyre. Science 329(5996), 1185–1188.

Lippmann, T. C., Holman, R. A., 1990. The spatial and temporal variability of sand bar morphology. J. Geophys. Res. 95(C7), 11575–11590.

Magome, S., Yamashita, T., Kohama, T., Kaneda, A., Hayami, Y., Takahashi, S., Takeoka, H., 2007. Jellyfish patch formation investigated by aerial photography and drifter experiment. J. Oceanogr. 63(5), 761–773.

Martinelli, L., Zanuttigh, B., Lamberti, A., 2006. Hydrodynamic and morphodynamic response of isolated and multiple low crested structures: Experiments and simulations. Coastal Eng. 53(4), 363–379.

Mato, Y., Isobe, T., Takada, H., Kanehiro, H., Ohtake, C., Kaminuma, T., 2001. Plastic resin pellets as a transport medium for toxic chemicals in the marine environment. Environ. Sci. Technol. 35(2), 318–324.

Maximenko, N., Hafner, J., Niiler, P., 2012. Pathways of marine debris derived from trajectories of Lagrangian drifters. Mar. Pollut. Bull. 65(1), 51–62.

McKinley, P., Levine, M., 1998. Cubic spline interpolation. Available at: http://online.redwoods.edu/instruct/darnold/LAPROJ/Fall98/SkyMeg/Proj.PDF

Moser, M.L., Lee, D.S., 1992. A fourteen-year survey of plastic ingestion by western North Atlantic seabirds. Colonial Waterbirds 15, 83–94.

Nakashima, E., Isobe, A., Magome, S., Kako, S., Deki, N., 2011. Using aerial photography and in situ measurements to estimate the quantity of macro-litter on beaches. Mar. Pollut. Bull. 62(4), 762–769.

Nakashima, E., Isobe, A., Kako, S. I., Itai, T., Takahashi, S., 2012. Quantification of toxic metals derived from macroplastic litter on Ookushi Beach, Japan. Environ. Sci. Technol. 46(18), 10099–10105.

Nordic Council of Ministers, 2003. Lead Review. Available at: http://www.who.int/ifcs/documents/forums/forum5/nmr_lead.pdf.

Northwest Pacific Region Environmental Cooperation Center (NPEC), 2007. Research on Washed-up Driftage on the Coasts. Available at: http://www.npec.or.jp/3_report/pdf/2008/2006hokoku.pdf

Ocean Conservancy, 2012. International Coastal Cleanup 2013 report: Working for clean beaches and clean water. Available at: http://www.oceanconservancy.org/

our-work/international-coastal-cleanup/2013-trash-free-seas-report.pdf.

Ogata, Y., Takada, H., Mizukawa, K., Hirai, H., Iwasa, S., Endo, S., Mato, Y., Saha, M., Okuda, K., Nakashima, A., Murakami, M., Zurcher, N., Booyatumanondo, R., Zakaria, M. P., Dung, L. Q., Gordon, M., Miguez, C., Suzuki, S., Moore, C., Karapanagioti, H. K., Weerts, S., McClurg, T., Burres, E., Smith, W., Velkenburg, M. V., Lang, J. S., Lang, R. C., Laursen, D., Danner, B., Stewardson, N., Thompson, R. C., 2009. International Pellet Watch: Global monitoring of persistent organic pollutants (POPs) in coastal waters. 1. Initial phase data on PCBs, DDTs, and HCHs. Mar. Pollut. Bull. 58(10), 1437–1446.

Peterson, N. P., Cederholm, C. J., 1984. A comparison of the removal and mark-recapture methods of population estimation for juvenile coho salmon in a small stream. N. Am. J. Fish. Mgmt. 4(1), 99–102.

Potemra, J. T., 2012. Numerical modeling with application to tracking marine debris. Mar. Pollut. Bull. 65(1), 42–50.

Ribic, C.A., 1998. Use of indicator items to monitor marine debris on a New Jersey beach from 1991 to 1996. Mar. Pollut. Bull. 36(11), 887–891.

Ribic, C.A., Sheavly, S.B., Rugg, D.J., Erdmann, E.S., 2010. Trends and drivers of marine debris on the Atlantic coast of the United States 1997–2007. Mar. Pollut. Bull. 60(8), 1231–1242.

Ribic, C. A., Sheavly, S. B., Rugg, D. J., Erdmann, E. S., 2012. Trends in marine debris along the US Pacific Coast and Hawai'i 1998–2007. Mar. Pollut. Bull. 64(5), 994–1004.

Ryan, P. G., 1988. Effects of ingested plastic on seabird feeding: evidence from chickens. Mar. Pollut. Bull. 19(3), 125–128.

Ryan, P. G., Moore, C. J., van Franeker, J. A., Moloney, C. L., 2009. Monitoring the abundance of plastic debris in the marine environment. Phil. Trans. R. Soc. B 364(1526), 1999–2012.

Seino, S., Kojima, A., Hinata, H., Magome, S. and Isobe, A., 2009. Multi-Sectoral research on East China Sea beach litter based on oceanographic methodology and local knowledge. J. Coast. Res. 56, 1289–1292.

Shaw, D.G., Day, R.H., 1994. Colour- and form-dependent loss of plastic microdebris from the North Pacific Ocean. Mar. Pollut. Bull. 28(1), 39–43.

Sheavly, S.B., 2007. National Marine Debris Monitoring Program: Final Program Report, Data Analysis and Summary. Final Report, US Environmental Protection Agency, Office of Water, Washington, DC.

Smith, T. D., Allen, J., Clapham, P. J., Hammond, P. S., Katona, S., Larsen, F., Lien, J.,

Mattila, D., Palsbøll, P. J., Sigurjónsson, J., Stevick, P. T., Ølen, N., 1999. An ocean-basin-wide mark-recapture study of the North Atlantic humpback whale (Megaptera novaeangliae). Mar. Mamm. Sci. 15(1), 1–32.

Spear, L. B., Ainley, D. G., Ribic, C. A., 1995. Incidence of plastic in seabirds from the Tropical Pacific, 1984–1991: relation with distribution of species, sex, age, season, year and body weight. Mar. Environ. Res. 40(2), 123–146.

Takada, H., 2006. Call for pellets! International Pellet Watch Global Monitoring of POPs using beached plastic resin pellets. Mar. Pollut. Bull. 52(12), 1547–1548.

Takeoka, H., 1984. Fundamental concepts of exchange and transport time scales in a coastal sea. Cont. Shelf Res. 3(3), 311–326.

Teuten, E. L., Saquing, J. M., Knappe, D. R., Barlaz, M. A., Jonsson, S., Björn, A., Rowland, S. J., Thompson, R. C., Galloway, T. S., Yamashita, R., Ochi, D., Watanuki, Y., Moore, C., Viet, P. H., Tana, T. S., Prudente, M., Boonyatumanond, R., Zakaria, M. P., Akkhavong, K., Ogata, Y., Hirai, H., Iwasa, S., Mizukawa, K., Hagino, Y., Imamura, A., Saha, M., Takada, H., 2009. Transport and release of chemicals from plastics to the environment and to wildlife. Phil. Trans. R. Soc. B 364(1526), 2027–2045.

Thompson, R. C., Olsen, Y., Mitchell, R. P., Davis, A., Rowland, S. J., John, A. W., McGonigle, D., Russell, A. E., 2004. Lost at sea: where is all the plastic?. Science 304(5672), 838–838.

Tsouk, E., Amir, S., Goldsmith, V., 1985. Natural self-cleaning of oil-polluted beaches by waves. Mar. Pollut. Bull. 16(1), 11-19.

van Franeker, J.A., Blaize, C., Danielsen, J., Fairclough, K., Gollan, J., Guse, N., Hansen, P.L., Heubeck, M., Jensen, J.K., Le Guillou, G., Olsen, B., Olsen, K.O., Pedersen, J., Stienen, E.W.M., Turner, D.M., 2011. Monitoring plastic ingestion by the northern fulmar Fulmarus glacilis in the North Sea. Environ. Pollut. 159(10), 2609–2615.

Walker, T. R., Reid, K., Arnould, J. P. Y., Croxall, J. P., 1997. Marine debris surveys at Bird Island, South Georgia 1990–1995. Mar. Pollut. Bull. 34(1), 61–65.

Williams, A. T., Tudor, D. T., 2001. Litter burial and exhumation: spatial and temporal distribution on a cobble pocket beach. Mar. Pollut. Bull. 42(11), 1031–1039.

ACKNOWLEDGMENTS

Firstly, I express my sincere gratitude to the chairmen of my committee, Professors Hiroshi Matsumoto and Takanobu Inoue, the Department of Architecture and Civil Engineering of the Toyohashi University of Technology, for their supervision, guidance and many valuable suggestions. I also thank the members of my committee, Associate Professors Shigeru Kato and Kuriko Yokota of the Toyohashi University of Technology and Professor Shin'ichi Aoki of Oosaka University for their support, encouragement and valuable comments.

I express my sincere gratitude to Dr. Hirofumi Hinata of the Coastal Zone Systems Division of the National Institute for Land and Infrastructure Management for helping to develop my skills as a researcher, and his instructive help during the field survey and analytical work. I also express my gratitude to Professors Atsuhiko Isobe of Ehime University, Hideshige Takada of the Tokyo University of Agriculture and Technology, Masahisa Kubota of the Tokai University, Associate Professor Yasuo Nihei of the Tokyo University of Science, Dr. Yoshiaki Kuriyama of the Port and Airport Research Institute and Dr. Nikolai Maximenko of the International Pacific Research Center for their many valuable comments. I thank Dr. Shin'ichiro Kako of Kagoshima University for his technical support, and Dr. Takumi Okabe of the Toyohashi University of Technology and Mr. Ryotaro Fuji of Kokusai Kogyo Co., Ltd. for their assistance with the field survey. I also thank the members of the JAPAN NUS Co., Ltd. for their support with the webcam monitoring, and the Tokyo Metropolitan Government's Oshima Island Branch Office for providing the bathymetry data in Wadahama Beach offshore.

I thank Dr. Takeshi Suzuki and the members of the Coastal, Marine and Disaster Prevention Department of the National Institute for Land and Infrastructure Management for their comments and encouragement during this research. I also thank the present and former managers of the National Institute for Land and Infrastructure Management for giving me the opportunity to carry out this research. I also thank the members of the Chubu Regional Bureau of the Ministry of Land, Infrastructure, Transport and Tourism for their understanding and support.

Finally, I sincerely thank my wife Fumi and our daughters Towa and Kii for their understanding and great support during this research.